

Version 1, July 12, 2018

Dark Matter phenomenology

Marco Cirelli

*Laboratoire de Physique Théorique et Hautes Energies (LPTHE),
CNRS & Sorbonne Université, 4 Place Jussieu, Paris, France*

Abstract

Lecture notes for the course given at the Institut de Physique Théorique (IPhT) de Saclay, during the months of June and July 2018. Extracted from: *M. Cirelli, A. Strumia and J. Zupan, Dark Matter*, a review in preparation. When ready, it will supersede these notes. In the meanwhile, a collection of recent reviews is given in the bibliography.

Contents

1 Why Dark Matter is needed?	4
1.1 Mini: galaxies	5
1.1.1 Rotation curves of spiral galaxies	5
1.1.2 Other galactic scale evidences	6
1.2 Midi: clusters of galaxies	7
1.2.1 Weak gravitational lensing: the bullet cluster and cosmic shear	8
1.3 Maxi: the Universe	9
1.3.1 Large scale structure formation	10
1.3.2 CMB acoustic peaks	15
1.3.3 Big Bang Nucleosynthesis	18
1.4 Alternatives to Dark Matter	18
2 What is Dark Matter?	21
2.1 DM as very massive objects	22
2.1.1 Primordial black holes	24
2.2 Very light Dark Matter	25
2.2.1 Fermionic DM	26
2.2.2 Bosonic DM	26
3 When was Dark Matter produced?	27
3.1 Freeze-out	28
3.1.1 Simple estimate of the thermal relic abundance	28
3.1.2 Precise computation of the thermal relic abundance	29
3.2 Asymmetric DM	31
3.3 Freeze-in	32
4 Where is Dark Matter?	33
4.1 Dark Matter density distribution	33
4.1.1 DM density functions	34
4.1.2 Milky Way parameters	34
4.2 Dark Matter velocity distribution	36
5 Direct detection	38
6 Collider searches	51

7 Indirect detection	53
7.1 Energy spectra at production	54
7.2 Positrons and electrons	57
7.3 Anti-protons	60
7.4 Gamma rays	62
7.5 Secondary photons	64
7.6 Neutrinos from the Sun and from the Earth	64
A Cosmology	67
A.1 Expansion	67
A.2 Matter-energy content	68
A.3 Particles in thermal equilibrium	69

Chapter 1

Why Dark Matter is needed?

Evidence for the existence of DM comes from a very wide range of astronomical scales, from a few kiloparsecs (the dimension of small galaxies) to essentially the whole size of the observable Universe. It is somewhat customary to focus on three main probes: observations of individual spiral galaxies (discussed in section 1.1), of clusters of galaxies (section 1.2) and of the CMB and Large Scale Structures at cosmological scales (section 1.3). All these probes are consistent and converge towards the same basic properties for DM¹. However, not all three have an equal status. The former (galaxies) is very intuitive and based on simple, classical physics, but it is arguably the least useful nowadays for quantitative determinations. The latter (cosmology) relies on the more complex physics underlying the standard cosmological model, based on the GR description of an expanding Universe; it delivers however the most statistically significant evidences and it is the most precise tool to measure DM quantities, as we will discuss below.

It is very important to stress that all these probes pertain to the *gravitational* effects of DM. No evidence based on DM effects other than gravitational is available yet. Hence, a natural alternative is to consider modifying gravity in order to explain the phenomena usually attributed to DM. Some of the proposals in this direction are discussed later on. Until then, we stick instead to the standard hypothesis that DM is made of undiscovered matter corpuscles, be they a new species of elementary particles or a new kind of macroscopical bodies.

The present cosmological DM density, averaged over the whole Universe, is expressed in terms of the combination of parameters $\Omega_{\text{DM}}h^2$ where $\Omega_i = \rho_i/\rho_{\text{cr}}$ is the density relative to the critical density $\rho_{\text{cr}} = 3H^2/8\pi G_N$, G_N is Newton's constant and the present Hubble constant is written as $H_0 = h \times 100 \text{ km/s} \cdot \text{Mpc}$, with $h = 0.678 \pm 0.009$.² The current best determination reads [4]

$$\Omega_{\text{DM}}h^2 = 0.1186 \pm 0.0020. \quad (1.1)$$

This trivially translates into $\Omega_{\text{DM}} = 0.258 \pm 0.004$, i.e. DM constitutes about 26% of the total *matter-energy* content of the current Universe. Since the density of normal baryonic matter is measured to be $\Omega_b = 0.02226 \pm 0.00023$, or 4.8%, DM constitutes about 84% of the total *matter* content.

¹Which does not exclude, however, that DM could be made of different substances at the different scales, provided that they share the common basic properties discussed below.

²This determination of h is based on PLANCK cosmological data [2]. Alternative determinations based on local HST data find higher values (around $h = 0.73$ in [3]) and are currently at odds with the value quoted above, originating an interesting debate. We use the cosmological value here for definiteness, as in [4].

The astrophysical and cosmological data are reproduced assuming that DM is cold, non-interacting, stable and with adiabatic inhomogeneities.

- *Cold* means that DM behaves as a non-relativistic fluid at the crucial time of matter-radiation equality (MReq), when structure formation begins. Assuming that DM is made of particles, this means that their typical momentum, p , is much smaller than their mass, $p \ll M$, i.e. their typical velocities, v , are much smaller than the speed of light, $v \ll c$, at the specific moment in time corresponding to MReq and, a fortiori, for the subsequent evolution of the Universe. If DM is made of thermalized particles, this implies that they must be heavier than a few keV, as discussed later in section 1.3.
- *Non-interacting* (or equivalently *collision-less*) means that the interactions among DM particles, or between DM and other particles, are small enough to be neglected. This is what differentiates DM from ordinary matter, which has significant interactions, notably electromagnetic. In the lack of interactions with light lies the origin of the *dark* in Dark Matter. This does not mean that DM has absolutely no interactions with itself or ordinary matter. Quite the contrary, most DM production models in cosmology and essentially all search strategies do rely on the existence of non-zero interactions. Notably, particles with SM weak interactions, or interactions with a similar strength, fit in the ‘non-interacting’ class. A corollary of non-interacting is *dissipation-less*: unlike ordinary matter, DM cannot emit electromagnetic radiation and therefore cannot easily dissipate its energy and cool down. This feature is at the core of the different behavior of ordinary and dark matter in cosmology. Of course, also in this case the prohibition is not absolute: interesting models exist in which DM has some small degree of dissipation.
- *Stable* means that DM is present since the early phases of the Universe and has not disappeared until essentially now. If DM is made of particles, it means that it does not decay, or, if it does, that its half-life is so much longer than the age of the Universe that the cosmological effects are negligible. Current limits sit at $\tau_{\text{DM}} \gtrsim 10^{28}$ s, to be compared with $t_{\text{Uni}} \simeq 13.8$ Gyr = $4.35 \cdot 10^{17}$ s.
- *Adiabatic* means that DM has the same primordial density inhomogeneity as other particles: DM is denser where ordinary matter and photons are denser. This happens in an inflationary context, when all inhomogeneities arise from the quantum fluctuations of one inflaton field.

1.1 Mini: galaxies

1.1.1 Rotation curves of spiral galaxies

Spiral galaxies³ rotate around their vertical axis. By measuring the Doppler shift of atomic lines, one can determine the circular velocity of stars and other tracers (e.g. hydrogen clouds and

³Traditionally, galaxies are classified according to their observed shape as: Ellipticals (E), Spirals (S) and Barred Spirals (SB). Elliptical galaxies are further labelled according to their elongation, from E0 (round) to E7 (very elongated). They do not exhibit any particular axe of rotation. Spiral and barred spiral galaxies are further marked according to how tight their spiral arms wrap around the center: Sa, Sb, Sc... and SBa, SBb, SBc..., in order of increasing openness of the arms. The Milky Way is a rather typical Sb galaxy. Irregular (Irr) and dwarf galaxies do not necessarily follow into one of the previous classes. This classification does not necessarily correspond to an evolution scheme: galaxies are not generically born as E and then evolve to S or SB (although

masers) as a function of their distance from the galactic center. This is what is called a *rotation curve*, of which some historical and recent examples are reported in fig. 1.1. Basic Newtonian dynamics predicts a simple relation between the circular velocity v_c of a test particle of mass m (e.g. a star) and the mass $M(r)$ contained within a distance r from the center:

$$m \frac{v_c^2(r)}{r} = \frac{G_N m M(r)}{r^2} \quad \Rightarrow \quad v_c(r) = \sqrt{\frac{G_N M(r)}{r}}. \quad (1.2)$$

In spiral galaxies, most of the (visible) mass is concentrated in a dense central bulge and in the arms of the disk, which typically extend to $\mathcal{O}(10)$ kpc. At large enough r , therefore, all the visible mass is contained within the orbit and can be replaced by a constant M thanks to Gauss' law: the velocity should then follow a ‘keplerian’ decline $v_c(r) \sim r^{1/2}$. The crucial point is that, instead, the observation of large samples of galaxies of this kind has shown the rotation curves to remain *flat* (i.e. constant with r) out to large distances from the center. Hence, additional invisible mass is needed to prevent the peripheral stars from flying away and the galaxies from breaking apart.

Assuming spherical symmetry, the above equations can be trivially integrated: for the velocity to remain approximately constant, the additional invisible matter should be distributed as a diffuse *halo* of particles with a density $\rho(r) \sim 1/r^2$ out to large r . Eventually, at even larger r , the halo is expected to die off and the curve to start declining. But typically no tracers are available at such large distances.

In 1970, Vera Rubin and W. Kent Ford [5] were the first to perform a precise measurement of the rotation curve of the Andromeda galaxy (M31), tracing about 70 hydrogen clouds. They determined the curve to be rather flat out to ~ 22 kpc.⁴ This was later corroborated by more observations, in tens of other galaxies and using radio as well as optical techniques, finding rotation curves that remain flat up to 50 kpc and beyond. The results were quickly interpreted as evidence for ‘missing mass’ and the problem of Dark Matter rose to prominence. To this day, with hundreds of spiral galaxies observed, the flatness of rotation curves remains probably the most intuitive and convincing evidence in favor of DM. Realistic studies, as opposed to the simplified proof of principle sketched above, carefully model the different luminous components (bulge, bar, disk, gas...) of the observed galaxies and determine by subtraction the DM contribution. In astrophysical terms, it is said that they determine the proportion of invisible to visible mass, i.e. the ‘mass-to-light ratio’, of a given galaxy. The studies can also try to determine the DM distribution, including in the Milky Way, although typically this is not very constraining.

1.1.2 Other galactic scale evidences

Some other pieces of evidences for DM have been claimed at the galactic scale [6].

Early numerical simulations in the ’70s, and their analytical interpretation, were showing that a dark spherical halo is needed to ensure the *stability of the disk* in spiral galaxies: in its absence, disks were seen disrupting within a few rotational periods and transforming into chaotic distributions of stars. Later more sophisticated work, on the other hand, showed that the DM halo has the negative effect of morphing a disk into a bar and eventually slowing the rotation of

initially it was believed so) nor they are created as S or SB and then merge into Ellipticals (although this is a recent hypothesis). This is a currently very active research domain in astrophysics.

⁴Previous observations were not as precise and as extended in r , so that their interpretation was not consensual. See especially the historical review by G. Bertone and D. Hooper in [1].

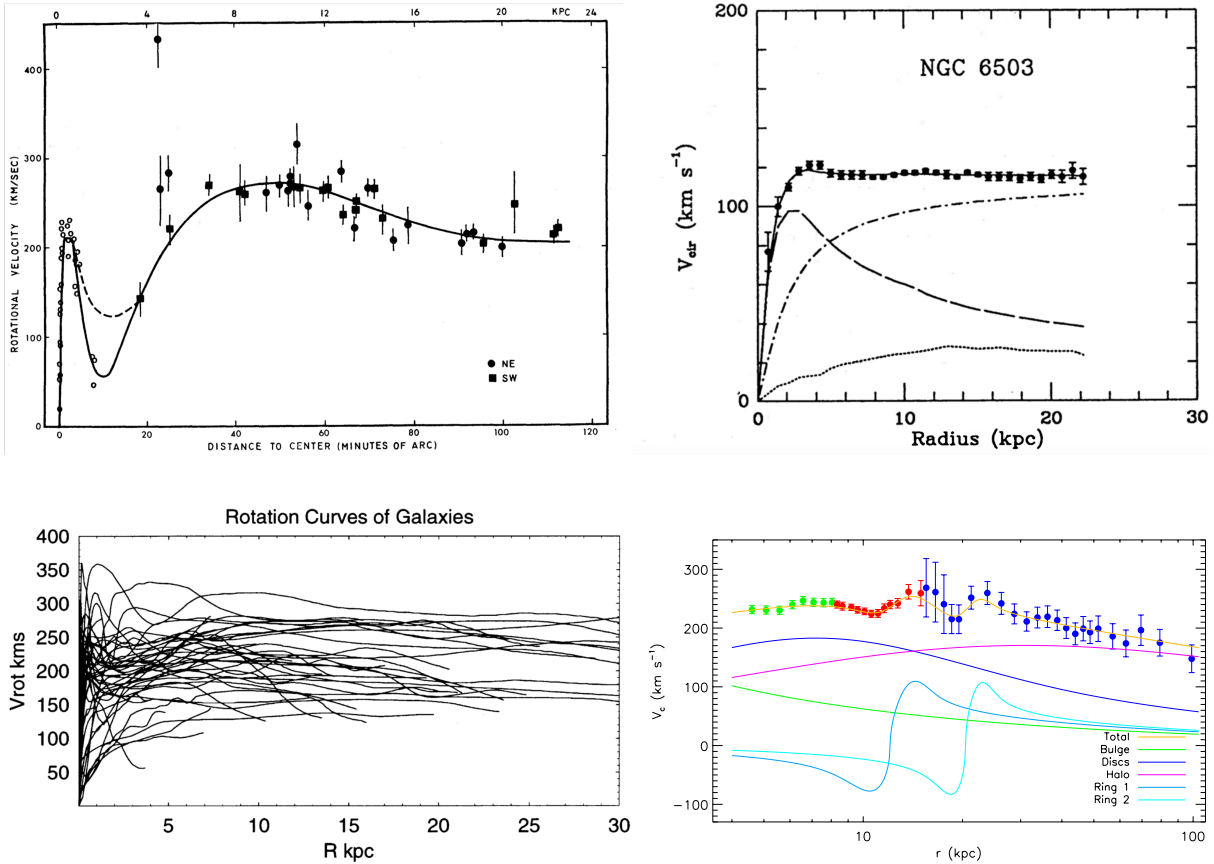


Figure 1.1: **Rotation curves of spiral galaxies.** *Top left:* The original rotation curve of Andromeda by Rubin and Ford (1970). *Top right:* the particularly neat curve of NGC6503 (from Begeman et al. 1991, where it is actually claimed that MOND is a better fit than DM). *Bottom left:* A compilation of about 50 galaxies, from Sofue et al. (1999). *Bottom right:* A recent rotation curve for the Milky Way by Huang et al. (2016).

the bar down, which is at odds with the observed existence of many spinning disks. It seems that no simple conclusion for the role of DM can be claimed, so that this topic is not currently often cited.

The existence of massive DM halos around galaxies can also be proven via *galaxy-galaxy lensing*. This is the distortion of the images of background galaxies induced by the gravitational lensing effect of foreground ones. By measuring average properties as in fig. 1.3a (because the weak lensing signal produced by an individual galaxy is too low to be detected), one can infer the amount of matter in a typical lens galaxy, finding that it is much larger than the visible mass. The same observations can also determine the typical shape of the DM halos, which are found to be somewhat flattened.

1.2 Midi: clusters of galaxies

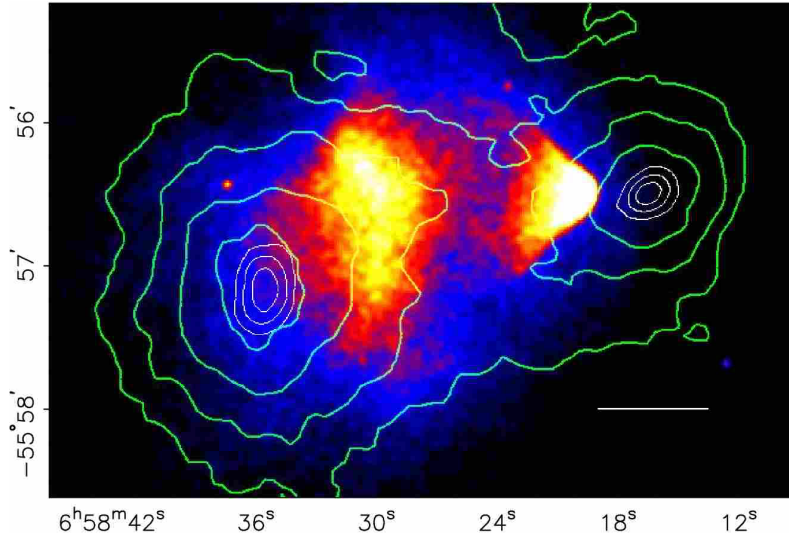


Figure 1.2: **Bullet cluster.** The collision of a pair of clusters of galaxies, with the colored map representing the X-ray image of the hot baryonic gas. This is displaced from the distribution of the total mass reconstructed through weak lensing, shown with green contours. The white bar corresponds to the length of 200 kpc. From Clowe et al. (2006).

In 1933 Fritz Zwicky was the first to claim evidence for DM⁵, by looking at the velocity dispersion in the Coma cluster of galaxies, and finding that extra matter was necessary to keep them together [7]. The clusters of galaxies are the largest gravitationally bound systems in the Universe. They contain hundreds to thousands of galaxies and extend to several Mpc in size. Because of their size, galaxy clusters are good probes of the ‘average’ Universe. While the most precise determinations of average DM density at present do not come from galaxy clusters, they do lead to $\Omega_{\text{DM}} \approx 0.2$.

Zwicky’s determination was based on the virial theorem. Because of its historic importance we briefly summarize the argument. The virial theorem links the average kinetic energy to the average potential energy, $\langle K \rangle = -\frac{1}{2}\langle V \rangle$. In a toy system with $N \gg 1$ objects of mass m at equal distance r interacting through gravity, this allows to determine their total mass mN from the velocity v and the size r :

$$N \frac{mv^2}{2} = \frac{1}{2} \frac{N^2}{2} \frac{G_N m^2}{r} \quad \Rightarrow \quad mN = \frac{2rv^2}{G_N}. \quad (1.3)$$

Applying this kind of considerations to clusters of galaxy, Zwicky claimed that the total mass in the cluster was larger than the visible mass, such that extra dark matter is needed. The DM hypothesis was not widely accepted, but it was also not disregarded. A common interpretation was that more information would be needed in order to understand these systems.

1.2.1 Weak gravitational lensing: the bullet cluster and cosmic shear

Today the most striking evidence for the presence of DM on the length scales of galaxy clusters comes from the observations of a pair of colliding clusters known as the ‘bullet cluster’ (located

⁵The concept and terminology of Dark Matter was already hoovering in the astronomy community, e.g. in the works by J. Kapteyn and J. Oort. However, like in the case of galaxy rotation curves, the early observations were somewhat contradictory and confused. See again G. Bertone and D. Hooper in [1].

3.7 Gyr away, with a catalog name 1E0657-558 and first observed in detail in 2006) and of similar systems [8]. Most of the baryonic mass in the bullet cluster is in the form of hot gas whose distribution can be traced through its X -ray emissions. The distribution of total mass, visible and dark, was independently measured through weak lensing.

The special feature of the system is that visible matter and dark matter are spatially separated. The interpretation is the following: in the past each of the two objects was an ordinary system, with the visible and dark matter mixed together. The two objects collided 150 million years ago. Visible matter interacts significantly with itself, so that the hot gas from the two clusters experienced a collisional shock wave. DM, on the other hand, experienced negligible collisions with itself and with normal matter, such that the DM clouds of the two systems simply passed through each other. This lead to the present separation of the visible and dark matter components, visible in fig. 1.2. After the observation of the bullet cluster, many similar system have been studied. Harvey et al. (2015) reports the results on 72 of them and concludes that the existence of DM can be established with a significance of more than 7σ .

This kind of observations puts a very severe strain on all alternative interpretations where DM is replaced by some modification of gravity that cannot get spatially separated from normal matter, so that the lensing would follow visible matter.

Incidentally, these systems also provide precious information about the particle physics properties of DM: the fact that the DM halos did not slow down compared to the collision-less trajectories implies an upper bound on the DM self-interaction cross section, assuming point interactions

$$\frac{\sigma}{M} \lesssim 1 \frac{\text{cm}^2}{\text{g}} = 1.8 \frac{\text{mb}}{\text{GeV}} = \frac{4580}{\text{GeV}^3}. \quad (1.4)$$

For comparison, we recall that 50 mb is a typical QCD cross section, for, e.g., pp scattering.

At length scales somewhat intermediate between the galactic, the cluster and the cosmic ones, the detection of *cosmic shear* also provides evidence for DM [9]. Cosmic shear refers to the deflection of light of very distant galaxies by the gravitational attraction of foreground mass concentrations, not in the form of the DM halos of galaxies or clusters (like in the case of the galaxy-galaxy lensing and of cluster collisions, discussed above) but in the form of much larger and diffuse structures like huge filaments and loose clumps. The measurements are performed statistically on a very large number (millions) of distant galaxies using multi-wavelength surveys, that have to be both very deep (detecting very distant galaxies) and very wide (exploring large portions of the sky). They allow to determine $\Omega_{\text{DM}} \simeq 0.25$. The importance of cosmic shear actually goes well beyond the mere additional evidence for the existence of DM: by reconstructing the matter distribution along the line of sight, one is effectively looking back at the formation history of the large DM structures that provide the scaffolding of the Universe, which we discuss next.

1.3 Maxi: the Universe

The most convincing and most precise evidence for the existence of Dark Matter comes nowadays from the largest scales possible, i.e. the entire observable Universe. The basic point, qualitatively, is that the Universe would not have acquired the appearance that we observe today if not for the role that DM played: galaxies would not be distributed in the way they are, and the CMB temperature anisotropies would not look the way they do, if it weren't for DM. DM acts as an

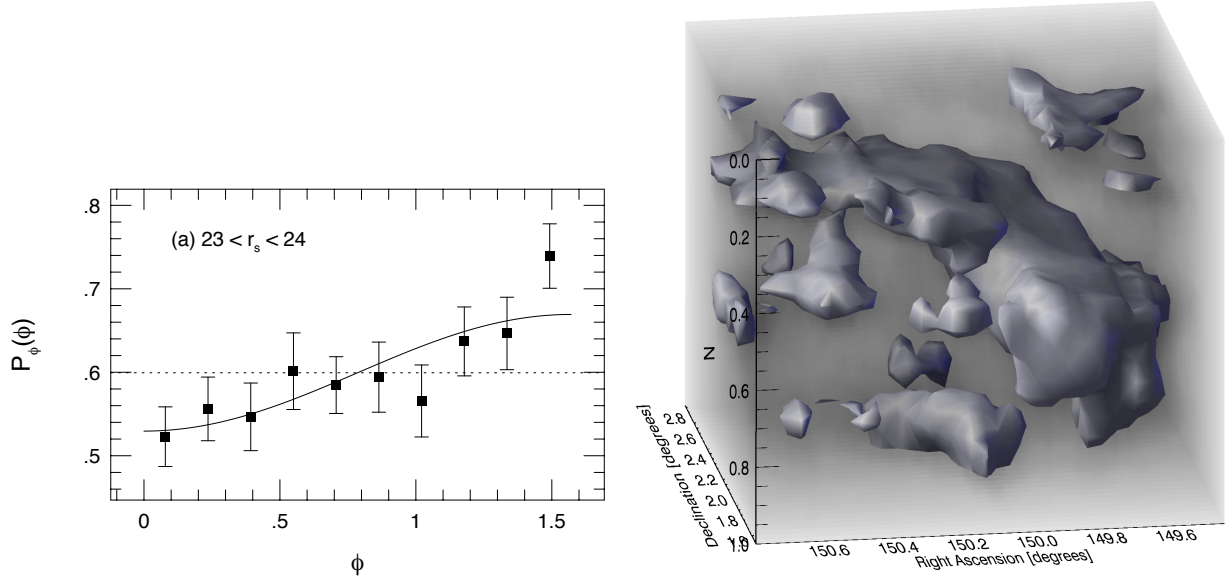


Figure 1.3: **Weak gravitational lensing** can be seen as a multi-length and multi-purpose tool to establish the existence of Dark Matter and determine its properties. At small scales, galaxy-galaxy lensing (discussed in sec. 1.1.2) is illustrated by the figure on the left. The images of background galaxies are statistically distorted to align on a ring pattern around a foreground galaxy i.e., for a certain bin in magnitude r_s of the source galaxies, the average probability of the orientation is measured to have a deficit of images oriented radially ($\phi = 0$) and an excess of images oriented tangentially ($\phi = \pi/2$). At very large scale, cosmic shear (sec. 1.2.1) is illustrated by the figure on the right. The clouds in the graph are just the constant density contours of the large scale DM formations, as reconstructed in 3D by the observations of the lensing of background sources. (Figures from Brainerd et al. 1995 in [6] and from Massey et al. 2007 in [9], credit: R. Massey/Nature, courtesy of R. Massey).

indispensable catalyzer for the formation of structures. It brings the Universe from the initial state characterized by almost perfect smoothness with only tiny inhomogeneities to a state rich of structures at many different scales. As we will see later, ordinary matter cannot accomplish this task, essentially because of its coupling to radiation.

In the next subsection we will deal with the formation of Large Scale Structures (LSS), while in sec. 1.3.2 we will discuss the imprint of DM in the acoustic peaks of the CMB. These two probes are illustrated in fig. 1.4.

1.3.1 Large scale structure formation

The Universe appears to be very clumpy today. Take for instance the results of galaxy surveys, like the one showed in fig. 1.4 (top right): a mere inspection by eye of the image, which corresponds to a 3D map of virtually all galaxies in the observable Universe, allows to appreciate a variety of structures like lumps, filaments, walls, voids..., at many different scales. Other astronomical observations, such as the Lyman- α forest, weak lensing measurements, cluster counts etc, concur in establishing the picture of a chunky Universe.

Quantitatively, from all these measurements one can extract the *matter power spectrum* $P(k)$

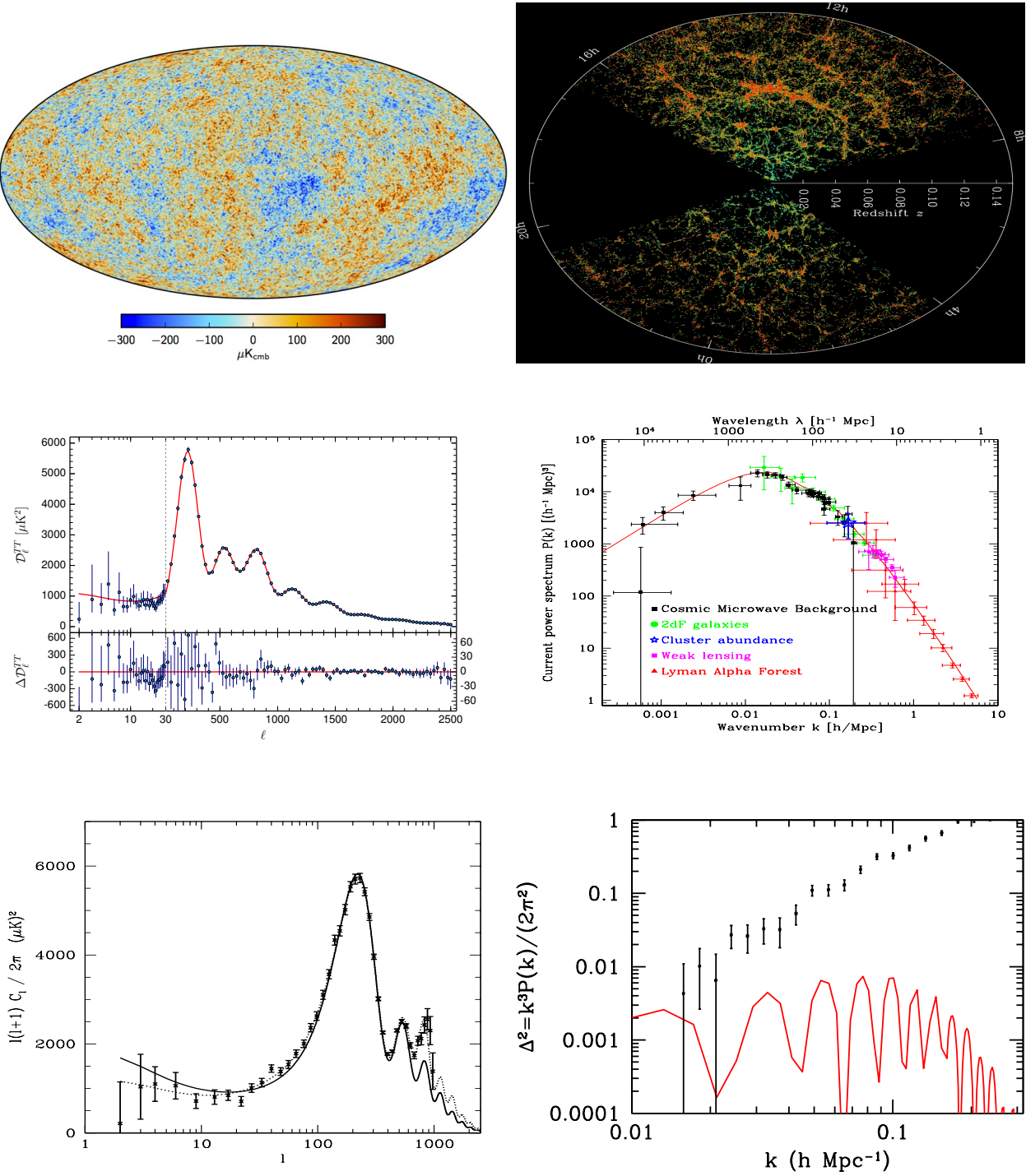


Figure 1.4: *The power spectrum of the CMB acoustic peaks (middle row, left) is extracted from the map of temperature anisotropies (top left). The matter power spectrum (middle row, right) is extracted from extensive galaxy surveys (top right) as well as from other mapping probes. The same quantities in absence of DM are illustrated in the bottom row. Figures from [2, 10–12] (credit M. Blanton and SDSS).*

plotted in fig. 1.4 (middle row on the right). It is defined via $\langle \delta_k \delta_{k'} \rangle = (2\pi)^3 P(k) \delta^3(\vec{k} - \vec{k}')$, where δ_k is the Fourier transform of the density contrast $\delta(\vec{r})$, as we will better specify below, and $\langle \rangle$ denotes an average over all \vec{k} -space.⁶ $P(k)$ conveniently expresses, in Fourier space, the inhomogeneity in matter: a large (small) value of $P(k)$ means that many (few) structures exist at the characteristic size $\sim 1/k$. The measurements therefore show that the Universe has ‘some power on all scales’. To make the case of clumpiness even stronger, one can also recast $P(k)$, which has units of $(\text{length})^3$, into the adimensional quantity called variance, $\Delta(k) = k^3 P(k)/(2\pi^2)$, plotted in fig. 1.4 (bottom right). Small values of Δ^2 correspond to small density contrasts, while $\Delta^2 \simeq 1$, for instance, indicates an overdensity which is 100% larger than the average. As the data show, on small scales (large k) the Universe exhibits large inhomogeneities.

On the other hand, in the standard cosmological model, inflation generated primordial inhomogeneities with very small amplitude $\delta \approx 10^{-5}$. This is indeed confirmed by the almost perfect homogeneity of the CMB. So the question is: how could these tiny primordial lumps grow from such small amplitudes to the large contrasts observed today? The answer, as anticipated above, is that the growth of the density perturbations is crucially driven by the presence of the DM. In order to quantitatively understand how that happened, we need to sketch their evolution in the early Universe.⁷

Let us consider a Universe filled with a generic matter fluid, whose exact nature we leave for the moment unspecified. The main features of the evolution of density perturbations in such a medium can be understood already by replacing the full general-relativistic computation with its Newtonian limit. This is a valid description of non-relativistic matter at length scales that are much smaller than the horizon. A non-relativistic fluid is fully characterized by its density, $\rho(\vec{r}, t)$, by its velocity field, $\vec{v}(\vec{r}, t)$ and by the equation of state for the pressure $P(\rho)$. Its gravitational interactions are described by the Newton potential Φ . These quantities are governed by the evolution (‘Euler’) equations

$$\left\{ \begin{array}{ll} \frac{\partial \rho}{\partial t} + \vec{\nabla} \cdot (\rho \vec{v}) = 0 & \text{continuity} \\ \frac{\partial \vec{v}}{\partial t} + (\vec{v} \cdot \vec{\nabla}) \vec{v} = -\frac{\vec{\nabla} P}{\rho} - \vec{\nabla} \Phi & \text{momentum conservation} \\ \nabla^2 \Phi = 4\pi G \rho & \text{Poisson,} \end{array} \right. \quad (1.5)$$

which form a system of non-linear differential equations. For a quasi-homogeneous universe it is possible to gain useful analytic information by expanding the above quantities to the 1st order in perturbations

$$\rho = \rho_0(t) + \rho_1(\vec{x}, t), \quad p = p_0 + p_1, \quad \vec{v} = \vec{v}_0 + \vec{v}_1, \quad \Phi = \Phi_0 + \Phi_1. \quad (1.6)$$

We first consider the case of a static universe (no expansion). Eq. (1.5) reduce to a set of coupled

⁶Here δ^3 denotes the Dirac delta that enforces $\vec{k} = \vec{k}'$, not to be confused with the δ that denotes the perturbations.

⁷Cosmological perturbation theory and structure formation is a whole research field in itself. We here focus only on the aspects that are instrumental to our goal, which is just showing the crucial role of DM in the growth of such structures. We follow quite closely the treatment found in classic textbooks [13].

equations for the perturbations

$$\left\{ \begin{array}{l} \frac{\partial \rho_1}{\partial t} + \rho_0 \vec{\nabla} \cdot \vec{v}_1 = 0 \\ \frac{\partial \vec{v}_1}{\partial t} + \frac{v_s^2}{\rho_0} \vec{\nabla} \rho_1 + \vec{\nabla} \Phi_1 = 0 \\ \nabla^2 \Phi_1 = 4\pi G \rho_1, \end{array} \right. \quad (1.7)$$

where we defined the quantity $v_s^2 = \partial p / \partial \rho = P_1 / \rho_1$ which is interpreted as the sound speed in the fluid (as we will see in a moment). By deriving the first equation again with respect to time, and substituting in it the second and third, one arrives at the evolution equation for the density perturbation ρ_1 , the *Jeans equation*

$$\frac{\partial^2 \rho_1}{\partial t^2} - v_s^2 \nabla^2 \rho_1 = 4\pi G \rho_0 \rho_1. \quad (1.8)$$

Ignoring gravity (i.e., setting $G = 0$) one indeed obtains density waves (i.e. sound) that travel at speed v_s . Including gravity, the full equation expresses the competition between a pressure term (on the left-hand side) and a collapse term (on the right). The Jeans length $\lambda_J = \sqrt{v_s^2 / (4\pi G \rho_0)}$ discriminates which term is dominant: perturbations on large scales $\lambda > \lambda_J$ will collapse and grow in time, while perturbations on small scales $\lambda < \lambda_J$ will be supported by pressure. Incidentally, the growth will be exponential in time, $\rho_1 \propto e^{\sqrt{4\pi G \rho_0} t}$, as one can easily check solving the 2nd order differential equation. This is the Jeans instability that, when applied to normal matter, explains how gas clouds collapse to form compact bodies, e.g. stars. The intuitive meaning of the Jeans scale is the size of the cloud of gas that is so big that its hydrostatic pressure, which prevents the collapse on time-scales $\tau_{\text{pressure}} \sim \lambda_J / v_s$, is too slow to stop the gravitational attraction, which has a typical time-scale $\tau_{\text{gravity}} \sim (G \rho_0)^{-1/2}$. One can also naturally define the Jeans mass $M_J = 4\pi/3 \rho_0 \lambda_J^3$, i.e the matter enclosed in a sphere of radius λ_J . Perturbations with mass $M > M_J$ are ‘Jeans unstable’ and will collapse.

We then move to the more realistic case of an expanding universe. This means that the zero-th order quantities describing the smooth background are subject to the laws of expansion

$$\rho_0(t) = \rho_0(t_0)/a^3, \quad \vec{v}_0 = H\vec{r}, \quad \vec{\nabla} \Phi_0 = \frac{4\pi G \rho_0}{3} \vec{r}. \quad (1.9)$$

The first relation is just the standard dilution of NR matter, with $a(t)$ satisfying the Friedmann equations (see Appendix A). The second is just the Hubble law for the velocity field of the homogeneous background, with respect to which the perturbations \vec{v}_1 can be seen as peculiar velocities. The third relation is a general solution of the Poisson equation. A series of tedious but rather straightforward passages lead to the 1st order linear equations

$$\left\{ \begin{array}{l} \frac{\partial \rho_1}{\partial t} + 3H\rho_1 + H(\vec{r} \cdot \vec{\nabla})\rho_1 + \rho_0 \vec{\nabla} \cdot \vec{v}_1 = 0, \\ \frac{\partial \vec{v}_1}{\partial t} + H\vec{v}_1 + H(\vec{r} \cdot \vec{\nabla})\vec{v}_1 + \frac{v_s^2}{\rho_0} \vec{\nabla} \rho_1 + \vec{\nabla} \Phi_1 = 0, \\ \nabla^2 \Phi_1 = 4\pi G \rho_1, \end{array} \right. \quad (1.10)$$

which replace eq. (1.7). The added terms due to the expansion are clearly identified by the appearance of H . We then define the relative density (or density contrast) $\delta(\vec{r})$ and expand it in

co-moving Fourier modes:

$$\delta(\vec{r}) \equiv \frac{\rho_1(\vec{r})}{\rho_0} = \frac{1}{(2\pi)^3} \int d^3k \delta_k(t) \exp[-i\vec{k} \cdot \vec{x}], \quad \vec{x} \equiv \frac{\vec{r}}{a(t)}. \quad (1.11)$$

The factor $a(t)$ means that the wavenumber $1/k$ follows the average evolution of the universe. This is very convenient because in this way modes with different k turn out to be decoupled. Similarly, we define \vec{v}_k and Φ_k , the Fourier transforms of the velocity perturbation \vec{v}_1 and of the gravitation potential one Φ_1 . In Fourier space, eq. (1.10) then become

$$\left\{ \begin{array}{l} \frac{\partial \delta_k}{\partial t} - i\frac{\vec{k}}{a} \vec{v}_k = 0, \\ \frac{\partial(a \vec{v}_k)}{\partial t} - i\vec{k} v_s^2 \delta_k - i\vec{k} \Phi_k = 0, \\ \Phi_k = -\frac{4\pi G \rho_0}{k^2} a^2 \delta_k. \end{array} \right. \quad (1.12)$$

The second equation can be further simplified. One can decompose the velocity perturbation as $\vec{v}_1 = \vec{v}_{1\perp} + \vec{v}_{1\parallel}$, where $\vec{\nabla} \cdot \vec{v}_{1\perp} = 0$ (divergence-free or soleinoidal component) and $\vec{\nabla} \times \vec{v}_{1\parallel} = 0$ (curl-free or irrotational component). In Fourier space $\vec{k} \cdot \vec{v}_{k\perp} = 0$, $\vec{k} \times \vec{v}_{k\parallel} = 0$. The second equation in (1.12) for $\vec{v}_{k\perp}$ just amounts to $\partial(a \vec{v}_{k\perp})/\partial t = 0$, solved by $\vec{v}_{k\perp} \propto 1/a$: the soleinoidal component dies away with the expansion of the Universe, only the irrotational one survives. Since the latter is parallel to \vec{k} , we can substitute everywhere in eq. (1.12) $\vec{v}_k \rightarrow v_k \hat{\vec{k}}$ (where $\hat{\vec{k}}$ is the unit vector along \vec{k}) and $\vec{k} \rightarrow |\vec{k}| \equiv k$. At this point we can combine the three equations to obtain a second order one. By taking v_k from the first one, plugging it into the second and using Φ_k from the third, we arrive at

$$\frac{\partial^2 \delta_k}{\partial t^2} + 2H \frac{\partial \delta_k}{\partial t} + \left(\frac{v_s^2 k^2}{a^2} - 4\pi G \rho_0 \right) \delta_k = 0. \quad (1.13)$$

This is the Jeans equation for density perturbations, analogous to eq. (1.8) but in Fourier space and in the context of an expanding Universe. Like before, the Jeans wavenumber $k_J = a\sqrt{4\pi G \rho_0/v_s^2}$, which now depends on a , discriminates whether the pressure term (proportional to v_s^2) wins or the collapse one (proportional to $G\rho_0$) does.

It is now time to specify which kind of matter fluid we are dealing with, and which epoch of the Universe's evolution it is in. Let us first consider the case of baryonic matter, and the epoch of Matter Domination (MD) before decoupling. The protons (and nuclei) and the electrons which constitute baryonic matter are *tightly coupled* by electromagnetism to the photons. They form a unique fluid which is effectively relativistic, as the photons supply their pressure to the plasma. The fluid has a very large speed of sound $v_s^2 \simeq 1/3$ (in units of c).⁸ In this case, we can then simplify eq. (1.13) by keeping only the pressure term. In MD, $a(t) = (\frac{3}{2}t H_0)^{2/3}$ (see Appendix A) and therefore $H = \dot{a}/a = 2/(3t)$. Hence one gets

$$\frac{\partial^2 \delta_k}{\partial t^2} + \frac{4}{3t} \frac{\partial \delta_k}{\partial t} + \frac{v_s^2 k^2}{\left(\frac{3}{2}H_0\right)^{4/3} t^{4/3}}, \quad \text{solved by} \quad \delta_k = \frac{c_1 \cos(c k t^{1/3}) + c_2 \sin(c k t^{1/3})}{k t^{1/3}}. \quad (1.14)$$

⁸Strictly speaking, this implies that the NR analysis done above may fail and we should move to the fully relativistic one. The qualitative results still hold though.

This is an oscillating solution, damped in time. Hence, inhomogeneities do not grow on scales $k < k_J(a) \sim aH/v_s$ (where in the last relation we have used $\rho_0 = 3H^2/(8\pi G)$ in MD). In other words, the baryonic, tightly-coupled fluid never clusters on any scale smaller than the horizon.

A Dark Matter fluid with $v_s = 0$ behaves differently and therefore makes a huge difference in cosmology. Using again the MD expressions for $a(t)$, $H(t)$ and ρ_0 , eq. (1.13) becomes

$$\frac{\partial^2 \delta_k}{\partial t^2} + \frac{4}{3t} \frac{\partial \delta_k}{\partial t} - \frac{2}{3t^2} \delta_k = 0, \quad \text{solved by} \quad \delta_k = c_{\text{grow}} t^{2/3} + c_{\text{decay}} t^{-1}. \quad (1.15)$$

The solution contains a decaying mode that will die off, but, most importantly, contains a mode that grows with a specific positive power of time. This is how the Universe evolved from a primordial quasi-homogeneous state with $\delta_k \sim 10^{-5}$ to the present clumpy state. Incidentally, note that the exponential growth found in the static case has become a power-law one, as if the expansion of the Universe acted as a brake to slow it down.

For completeness, we can also consider the DM fluid in the Radiation-Dominated (RD) epoch, described by $H = 1/(2t)$. In this case, one can show that eq. (1.13) loses both the $v_s^2 k^2 \delta_k / a^2$ term (because $v_s = 0$ for the DM fluid) and the $4\pi G \rho_0 \delta_k$ term (because the relevant δ_k would be the one of radiation, which however does not cluster and therefore does not source perturbations in the gravitational potential), reducing to

$$\frac{\partial^2 \delta_k}{\partial t^2} + \frac{1}{t} \frac{\partial \delta_k}{\partial t} = 0, \quad \text{solved by} \quad \delta_k \propto \ln t + \text{const..} \quad (1.16)$$

Hence, DM perturbations grow only negligibly (logarithmically) during RD. Similar computations show that DM does not efficiently cluster when the Universe is dominated by vacuum energy, or by curvature.

In summary, the standard story of structure formation goes as follows. The Universe became matter-dominated when the scale factor was $a_{\text{eq}} \sim 1/3400$. At that point, DM inhomogeneities δ_k started growing as $t^{2/3}$ on scales $1/k$ which are 3400 times smaller than the present horizon. Larger scales started clustering later, as soon as they became smaller than the expanding horizon. Normal matter, in contrast, could not cluster because it was tightly coupled by electromagnetism to photons and was forming pressure waves. Later in the evolution of the Universe, at $a_{\text{recomb}} \sim 1/1100$, the temperature became low enough and the photon bath diluted enough that electrons and positrons could bind to form neutral hydrogen. At that point normal matter decoupled from radiation and began falling into the gravitational potential wells that DM had already started to form. In this sense, DM is the crucial ingredient to construct the ‘cosmic scaffolding’ observed in the Universe. If the Universe contained baryonic matter only, perturbations would have a much smaller power and would exhibit evident oscillations. This is what is depicted in the bottom right panel of fig. 1.4, in clear disagreement with observations.

1.3.2 CMB acoustic peaks

The power spectrum of the cosmic microwave background (CMB) (middle left panel in fig. 1.4) is the equivalent of a Fourier transform for the photon temperature field. It is very well measured and provides a large amount of precise information on the contents of the Universe, including in particular DM. The position of the acoustic peaks depends on the DM density and their amplitude is very sensitive to the ratio between the baryon density and the DM density, given that only

normal matter undergoes acoustic oscillations. The minimal Λ CDM model allows to reproduce the detailed features of these inhomogeneities (provided that primordial inhomogeneities are adiabatic) and to extract from a global fit the precise values of the cosmological parameters. This is how the precise numbers for Ω_{DM} and Ω_b given above are determined. It is also possible, however, to understand qualitatively how DM affects the shape of the spectrum by drastically simplifying the analysis and focussing only on the main features, which is what we do below.

The CMB power spectrum has the same intuitive meaning as the matter one $P(k)$, but now for the photon anisotropy field. A large (small) power at a given ℓ signifies abundance (paucity) of correlation between the hot and cold spots in the map at the angular scale $\theta \sim \pi/\ell$. An angular scale θ imprinted on the Last Scattering Surface (LSS) corresponds to physical sizes λ (or $1/k$ in Fourier space) observed from the distance that separates us from the LSS: $\theta \sim \lambda/(\eta_0 - \eta_{\text{LSS}}) \sim 1/(k\eta_0)$. Here η expresses the distance travelled by the CMB photons (see Appendix A), with η_0 the distance travelled up to today and η_{LSS} the distance up to the LSS instant. In the last passage we used the fact that the latter is negligible with respect to the former. Hence, the shape of the power spectrum in ℓ is the resemblance of the structures in $k\eta_0$ in the photon temperature field at the LSS.

The peaks decline as ℓ increases, due to ‘Silk damping’ i.e. the smoothing of small scale structures due to photon diffusion. However the 2nd and the 3rd peaks have roughly equal size. This suggests that, if one could remove Silk damping, the 3rd peak would be particularly prominent and higher than the 2nd. This is the footprint of DM, as we proceed to illustrate.

One denotes the temperature anisotropies $\delta T/T \sim 10^{-5}$ as $\Theta(\vec{r}, \vec{p}, t)$, and expands them in spherical harmonics $\Theta(\vec{r}, \vec{p}, t) = \sum_{\ell=1}^{\infty} \sum_{m=-\ell}^{+\ell} a_{\ell m}(\vec{r}, t) Y_{\ell m}(\vec{p})$. The C_ℓ s of the power spectrum are defined as the variance of the coefficients: $\langle a_{\ell m} a_{\ell' m'} \rangle = \delta_{\ell\ell'} \delta_{mm'} C_\ell$, so roughly speaking $C_\ell \propto |\Theta_\ell|^2$. The evolution of the perturbations in the photon fluid is governed by a set of Boltzmann equations. They are coupled to the evolution equations for matter. The full system reads [13]

$$\text{DM} \left\{ \begin{array}{l} \dot{\delta}_k - i \frac{k}{a} v_k + 3\dot{\Psi}_k = 0, \\ a\dot{v}_k + \dot{a}v_k - ik\Phi_k = 0, \end{array} \right. \quad (1.17)$$

$$\text{baryons} \left\{ \begin{array}{l} \dot{\delta}_{bk} - i \frac{k}{a} v_{bk} + 3\dot{\Psi}_k = 0, \\ a\dot{v}_{bk} + \dot{a}v_{bk} - ik\Phi_k = a \frac{\dot{\tau}}{R} [3i\Theta_1 + v_{bk}], \end{array} \right. \quad (1.18)$$

$$\text{photons} \left\{ \begin{array}{l} \dot{\Theta}_0 + \frac{k}{a} \Theta_1 + \dot{\Psi}_k = 0, \\ \dot{\Theta}_1 - \frac{k}{3a} \Theta_0 + \frac{k}{3a} \Phi_k = \dot{\tau} \left[\Theta_1 - \frac{iv_{bk}}{3} \right], \end{array} \right. \quad (1.19)$$

where $R = 3\rho_b/(4\rho_\gamma)$ and $\tau = \int d\eta n_e \sigma_{\text{Th}} a$ is the optical depth, expressed in terms of the number density of electrons n_e and the cross section of Thomson scattering σ_{rmT} . A few comments are in order. The equations for matter (baryonic or dark) should look familiar: they correspond to those derived in eq. (1.12), with a couple of differences: we are here considering the full relativistic treatment, so that the perturbation to curvature Ψ_k appears (the gravitational potential Φ is still present); we have made the coupling between baryons and photons explicit with the Thomson scattering term (rhs of eq. (1.18)). As expected, the only difference between DM and baryons is

precisely the coupling with photons. The equations for photons contain only the first moments Θ_0 and Θ_1 , as one can show that all higher momenta are damped in the tight coupling limit. The rhs of the second equation in (1.19) is again the Thomson scattering term that couples to baryons. Hence, just the inspection of these system of coupled equations allows to appreciate the following crucial point. Photons are coupled to matter in two ways: via electromagnetism, as expressed by Thomson scattering, and via gravity, as expressed by the gravitational potentials Φ and Ψ that appear in the equations for all fluids. Physically, the latter point means that photons will be redshifted (blueshifted) when spending (gaining) energy to climb out of (fall in) the gravitational potential wells created by matter perturbations. In other words, the CMB photons are *separately sensitive to matter that gravitates* and to matter that also *has an electric charge*. In this resides its ability of measuring the densities of DM and baryonic matter separately. Massaging the above equations will show, qualitatively, how this works in practice.

In the second equation for baryons, one can consider that the dominant term is the rhs, due to the large \dot{r} , so that $v_{bk} \simeq -3i\Theta_1$ and the equation can be rewritten as

$$\left[\Theta_1 - \frac{iv_{bk}}{3} \right] \dot{r} = -R \left[\dot{\Theta}_1 + H\Theta_1 + \frac{k}{3a}\Phi_k \right]. \quad (1.20)$$

This can be plugged in the second equation for photons obtaining

$$\Theta_1 + H\frac{R}{1+R}\Theta_1 - \frac{k}{3a(1+R)}\Theta_0 = -\frac{k}{3a}\Phi_k. \quad (1.21)$$

It is now convenient to convert the photon equations to derivatives with respect to conformal time η , which we denote by $'$. One obtains

$$\begin{cases} \Theta'_0 + k\Theta_1 = -\Psi'_k, \\ \Theta'_1 + \frac{a'}{a}\frac{R}{1+R}\Theta_1 - \frac{k}{3(1+R)}\Theta_0 = -\frac{k}{3}\Phi_k. \end{cases} \quad (1.22)$$

These can be combined in a single second order equation for Θ_0 , by deriving the first one more time with respect to η and plugging in Θ'_1 from the second and Θ_1 from the first. When the dust settles, one has

$$\Theta''_0 + \frac{a'}{a}\frac{R}{1+R}\Theta'_0 + \frac{k^2}{3(1+R)}\Theta_0 = -\frac{k^2}{3}\Phi_k - \frac{a'}{a}\frac{R}{1+R}\Psi'_k - \Psi''_k. \quad (1.23)$$

This is the familiar equation of a damped, forced harmonic oscillator. The damping (the second term on the left) is due as usual to the expansion of the Universe, and indeed it features $a'/a = aH$: for simplicity we will neglect it in the following. The external forcing (the right hand side) is provided by gravity: for simplicity we neglect the curvature terms and keep the gravitational potential Φ_k . If we could neglect the forcing, the equation would read

$$\Theta''_0 + \frac{k^2}{3(1+R)}\Theta_0 = 0, \quad \text{solved by} \quad \Theta_0 = c_1 \cos\left(\frac{k\eta_0}{v_s}\right) + c_2 \sin\left(\frac{k\eta_0}{v_s}\right), \quad (1.24)$$

where $v_s = 1/\sqrt{3(1+R)}$. This is an oscillating solution for Θ_0 as a function of $k\eta_0$, with all peaks and troughs of the same amplitude (as obvious for sine and cosine functions). When we take the square (remember that $C_\ell \propto |\Theta_\ell|^2$), we would get peaks in the C_ℓ distribution that have all the same height.

Including the forcing, the (simplified) equation reads

$$\Theta_0'' + \frac{k^2}{3(1+R)}\Theta_0 = -\frac{k^2}{3}\Phi_k, \quad \text{solved by} \quad \Theta_0 = c_1 \cos\left(\frac{k\eta_0}{v_s}\right) + c_2 \sin\left(\frac{k\eta_0}{v_s}\right) - (1+R)\Phi_k. \quad (1.25)$$

In this case, oscillations occur on top of an ‘offset’ proportional to the gravitational potential Φ_k . When taking the square, the peaks will not have the same height any longer. This simplified analysis cannot capture all the complexity of the system, but the main message is clear: in the relative height of two neighboring peaks in the CMB power spectrum (in particular the 2nd and the 3rd) one reads the abundances of two kinds of matter: matter that is coupled by electromagnetism to photons (baryons, that provide the term with R) and matter that provides the gravitational forcing Φ . The latter turns out to be much larger than the former, providing a very convincing evidence for the existence of DM. If the Universe contained baryonic matter only, the 3rd peak would be suppressed, as shown in the bottom left plot of fig. 1.4, in clear disagreement with the data.

1.3.3 Big Bang Nucleosynthesis

The density of normal matter obtained from a global fit to the CMB data agrees closely with another precision determination, from Big Bang Nucleosynthesis (BBN). BBN probes an earlier phase of the Universe, at much larger temperature, $T \sim$ MeV. It is the theory describing the synthesis of the light elements (D , 3He , 4He and 7Li) starting from their building blocks: the free protons and neutrons present in the primordial plasma. More precisely, BBN is sensitive to the baryon-to-photon ratio $\eta \equiv n_b/n_\gamma$, which trivially translates into $\Omega_b \equiv \rho_b/\rho_{\text{crit}} = n_b m_p / \rho_{\text{crit}} = \eta n_\gamma m_p / \rho_{\text{crit}}$, where m_p is the mass of the proton and the density of photons today $n_\gamma = 410.5 \text{ cm}^{-3}$ as determined from the CMB temperature. The measurements give [4]

$$5.8 \leq \eta_{10} \leq 6.6 \quad \Rightarrow \quad 0.021 \leq \Omega_b h^2 \leq 0.024 \quad (1.26)$$

(with $\eta_{10} \equiv \eta \times 10^{10}$), in perfect agreement with the CMB value quoted in page 4. The concordance between the two determinations gives us confidence that we have well understood the evolution of the early Universe. Quantitatively, the fact that $\Omega_b < \Omega_M \simeq 0.30$ (where the subscript M denotes matter in any form) provides further evidence for the need of additional stuff, that behaves as non-baryonic and that is needed for the structure formation process discussed above. This has been important historically, before CMB and LSS measurements were able to pin down by their own the relative proportions of baryons and DM.

1.4 Alternatives to Dark Matter

In 1840s the astronomy community was facing a puzzling mystery: the orbit of the planet Uranus, at the time the farthest known planet in the solar system, had been observed to violate the standard newtonian laws of celestial mechanics. This led Urbain Jean Joseph Le Verrier, an astronomer working at the Paris Observatory, to postulate the existence of one extra planet whose gravitational effect would explain the anomalies in Uranus’s behavior.⁹ Indeed such a planet,

⁹Independently, John Couch Adams, working at Cambridge in England, put forward the same idea, but his works were not published until later.

named Neptune, was observed in 1846 by Johann Gottfried Galle, an astronomer working in Berlin, almost exactly at the position indicated by Le Verrier on the basis of his computations [14]. At the same time, the planet Mercury was also displaying a puzzling feature not predicted by newtonian gravity – the precession of its perihelion. This led once again Le Verrier to interpret the anomaly as the gravitational effect of another hypothetical planet, which was named Vulcan. Despite decades of searches and even some false discoveries, Vulcan was never proved to exist. Instead, the anomaly was later understood by Albert Einstein as a correction to newtonian gravity due to General Relativity [15].

The analogy with the topic of this review is evident: we are now in a similar situation since we only have indirect gravitational ‘anomalies’. Are they due to some extra (dark) matter, as was the case of Neptune, or are they due to extra gravitational physics, as in the case of the non-existent Vulcan? So far, no convincing modification of gravity has been proposed which could be able to reproduce all the anomalies described above. Hence, most of the community currently directs its efforts towards the former option, the one of additional matter. Nevertheless, DM has never been observed directly. Interesting alternative ideas have been proposed that can fit a sub-set of the gravitational anomalies. Below we review these ideas.

We focus on galaxies. The fact that rotation curves $v(r)$ of almost all galaxies tend to a constant velocity at large radii has been tentatively interpreted as a general phenomenon that is not due to DM, especially because data hint to a puzzling regularity. Even though galaxies have different sizes and masses, their rotation curves tend to flatten when the acceleration a falls below a common critical value

$$a_* \sim 10^{-10} \text{ m/s}^2. \quad (1.27)$$

It is debated whether DM can naturally reproduce this common behaviour observed in different galaxies [16–19]. The answer is possibly yes, because galaxies tend to have a common formation history: normal matter falls into potential wells formed by DM. However, normal matter gets later partially expelled by astrophysical effects (such as supernova explosions) that are not under good theoretical control and which presumably depend on the escape velocity of the specific galaxy. If this is the case, the observed regularity does not have a profound significance.

Alternatively, this regularity might point to a new physics law, a possibility proposed by Milgrom, and known as Modified Newtonian dynamics (MOND) [20]. It postulates that below some critical acceleration a_* the usual Newton law $F = ma$ changes to $F = ma^2/a_*$, where the quadratic dependence has been chosen such that rotation curves become flat at accelerations below a_* . In spherical approximation:

$$\frac{GmM(r)}{r^2} = F = \begin{cases} ma & a > a_*, \\ ma^2/a_* & a < a_*, \end{cases} \quad v(r) = \begin{cases} (GM(r)/r)^{1/2} & \text{Newton,} \\ (GM(r)a_*)^{1/4} & \text{MOND,} \end{cases} \quad (1.28)$$

where $M(r)$ is the baryonic mass inside a sphere of radius r . The empirical relation $M(r) \propto v^4$ is known as Tully-Fisher relation. The MOND idea faces the following difficulties:

1. Some globular clusters seems to behave differently from MOND predictions [21].
2. The observation of the bullet cluster [8], discussed in section 1.2, shows that whatever is responsible for ‘dark matter’ is not tied to normal matter.
3. Evidence for Dark Matter comes not only from rotation curves of galaxies, but also from galaxy clusters and cosmology.

Trying to promote the empirical law to a theory, some possible field theories have been proposed, which employ appropriate extra fields. For example, assuming the bizarre non-relativistic Lagrangian density $|\vec{\nabla}\phi|^3 + \phi\rho$, where ρ is the mass density, a mass M sources an extra force proportional to \sqrt{M}/r , giving a $v(r)$ as in eq. (1.28). Such fields can behave as DM, making MOND a special property of DM, rather than an alternative to it, allowing to avoid the wrong predictions of MOND [22]. For example, MOND could be a manifestation of a superfluid state of DM. Alternatively, it has been proposed [23] that gravity is an emergent phenomenon related to entanglement entropy, and that this could explain Newtonian gravity together with a MOND-like modification below a critical acceleration comparable to the current acceleration of the Universe,

$$H_0 = 100h \text{ km/sec} \cdot \text{Mpc} = 9.7h \cdot 10^{-10} \text{ m/sec}^2 \quad (1.29)$$

which is comparable to a_* . It's not clear if this idea can reproduce relativistic gravity, the behavior of the bullet cluster, and the observed features in CMB anisotropies. The numerical coincidence of a_* with the acceleration indicated by the defunct Pioneer anomaly reminds us of the dangers of numerology.

In conclusion, the flatness of most galactic rotation curves is presently considered by most (but not all) authors as an accidental consequence of how DM tends to cluster, with no deeper meaning.

Chapter 2

What is Dark Matter?

Despite decades of theoretical and experimental work the Dark Matter mass, M , is still largely unconstrained. The viable range spans more than 90 orders of magnitude,

$$10^{-21} \text{ eV} < M < 10^{35} \text{ kg}. \quad (2.1)$$

This range contains three main qualitatively different regions, illustrated in fig. 2.1. The DM behaves as a classical field if $M \lesssim \text{eV}$, is in the form of macroscopic objects for $M \gtrsim M_{\text{Pl}} = 1.2 \times 10^{19} \text{ GeV}$, and is a particle for intermediate values of M . The boundaries arise as follows.

If Einstein gravity holds up to the Planck scale, M_{Pl} , this is the ultimate frontier of particle physics¹. An elementary particle with mass $M > M_{\text{Pl}}$ would be a black hole, because its wavelength, $1/M$, would be smaller than its Schwarzschild radius, $2M/M_{\text{Pl}}^2$. Hence DM heavier than M_{Pl} can be viewed as a macroscopic object.

The boundary between fields and particles is reached in galaxies, where the observed DM density can be reproduced by particles lighter than about an eV only if many quanta occupy the same phase space volume. In this limit photons are more simply described by classical electromagnetism. Similarly, DM could be a massive boson that, in dense environments, is more simply described as a classical field. From a fundamental point of view both cases (particles and fields) are described by Quantum Field Theory. From a practical point of view, they are different enough to be studied separately.

These three general possibilities are described in the following:

1. Section 2.1 discusses DM as composite objects heavier than Planck scale; primordial black holes are one possible candidate.
2. Section 2.2 discusses the general properties of DM as ultra-light bosons.
3. By far the most studied possibility is that DM is made of particles. They must have the properties presented in page 5. They might have been produced according to one of the mechanisms discussed in chapter 3. They are searched for with the strategies discussed in chapters 5, 7, 6.

¹ Experimentally, however, we do not know that Einstein gravity is not modified at energy scales larger than about an eV.

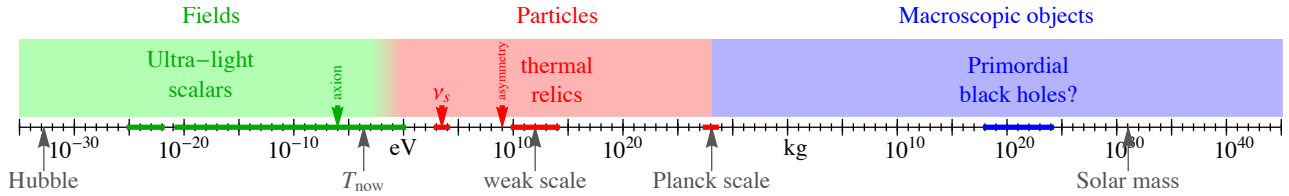


Figure 2.1: Possible range for the DM mass, and some notable candidates.

2.1 DM as very massive objects

DM could be made of MAssive Compact Halo Objects (MACHOs²), i.e., ordinary astrophysical objects of macroscopic mass M , such as large planets, small dead stars or stray black holes. These objects do not emit light and therefore fulfill the definition of dark matter. If they are baryonic *and* if they have been created in the late Universe like the rest of the astrophysical objects, which would be the most natural expectation, then the abundance required to explain the observed DM density would contradict the bounds from BBN and CMB that we will discuss in sec. 1.3. Still, it is interesting to consider their role as DM candidates, even if it is mainly for historical reasons.

One way of identifying the presence of MACHOs in the Milky Way halo is via gravitational microlensing. When a MACHO happens to cross the line of sight between the observer and a background star, the light of such a star is lensed and its flux towards the Earth temporarily increases (two related effects – creating a second image or modifying the apparent size of the star – are typically too small to be observable).

Since the time that MACHOs were first proposed in the '80s [24] a number of surveys, EROS-1 and -2, MACHO, OGLE-I, -II, -III, tried to detect lensing signals by monitoring for several years millions of stars in the Magellanic clouds, which are relatively nearby and known environments just outside of our Galaxy. More recently, similar analyses has been done with KEPLER data using local stars and with the SUBARU HSC camera using stars in our neighbour galaxy Andromeda. Despite the excitement generated by the MACHO collaboration, which initially reported that between 8% and 50% of the Milky Way halo could be made by massive objects with preferred mass of about half a M_\odot , most surveys only found upper limits on f , the fraction of halo dark mass consisting of massive objects.³ Combining the results of different campaigns one finds,

$$f \lesssim 5\% \quad \text{for} \quad 10^{-13} M_\odot \lesssim M \lesssim 10 M_\odot \\ (\text{exclusion by EROS, OGLE, MACHO, KEPLER, SUBARU HSC}). \quad (2.2)$$

(We recall that $M_\odot = 1.9984 \times 10^{30}$ kg is the mass of the Sun). The detailed bounds are reported in fig. 2.2 (left). They hold under standard assumptions for the density and the distribution of the lensing objects, but could be weakened if, for instance, MACHOs are clustered (as this reduces the relative probability of their crossing a line of sight) or if their velocity dispersion is small. Such effects are however typically not sufficient to lift the bounds significantly (see Green in [24]). Other surveys, some still ongoing, include MOA, OGLE-4 and SUPER-MACHO [24].

²The name was coined, in witty opposition to WIMPs, in the early '90s (see K. Griest (1991) in [24]).

³An implicit assumption is that the fraction f is the same in the whole Universe.

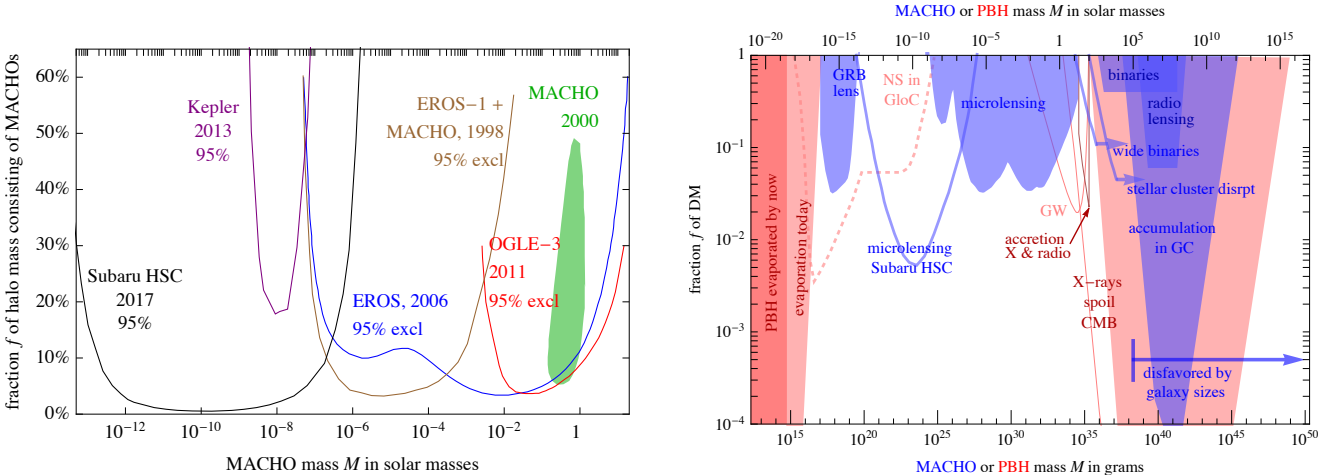


Figure 2.2: **MACHO searches.** **Left:** Results of microlensing surveys (mostly towards the Magellanic Clouds): the bounds on the fraction f of the Milky Way halo’s mass which can be due to MACHOs, as a function of the object’s mass M , together with the region identified by the MACHO collaboration in 2000. **Right:** A collection of bounds on the fraction f of DM consisting of massive astrophysical objects. The blue bounds apply to any MACHO, including Primordial Black Holes (PBH). The red bounds only to PBHs. The most recent or the most debated bounds are shown as dashed lines or as open (unshaded) contours.

Besides bounds from microlensing, there are also other constraints [24], a selection of which is illustrated in fig. 2.2 (right). The non-observation of lensing effects towards gamma ray bursts (GRBs) disfavors the range of masses $5 \times 10^{-17} - 2.5 \times 10^{-14} M_{\odot}$. The absence of lensing towards compact radio sources excludes the portion of the parameter space between $10^6 - 10^8 M_{\odot}$. Requiring that the binary star systems observed in the Galaxy are not disrupted by encounters with MACHOs rules out a portion around $10^3 - 10^8 M_{\odot}$. The constraint extends to $10^{10} M_{\odot}$ (not shown in fig. 2.2), if the survival of globular clusters is taken into consideration as well. Recent results on wide halo binaries even lower the bound to $10 M_{\odot}$. In a similar spirit, requiring that the stellar clusters observed at the center of ultra-faint dwarf galaxies, in particular Eridanus II, are not disrupted by the passage of MACHOs can impose a bound that, in its most conservative version, rules out a portion above $100 M_{\odot}$. Imposing that the amount of MACHOs being dragged (along with the stars) by dynamical friction into the galactic center region does not exceed the observed mass of the GC region itself, disfavors the large portion around $2 \times 10^4 - 10^{12} M_{\odot}$. Note that this constraint is sensitive to the detailed galactic dynamics. For instance, an in-falling MACHO could kick stars or other MACHOs out of the GC via gravitational slingshot effects, reducing the accumulation rate. Another bound excluding MACHOs with masses $10^4 - 10^{10} M_{\odot}$ (not shown in fig. 2.2) comes from requiring that DM behaves like a fluid, and not as a collection of discrete massive objects, in the formation of Large Scale Structures. Finally, we should mention that the whole large mass portion of the range in fig. 2.2 (right) is highly disfavored by the simple consideration that a single DM ‘particle’ cannot be heavier than the smallest of the objects which it is supposed to inhabit: the sizes of dwarf galaxies such as Segue 1 ($\sim 5 \times 10^5 M_{\odot}$) or even of the Milky Way ($\sim 5 \times 10^{11} M_{\odot}$) arguably impose robust upper bounds, unless one is willing to allow taylor-made MACHOs for each galaxy... More stringent bounds could be derived by imposing that a sizable number of DM ‘particles’ must constitute the halos of these objects (to

avoid granularities) or by detailed modelling of even smaller bodies (e.g. globular clusters).

In summary, the various observational and dynamical bounds only leave open the region at small masses ($M \lesssim 2 \times 10^{-15} M_\odot$). Before the 2017 lensing bounds from SUBARU HSC, the window $5 \times 10^{-13} M_\odot \rightarrow 2 \times 10^{-9} M_\odot$) was open too. In addition, if the wide binaries and the Eridanus II bounds are neglected, the region around 10 to 1000 M_\odot is viable too. This latter region as attracted particular attention in the wake of the detection of gravitational waves by LIGO, as we mention in the following subsection. However, let us recall: all the discussion above is subject to the fact that BBN and CMB constraints actually contradict the existence of baryonic bodies of astrophysical nature, of any mass, as an explanation for DM abundance.

2.1.1 Primordial black holes

Astrophysical objects that consist of baryonic matter but have been created *before* BBN are not subject to the cosmological constraints of sec. 1.3, since the material of which they are made is subtracted very early on from the baryonic budget. This is the case of *primordial* black holes (PBHs) [25].

The formation of PBHs is not predicted by standard cosmology. One has to invoke exotic ingredients such as very large primordial density fluctuations in multi-stage inflation scenarios; some sort of specific phase transition; a collapse of peculiar objects like cosmic strings or cosmic walls, etc [25]. For instance, inflationary models could produce $\gamma(1)$ inhomogeneities that exit the horizon N e -folds before the end of inflation; when the length scale of the inhomogeneity re-enters the horizon, the matter within it collapses into a PBH of mass $M \sim M_{\text{Pl}}^2 e^{2N}/H$ (with H the Hubble constant). Alternatively, a first-order phase transition at temperature T could generate BH with mass again given by the mass contained by the horizon, $M \sim \rho/H^3 \sim M_{\text{Pl}}^3/T^2 \sim M_\odot(\Lambda_{\text{QCD}}/T)^2$ where $\rho \sim T^4$ during radiation domination, $H \sim \rho^{1/2}/M_{\text{Pl}}$ and $\Lambda_{\text{QCD}} \approx 0.3$ GeV is the QCD scale. This in particular illustrates that a large range of masses is possible. At one extremum, PBHs created at the Planck temperature would have a Planck mass $M \sim M_{\text{Pl}} \sim 10^{-5}$ g. At the other extremum, PBH generated just before BBN ($T \sim$ MeV) would have a mass of comparable to the supermassive BHs at the center of current galaxies, $M \sim 10^5 M_\odot$.

Several phenomenological constraints apply to PBHs as candidates for DM, shown in fig. 2.2 (right). First of all, the bounds already discussed in section 2.1 also apply to PBHs. In addition, one has to impose that PBHs have not evaporated by now. Indeed, quantum fluctuations of fields around any black hole imply that it emits ‘Hawking radiation’, a thermal spectrum of particles at a temperature $T_{\text{BH}} = (8\pi G_N M)^{-1}$. The total radiated power is $P = (15360 \pi G_N^2 M^2)^{-1}$, and thus the BH loses mass at the same rate. As a consequence, a black hole evaporates after a life-time of $\tau_{\text{BH}} = 5120 \pi G_N^2 M^3$. Imposing that the PBH’s life-time is longer than the age of the Universe implies $M \gtrsim 10^{-19} M_\odot$ (a detailed computation gives $M > 2.5 \cdot 10^{-19} M_\odot$).⁴ PBHs with a mass slightly above the latter value would be in the process of evaporating at the present time, emitting particles with a temperature of around 80 MeV. The non observation of such Hawking radiation, e.g., in the extragalactic γ -ray flux, imposes $M \gtrsim 6 \cdot 10^{-17} M_\odot$ (or, rather, the evaporating PBHs must have a very small abundance, $\Omega \lesssim 10^{-9}$, which for our purposes is the same constraint).

Constraints based on the survival rates of neutron stars (NS) in Globular Clusters (GloC) affect the mass range $10^{-18} \rightarrow 10^{-9} M_\odot$. PBHs could sink to the interior of such stars, either

⁴A possible loophole to this argument occurs if PBHs evaporate leaving behind stable Planck-mass relics. These relics could constitute the DM [25].

during the formation of the star or by subsequent capture, and quickly destroy them by eating them from the inside. The mere observation of existing neutron stars thus imposes the constraint. However, such bounds rely on the assumption of a very large density of DM in Globular Clusters (of the order of 10^3 GeV/cm 3 and higher), which is far from certain. For this reason the bound is indicated as an open dashed contour in fig. 2.2 (right).

Finally, PBHs, like any other BH, would be accreting material. This could explain why some denser structures are heavily dominated by DM [26]. However, the infalling gas would emit X-rays, which would ionize matter, affecting the spectrum and the anisotropies of the CMB. This rules out a very large portion of the parameter space around $10^2 - 10^{12} M_\odot$.⁵ By refining the accretion model, Poulin et al. (2017) [25] move the exclusion line to the left by about 2 orders of magnitude. On the other hand, the same X-rays (and radio) emission from accretion should be visible if PBHs are present in our Galaxy. Its non-observation allowed Gaggero et al. (2017) [25] to impose a bound in the mass window $10 - 100 M_\odot$. It should be added, however, that all these bounds are subject to the uncertainties related to the modelling of the accretion process, which is a whole unsettled problem by itself in astrophysics, especially in these conditions of BH masses, gas densities and relative speeds.

The $10 - 100 M_\odot$ mass interval is, by the way, a range which has attracted a lot of attention recently: the LIGO events in gravitational waves [27] have been advocated by some groups to be due to mergings of PBHs with such mass. For this to be viable, however, the bounds from accretion, wide binaries and possibly CMB distortions and stellar cluster disruptions in Eridanus II have to be dismissed. Carr et al. (2017) and Ali-Haïmoud et al. (2017) [25] have, on the other hand, used the same LIGO observations to impose exclusion bounds, denoted with GW in fig. 2.2 (right).

All in all, taking into account the recent stringent constraints in different ranges of mass, PBHs can not constitute the whole of Dark Matter for any mass (with the possible exception of a very narrow window around $M \approx 10^{-16} M_\odot$). Some of the constraints are however still under discussion, as we mentioned above, so that the situation could change.

It should also be stressed that the above discussions refer to the case in which all the PBHs have a unique mass. In the more general (and probably more realistic) case in which they are distributed according to an extended mass function, each mass could in principle lie below the various constraints and they could sum up to the needed total amount. The analysis is actually complex as constraints need to be re-evaluated. Current results seem to indicate that PBHs might still account for the whole of DM in some windows [25]. For instance, in the suggestion that creation of PBHs explaining DM could be due to the Standard Model Higgs vacuum instability [28], the PBHs have masses that span about an order of magnitude, $10^{-17} - 10^{-16}$ solar masses, and presently seem not to be excluded.

Future prospects to further explore the PBH parameter space include for instance detecting the seismic oscillations that a PBH would produce when piercing the body of the Sun or another star, or sensing their motion in the Galaxy via pulsar timing arrays [25].

2.2 Very light Dark Matter

⁵Note that the early computation in Ricotti et al. (2007) [25], which had found more constraining bounds down to $10^{-1} M_\odot$, has recently been revisited and relaxed.

What is the smallest possible mass for DM? Cosmological observations tell us that Dark Matter is cold. If DM is thermalized, this places a bound $M \gtrsim \text{KeV}$. However, if DM is not thermalized (requiring DM with small enough interactions), then DM can be much lighter. To be viable one also needs a special cosmological production mechanism that produces DM particles ‘at rest’. A reasonable mechanism known as “initial misalignement” applies to axions, for instance.

In this case the smallest possible DM mass M is limited by quantum mechanics: the de Broglie wave-length $\lambda = 2\pi/Mv$ of DM cannot be “too large”. What “too large” means depends on whether the particle is a boson ϕ or a fermion ψ .

2.2.1 Fermionic DM

Gunn and Tremaine derived the bound on mass of the fermionic DM using the Pauli exclusion principle [29]. For concreteness we consider the Milky Way, where the local DM density is $\rho \approx 0.3 \text{ GeV/cm}^3 = (0.04 \text{ eV})^4$ and the galactic escape velocity $v_{\text{esc}} \approx 10^{-3}$. DM has a de Broglie wave-length $\lambda = 2\pi/Mv$, and v must be smaller than the escape velocity. The requirement that the DM quantum occupation number is smaller than one, implies that the maximal DM density is $\rho \lesssim M/\lambda^3$, which in turn gives $M \gtrsim 1 \text{ keV}$. A detailed study of dwarf spheroidal galaxies finds a bound $M > 0.1 \text{ keV}$ [30]. This bound is robust and independent from the model of DM formation and DM decoupling.

2.2.2 Bosonic DM

The Gunn-Tremaine bound does not apply to bosonic DM. The mass of DM is in this case bound by the requirement that its de Broglie wave-length

$$\lambda = \frac{2\pi}{Mv} = 2 \text{ kpc} \frac{10^{-21} \text{ eV}}{M} \frac{3 \cdot 10^{-5}}{v}, \quad (2.3)$$

is smaller than a small galaxy, which has a size of about 2 kpc and contains DM with a velocity of about 10 km/s.

Chapter 3

When was Dark Matter produced?

In this section we summarize the main cosmological production mechanisms that can reproduce the observed DM abundance ¹.

Section 3.1 discusses DM as a thermal relic (freeze-out). This is often considered as the most plausible mechanism and is certainly the one that has been most popular in the community in the past decades. As we will elaborate below, its appeal is essentially due to two facts: i) it is rather natural (just throw a feebly interacting particle in the primordial thermal bath and watch it come out with the correct abundance) and ii) it fits well in a number of particle physics theories beyond the Standard Model (BSM) that predict DM (such as SuperSymmetry or ExtraDimensions). If the latter point is arguably losing attractiveness (since the mentioned BSM physics does not show up yet in searches), the former still stays. Section 3.2 discusses Asymmetric DM. The attractiveness of this mechanism is that it parallels the supposed production mechanism of ordinary matter, i.e. baryogenesis, thereby potentially providing a natural reason for why the dark and ordinary matter abundances are comparable. On the other hand, no full baryogenesis theory is known yet. Section 3.3 discusses the freeze-in mechanism and some of its variants. This mechanism is somewhat opposite to freeze-out, as we discuss below, but also provides a natural paradigm to explain the abundance of DM in terms of its measurable particle physics properties.

It is important to stress that all the production mechanisms require the DM to have some kind of interactions with ordinary matter and/or with itself, other than gravitational. The size of these interactions is small enough that it does not contradict the ‘non-interacting’ requirement discussed in page 5. Still, as we already mentioned above, the existence of these interactions is not implied in any way by the cosmological and astrophysical evidences discussed in chapter 1.

Before presenting the various possible mechanism it is useful to introduce a quantity that expresses the DM density in a form which will be useful for cosmological computations. Indeed, the number density $n_{\text{DM}} = \rho_{\text{DM}}/M$ has the ‘drawback’ of depending on the unknown DM mass M and of evolving significantly during cosmological history, as function of either time t or temperature T . Ratios such as n_{DM}/n_{γ} would be more constant, but photons have their own cosmological history, being periodically heated by annihilations of charged particles that become non-relativistic. A more useful quantity to measure the cosmological DM abundance in this context is

$$Y_{\text{DM}}(T) \equiv \frac{n_{\text{DM}}(T)}{s(T)} \tag{3.1}$$

¹In this Chapter we always assume DM to be a particle. The production of primordial black hole DM is briefly discussed in sec. 2.1.1.

where $s = 2\pi^2 g_s(T)T^3/45$ is the total entropy density (see Appendix A). The total entropy in a comoving volume V , $S = sV$, is conserved during cosmological evolution as long as thermal equilibrium holds. The quantity $Y_{\text{DM}}(T)$ is useful because it stays constant during most of the cosmological history, whenever the number of DM particles per comoving volume is conserved: at later times when DM is decoupled, and at early times when DM possibly was in thermal equilibrium.

It is therefore useful to match cosmological computations of the DM density to $Y_{\text{DM}0} = Y_{\text{DM}}(T_0)$, the present value of Y_{DM} , which is linked to the DM mass density Ω_{DM} as

$$\Omega_{\text{DM}} = \frac{\rho_{\text{DM}}}{\rho_{\text{cr}}} = \frac{s_0 Y_{\text{DM}0} M}{3H_0^2/8\pi G} = \frac{688\pi^3 T_0^3 Y_{\text{DM}0} M}{1485 M_{\text{Pl}}^2 H_0^2}. \quad (3.2)$$

3.1 Freeze-out: DM as a thermal relic

The basic idea of the freeze-out mechanism is simple. DM was initially a component of the thermal bath but eventually decoupled: the current abundance is a left-over (a ‘relic’) of an incomplete (‘frozen’) annihilation process.

In sec. 3.1.1 we sketch the history of the process and provide an estimate of the resulting abundance. In sec. 3.1.2 we introduce the tool for the precise computation and derive its (approximate) analytic solution.

3.1.1 Simple estimate of the thermal relic abundance

We assume that DM is a stable particle with mass M , that in the Early Universe is in thermal equilibrium with the thermal bath of SM particles at temperature T . For DM we do not assume any special properties, such as conserved quantum numbers. When the temperature of the Universe drops below the DM mass, M , the annihilation processes with total cross section σ , such as

$$\text{DM DM} \leftrightarrow \text{SM SM}, \quad \text{where SM is any SM particle,} \quad (3.3)$$

try to maintain the thermal equilibrium such that the DM number density gets Boltzmann-suppressed,

$$n_{\text{DM}} \propto e^{-M/T}. \quad (3.4)$$

At some point the DM density becomes so small that the DM DM annihilation rate Γ is slower than the expansion rate H and the thermal equilibrium can no longer be maintained. At this point DM stops annihilating and its abundance “freezes out”. This happens when

$$\Gamma \sim n_{\text{DM}} \langle \sigma v \rangle \lesssim H = \sqrt{\frac{8\pi^3}{90} g_\rho} T^2 / M_{\text{Pl}}. \quad (3.5)$$

In the last passage we have used the Friedmann equation (A.3) to express H in terms of the energy density, which we have expressed with eq. (A.21) since the process happens in radiation domination. Using the above relation the out-of-equilibrium DM relic abundance is conveniently estimated by using the quantity Y introduced above, i.e. in units of the entropy density s , as

$$Y_{\text{DM}} \equiv \frac{n_{\text{DM}}}{s} \simeq \frac{\sqrt{\frac{8\pi^3}{90} g_\rho} T^2 / M_{\text{Pl}} \langle \sigma v \rangle}{\frac{2\pi^2}{45} g_s} \simeq 0.4 \frac{1}{M_{\text{Pl}} \langle \sigma v \rangle T_{\text{fo}}}. \quad (3.6)$$

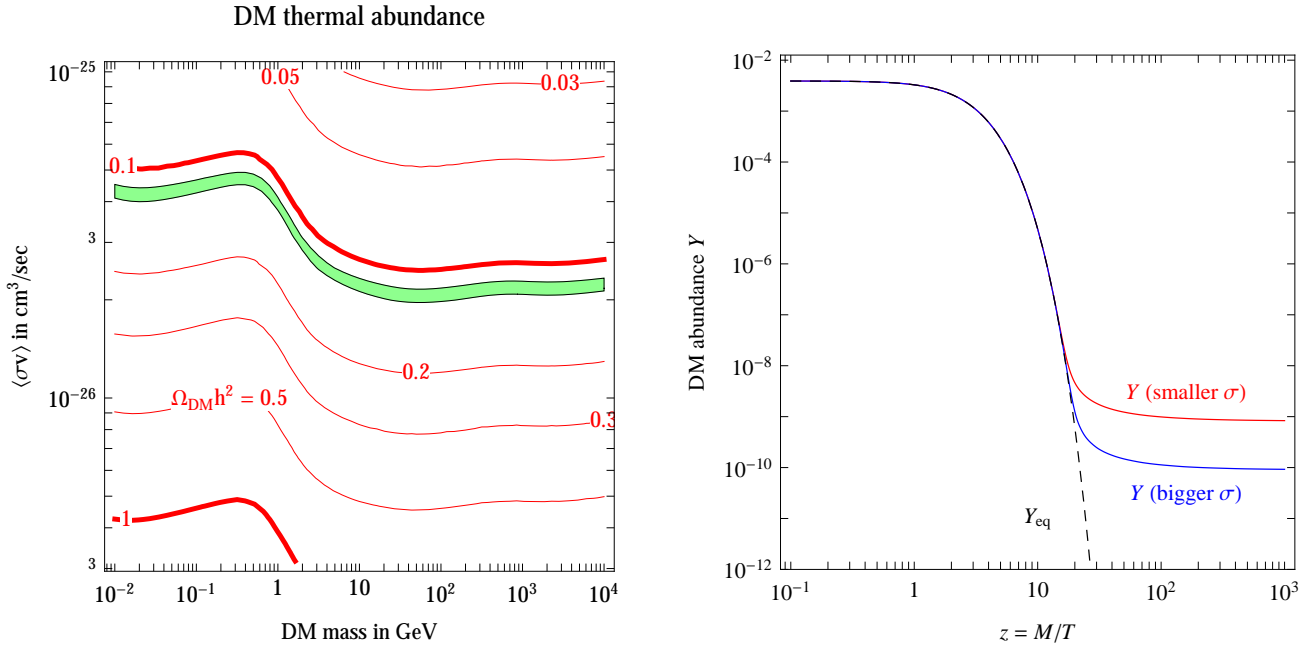


Figure 3.1: **Left:** *DM freeze-out abundance $\Omega_{\text{DM}}h^2$ as function of the DM mass and of the DM annihilation cross section $\langle\sigma v\rangle$ for Majorana DM. The measured cosmological DM abundance is reproduced within the green band at 3 standard deviations.* **Right:** *Sample of the evolution of the DM abundance $Y = n/s$ as function of $z = T/M$.*

In the last passage, apart from plugging in the numbers and using the fact that $g_\rho \simeq g_s \simeq \mathcal{O}(100)$ at high temperatures (see Appendix A), we have made explicit that the relation holds at the temperature of freeze-out. One could now show (e.g. by solving the actual equation, see below) that $T_{\text{fo}} \approx M/20$: we are going to use this in eq. (3.6) without questioning. Next, since the Y quantity does not evolve after annihilations have stopped (as discussed above), we realize that eq. (3.6) also corresponds to $Y_{\text{DM}0}$. Therefore, using eq. (3.2) and inserting all the numerical constants, we arrive at the final result

$$\Omega_{\text{DM}}h^2 \approx 0.11 \frac{\sigma v_{\text{cosmo}}}{\langle\sigma v\rangle_{T \approx M/20}}, \quad (3.7)$$

where

$$\sigma v_{\text{cosmo}} \approx 3 \times 10^{-26} \text{ cm}^3/\text{sec} \approx 1 \text{ pb}. \quad (3.8)$$

Notice the inverse dependence on the annihilation cross section σ . As a result, if there are several stable particles, the relic density of the universe will be dominated by the one with the smallest annihilation cross section – the weakest particle wins.

The precise numerical result for the special value σv_{cosmo} , needed to reproduce the cosmological DM abundance, is plotted in fig. 3.1.

3.1.2 Precise computation of the thermal relic abundance

The standard tool to perform this kind of cosmological computation is the classical Boltzmann equation. It describes the evolution of the DM number density, $dn_i(t, \vec{x}, \vec{p})/d^3x d^3p$ where i denotes DM polarizations, internal degrees of freedom, etc. In early cosmology inhomogeneities are at the 10^{-5} level, and one can neglect them. Furthermore, scatterings that maintain kinetic equilibrium are fast enough that one can assume a Fermi-Dirac or Bose-Einstein distribution in \vec{p} (both reduce to the Maxwell distribution in the relevant non-relativistic limit) and write a single equation for the total DM number density $n(t)$, summed over all DM polarizations, internal degrees of freedom, etc. This equation has the intuitive form

$$\frac{1}{a^3} \frac{d(na^3)}{dt} = \frac{dn}{dt} + 3Hn = \langle \sigma v \rangle (n_{\text{eq}}^2 - n^2) \quad (3.9)$$

where $a(t)$ is the universe scale factor, $H = \dot{a}/a$ is the Hubble rate; n_{eq} is the number density that DM would have had in thermal equilibrium; $\langle \sigma v \rangle$ is the thermal average of the total annihilation cross section times the relative velocity v between annihilating DM particles. The two terms describe DM depletion due to annihilations (proportional to n^2) and DM creation via inverse annihilations (proportional to n_{eq}^2). For large enough $\langle \sigma v \rangle$ the DM abundance stays in thermal equilibrium, $n = n_{\text{eq}}$, until DM becomes non-relativistic, such that $n_{\text{eq}} = g_{\text{DM}}(MT/2\pi)^{3/2}e^{-M/T}$ becomes exponentially suppressed. Here g_{DM} is the number of degrees of freedom of the DM particle.

For numerical or semi-analytical solutions, it is convenient to a) study the evolution of DM abundance as a function of a dimensionless parameter $z \equiv M/T$, which is $\mathcal{O}(1)$ during freeze out, and that grows with time; b) factor out the overall expansion of the Universe by writing equations for $Y = n/s$, as discussed above. In terms of these two variables, the Boltzmann equation becomes

$$sHZz \frac{dY}{dz} = -2\gamma_{\text{ann}} \left(\frac{Y^2}{Y_{\text{eq}}^2} - 1 \right), \quad (3.10)$$

where the factor $Z = 1/(1 + \frac{1}{3} \frac{d \ln g_{*s}}{d \ln T})$ can often be approximated as 1, and γ_{ann} is the space-time density of annihilations in thermal equilibrium, summed over initial state and final states and their polarisations. In the non-relativistic limit one has

$$2\gamma_{\text{ann}} \stackrel{T \ll M}{\simeq} n_{\text{eq}}^2 \langle \sigma v \rangle, \quad (3.11)$$

while the generally valid expression for it is more complex and out of our scope. The annihilation cross section can usually be expanded in powers of $v \ll 1$ as $\langle \sigma v \rangle = \sigma_0 + v^2 \sigma_1$, keeping only the s -wave term, σ_0 , and the usually sub-leading p -wave term, $v^2 \sigma_1$. Its thermal average is

$$\langle \sigma v \rangle = \sigma_0 + \frac{6T}{M} \sigma_1 + \dots \quad (3.12)$$

The Boltzmann equation for the total DM abundance then simplifies to

$$\frac{dY}{dz} = -f(z)(Y^2 - Y_{\text{eq}}^2), \quad f(z) \equiv \frac{s \langle \sigma v \rangle}{HZz} \stackrel{z=1}{\approx} \frac{\lambda}{z^2} \left(1 + \frac{6\sigma_1}{z\sigma_0} \right), \quad (3.13)$$

where $Y_{\text{eq}} = n_{\text{eq}}/s$ with n_{eq} defined in Appendix A. The dimension-less constant λ is

$$\lambda = \left. \frac{s \langle \sigma v \rangle}{H} \right|_{T=M} = M_{\text{Pl}} M \langle \sigma v \rangle \sqrt{\frac{\pi g_{\text{SM}}}{45}} \gg 1. \quad (3.14)$$

We have the following approximate solutions, plotted in fig. 3.1:

- Long before freeze-out, i.e., at early $z \ll z_f$, one can expand eq. (3.13) to the first order in small $Y - Y_{\text{eq}}$, finding

$$Y(z) \stackrel{z \ll z_f}{\simeq} Y_{\text{eq}} - \frac{Y'_{\text{eq}}}{2fY_{\text{eq}}} \approx Y_{\text{eq}} + \frac{z^2}{2\lambda}. \quad (3.15)$$

We can define z_f by imposing that the last two terms are equal, obtaining the equation

$$z_f = \ln \frac{2\lambda Y_{\text{eq}}(1)}{\sqrt{z_f}}, \quad (3.16)$$

which can be iteratively solved stating from $z_f \approx \ln \lambda Y_{\text{eq}}(1) \approx 1/25$.

- Long after freeze-out, i.e. at late $z \gg z_f \approx 25$, we can neglect the Y_{eq}^2 term in eq. (3.13) obtaining the integrable approximated equation $dY/dz = -fY^2$ with the solution

$$\frac{1}{Y_\infty} - \frac{1}{Y(z)} \stackrel{z \gg z_f}{\simeq} \int_\infty^z f(z) dz = \frac{\lambda}{z} \left(1 + \frac{3\sigma_1}{z\sigma_0} \right) \quad (3.17)$$

Since $Y(z_f) \gg Y_\infty$ we have the approximate solution

$$Y_\infty = \frac{z_f \sqrt{45/\pi g_{\text{SM}}}}{M_{\text{Pl}} M (\sigma_0 + 3\sigma_1/z_f)}. \quad (3.18)$$

If nothing more happens after freeze-out, Y_∞ can be identified with the present DM entropy density, $Y_{\text{DM}0}$. Then, converting it into DM mass density using eq. (3.2) we obtain the precise version of the result announced in eq. (3.7)

$$\frac{\Omega_{\text{DM}} h^2}{0.110} = \frac{Y_\infty M}{0.40 \text{ eV}} = \frac{z_f}{25} \frac{2.18 \cdot 10^{-26} \text{ cm}^3/\text{sec}}{\sigma_0 + 3\sigma_1/z_f}. \quad (3.19)$$

3.2 Asymmetric DM (darkogenesis)

The ordinary (baryonic) matter does not have its origin in a freeze-out process, but rather in the existence of very small primordial asymmetry that the Universe happens to have. Explaining how and why this asymmetry was created is the task of the theory of baryogenesis (and/or leptogenesis). Different versions, working at different epochs, exist.

The same mechanism may be behind the relic abundance of DM: an initial small asymmetry (e.g. a small overabundance of the number of DM particles versus antiparticles, to fix the ideas) would translate into a relic population of particles. In which case we could talk about ‘darkogenesis’ [32]. This could explain the observed proximity of the DM density with the matter density, $\Omega_{\text{DM}} \simeq 5.4\Omega_m$, which may or may not be a coincidence. Or it can be interpreted as an indication that both DM and matter have a common cosmological origin.

The overall picture is simple: if there is an asymmetry in the dark sector, as soon as annihilations have wiped out the density of (say) antiparticles, the number density of particles remains frozen for lack of targets, and is entirely controlled by the primordial asymmetry rather than by the value of the annihilation cross section. Indeed, the relic abundance is just given by

$$\Omega_{\text{DM}} h^2 = \frac{M n_{\text{DM}}}{\rho_{\text{crit}}} h^2 \simeq 0.1186 \frac{M}{5 \text{ GeV}} \frac{\eta_{\text{DM}}}{6 \cdot 10^{-10}}, \quad (3.20)$$

where $\eta_{\text{DM}} \equiv n_{\text{DM}}/n_\gamma$ in exact analogy with the baryon to photon ratio η defined in sec. 1.3.3. The equation is cast in a form that suggests the obvious following conclusion. If $\eta_{\text{DM}} = \eta$, e.g. because the dark and the visible sector share the production mechanism, then the correct relic abundance is obtained for a DM mass $M \simeq 5$ GeV. In other words, the simplest realization of this scenario provides a prediction for the DM mass.

3.3 Freeze-in

The basic idea of the freeze-in mechanism [33] is somewhat opposite to the one of freeze-out. In this case, one assumes that the DM particle is absent in the thermal bath of the Early Universe (zero initial abundance). The particle, however, is coupled to the SM particles by reactions like

$$\text{SM SM} \leftrightarrow \text{DM DM}, \quad \text{SM SM} \leftrightarrow \text{DM}, \quad \text{SM} \leftrightarrow \text{DM DM}. \quad (3.21)$$

The coupling λ entering these reactions is assumed to be extremely feeble (typically $\lambda \lesssim 10^{-13}$, as we will see later), so that DM is slowly but steadily produced. At some point, the production will stop and the DM abundance is ‘frozen-in’. This happens either because the temperature of the thermal bath drops below the DM mass M or because the temperature drops below the mass of the SM particle from which DM is produced (so that the SM particle’s abundance becomes Boltzmann suppressed), or both.

An estimate of the frozen-in abundance can be obtained as follows, assuming for definiteness that the third reaction (decay) in eq. (3.21) is dominant.

$$Y_{\text{DM}} = \frac{n_{\text{DM}}}{s} \sim \frac{\Gamma_{\text{SM} \rightarrow \text{DM DM}} t_H n_{\text{SM}}}{s} \sim \frac{\lambda^2 T \cdot (M_{\text{Pl}}/T^2) \cdot T^3}{T^3} \sim \frac{\lambda^2 M_{\text{Pl}}}{T}. \quad (3.22)$$

In the second passage we have expressed the number density of produced DM particles in a Hubble time as the rate Γ of the production reaction times the time $t_H \sim 1/H$ and the number of decaying SM particles. In the third passage we have expressed the rate in terms of the only relevant mass scale in the system (the temperature) and substituted the formulae for the other quantities in radiation domination. The chain of estimates shows therefore that the yield is maximal at low temperature. Since the production will stop as soon as $T \lesssim M$, we can plug this value in the estimate. Thus

$$Y_{\text{DM}} = \frac{\lambda^2 M_{\text{Pl}}}{M} \quad (3.23)$$

As usual, the quantity Y is translated into the present DM abundance thanks to eq. (3.2). Plugging in the numbers:

$$\Omega_{\text{DM}} h^2 = \frac{M Y_{\text{DM}0} s_0}{\rho_{\text{crit}}} h^2 = 3 \cdot 10^{+27} \lambda^2. \quad (3.24)$$

Chapter 4

Where is Dark Matter?

For interpreting direct and indirect DM detection experiments (discussed in chapters 5 and 7) we need to know what is the DM density and DM velocity distribution in the Milky Way and in other galaxies. Presently, only educated guesses for these are known, with significant uncertainties.

On the experimental side, observations of rotation curves do not give precise results, because it is difficult to take and interpret data, especially around the center of the Galaxy where DM is not the main component. On the theoretical side, gravity is attractive so there is no ground state. This means that ultimately the DM density distribution will tend to $\rho(\vec{x}) = M\delta^3(\vec{x})$, so that everything will accumulate in the center, at least in principle. However, in practice this process is slow because DM has slow dissipative interactions.

Quantitative properties of the DM halo, such as the local density in the solar system or the velocity distribution of DM, rely either on N -body simulations or on observations of the Milky way rotation curves or velocity field in our local neighbourhood. In the rest of the chapter we review these constraints.

4.1 Dark Matter density distribution

Tentative determinations of the DM density profile $\rho(r)$ proceed in two steps:

1. Guesses of the functional form of the spherical $\rho(r)$ in terms of a minimal number of free parameters, as discussed in section 4.1.1.
2. Determination of the free parameters in terms of safe observations of DM in our Galaxy, or in other galaxies, as discussed in section 4.1.2.

4.1.1 DM density functions

For the galactic distribution $\rho(r)$ we list the functional forms considered most plausible (see also fig. 4.1):

$$\begin{aligned}
 \text{NFW : } \rho_{\text{NFW}}(r) &= \rho_s \frac{r_s}{r} \left(1 + \frac{r}{r_s}\right)^{-2}, \\
 \text{Einasto : } \rho_{\text{Ein}}(r) &= \rho_s \exp \left\{ -\frac{2}{\alpha} \left[\left(\frac{r}{r_s}\right)^\alpha - 1 \right] \right\}, \\
 \text{Isothermal : } \rho_{\text{Iso}}(r) &= \frac{\rho_s}{1 + (r/r_s)^2}, \\
 \text{Burkert : } \rho_{\text{Bur}}(r) &= \frac{\rho_s}{(1 + r/r_s)(1 + (r/r_s)^2)}, \\
 \text{Moore : } \rho_{\text{Moo}}(r) &= \rho_s \left(\frac{r_s}{r}\right)^{1.16} \left(1 + \frac{r}{r_s}\right)^{-1.84}.
 \end{aligned} \tag{4.1}$$

All profiles assume spherical symmetry, with r the coordinate centered in the Galactic Center, while r_s , ρ_s and α are free parameters. These functions are motivated by the following considerations:

- The Navarro, Frenk and White (**NFW**) [34] profile peaks as r^{-1} close to the Galactic Center (GC). It is a common benchmark choice motivated by N -body simulations.
- The **Einasto** [35, 36] profile does not converge to a power law at the GC, and is somewhat wider than NFW on kpc scales. It is a better fit to more recent numerical simulations. The shape parameter α varies from simulation to simulation. We adopt $\alpha = 0.17$, representing a reasonable average over simulations.
- Cored profiles, such as the truncated **Isothermal** profile [37, 38] or the **Burkert** profile [39], are motivated by the observations of galactic rotation curves that may be pointing toward cored profiles. They do seem to be in conflict with the results of numerical simulations, though.
- Profiles steeper than NFW had been previously found by **Moore** and collaborators [40]. Such profiles, despite being less plausible, are often considered because they imply larger DM indirect signals from the center of the Galaxy.

In some of the considered profiles $\rho(r)$ diverges as $r \rightarrow 0$, but in all profiles $r^2\rho(r) \rightarrow 0$ such that the central region of the Galaxy contains a small amount of DM. Even so, since the DM indirect signal scales as $r^2\rho(r)^2$ this signal is peaked toward GC.

4.1.2 Determination of the Milky Way parameters

Next, we determine the parameters that govern the typical DM halo radius, r_s , and the typical density, ρ_s , both of which enter in the above parametrizations of the DM distribution, $\rho(r)$. We impose that the resulting profiles satisfy the following, from astrophysical observations relatively well determined, properties

- A) The density of DM at the location of the Sun is taken to be

$$\rho_\odot = \rho(r_\odot) = 0.3 \text{ GeV/cm}^3. \tag{4.2}$$

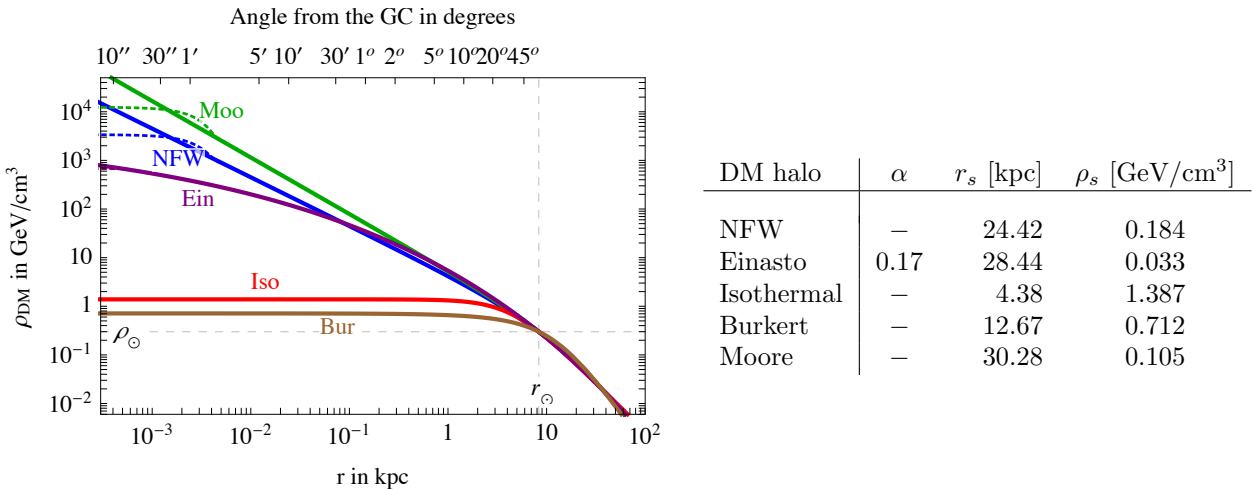


Figure 4.1: **DM profiles** (fig. left) and (table right) the corresponding parameters in the parametrizations of the profiles in eq. (4.1). The dashed lines show the smoothed functions adopted for some computations. In the table we provide r_s (ρ_s) to 2 (3) significant digits, a precision sufficient for most computations.

This is the canonical value routinely adopted in the literature, with a typical associated error bar of ± 0.1 GeV/cm³ and a possible spread up to $0.2 \rightarrow 0.8$ GeV/cm³ (sometimes referred to as ‘a factor of 2’). Recent determination found a higher central value and possibly smaller associated error, still subject to debate [41–44].

B) That the total DM mass contained in a 60 kpc radius centered around GC is

$$M_{60} \equiv 4.7 \times 10^{11} M_\odot. \quad (4.3)$$

(The distance of 60kpc is just a bit larger than the distance from GC to the Large Magellanic Cloud, which is 50 kpc). The value for M_{60} in (4.3) is based on the recent kinematical surveys of stars in SDSS [45]. We adopt the upper edge of their 95% C.L. interval to conservatively take into account that previous studies had found somewhat larger values (see, e.g., [46,47]).

Below we will also need the distance of the Sun from the Galactic Center, which is also somehow uncertain. We assume $r_\odot = 8.33$ kpc (see [48–50]), with an uncertainty of ± 0.2 kpc.

The parameters that we adopt for each of the $\rho(r)$ parametrizations are given in fig. 4.1, where we also plot the resulting profiles.

While the various density profiles give similar results above a few kiloparsecs, including around the location of the Earth, they do differ considerably — by orders of magnitudes — at smaller distances. Close to the GC there are no observational data on DM profile and the value of $\rho(r)$ is simply governed by the assumed asymptotic functional form as $r \rightarrow 0$. As a consequence, indirect DM signals from the inner Galaxy, such as gamma ray fluxes from regions a few degrees around the GC, will be highly sensitive to the choice of the DM profile. This is unlike DM signals that depend on the DM density around the Earth (e.g., direct detection), or DM signals that probe the local Galactic neighborhood (e.g., the fluxes of high energy positrons, produced at most a few kpc away from the Earth), or DM signals that probe regions distant from the GC (e.g., gamma rays from high latitudes).

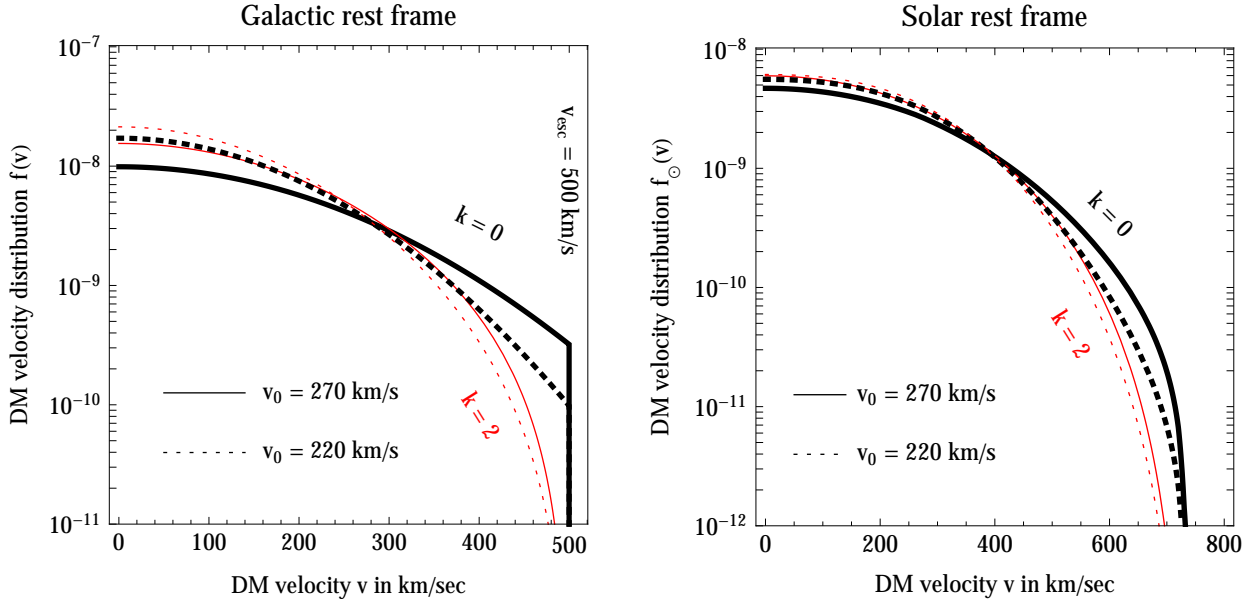


Figure 4.2: **DM velocity distributions:** the Maxwell-Boltzmann distribution with sharp cutoff at $v = v_{\text{esc}} = 500 \text{ km/s}$ (thick black curve), and the distribution motivated by N -body simulations, eq. (4.7), with a smooth cutoff computed for $k = 2$ (red). Two different values of v_0 are shown: 220 km/s (dotted) and 270 km/s (solid). The DM velocity distribution is plotted with respect to the galactic rest frame in the left picture and with respect to the solar rest frame in the right picture.

4.2 Dark Matter velocity distribution

The energy, E , of a DM particle changes with time because DM particles form a dynamical gravitationally bound system, where the gravitational potential, φ , changes with time, such that $dE/dt = \partial\varphi/\partial t$. This effectively amounts to DM particles undergoing many gravitational scatterings. As a consequence their final velocities are given by a sum of many random contributions. Due to the Central Limit Theorem their energy distribution will tend toward Gaussian.

However, the distribution will not be exactly Gaussian, since DM particles that happen to acquire a velocity larger than the galactic escape velocity, v_{esc} , tend to evaporate away. Consequently, the DM velocity distribution, $f(v)$, in the galactic rest frame is often assumed to be a Maxwell-Boltzmann (MB) distribution that is sharply cut off at a finite escape velocity,

$$f(v) = N \times e^{-v^2/v_0^2} \Theta(v_{\text{esc}} - v). \quad (4.4)$$

The normalization constant $N = 1/(\sqrt{\pi}v_0)^3 + \mathcal{O}(v_0^2/v_{\text{esc}}^2)$ is fixed such that $\int d^3v f(v) = 1$. Here v_0 is the root mean square velocity, and lies in the range,

$$220 \text{ km/s} < v_0 < 270 \text{ km/s}, \quad (4.5)$$

while the escape velocity from the Milky Way is [58],

$$450 \text{ km/s} < v_{\text{esc}} < 650 \text{ km/s}. \quad (4.6)$$

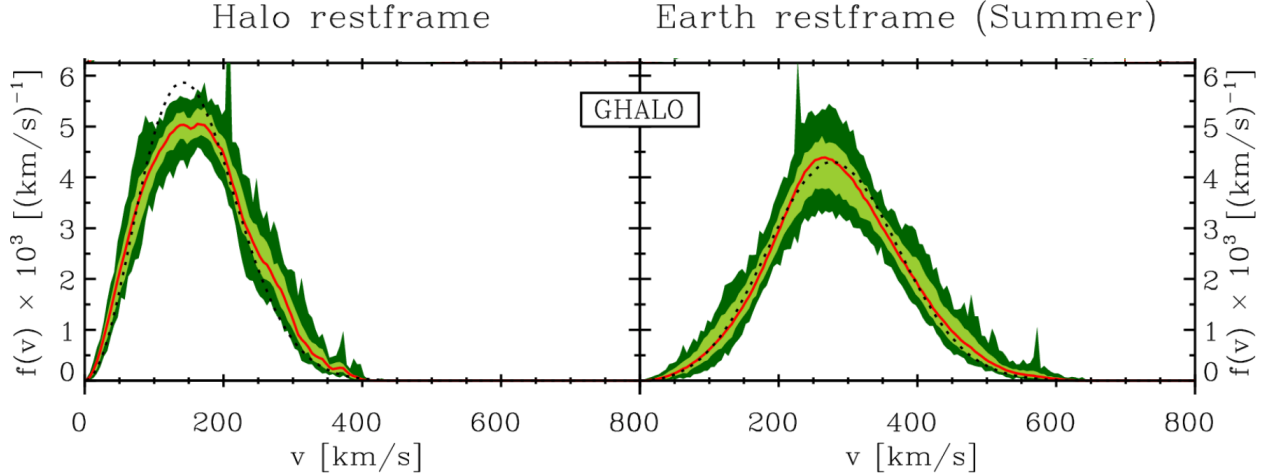


Figure 4.3: *DM velocity distributions in the galactic rest frame (left) and Earth's rest frame on June 2nd (right)* as obtained from GHALO N body simulation [56]. The solid red line is the average distribution, with the light (dark) green shaded regions giving the 68% scatter (envelope) over 100 sample spheres of 1kpc radius centered at 8.5kpc. The dotted line represents the best-fitting Maxwell-Boltzmann distribution (adapted from [57]).

The N -body simulations [51–54] suggest a smoother cut-off at $v < v_{\text{esc}}$, which can be parameterized as

$$f(v) = N_k \left[\exp \left(\frac{v_{\text{esc}}^2 - v^2}{kv_0^2} \right) - 1 \right]^k \Theta(v_{\text{esc}} - v), \quad (4.7)$$

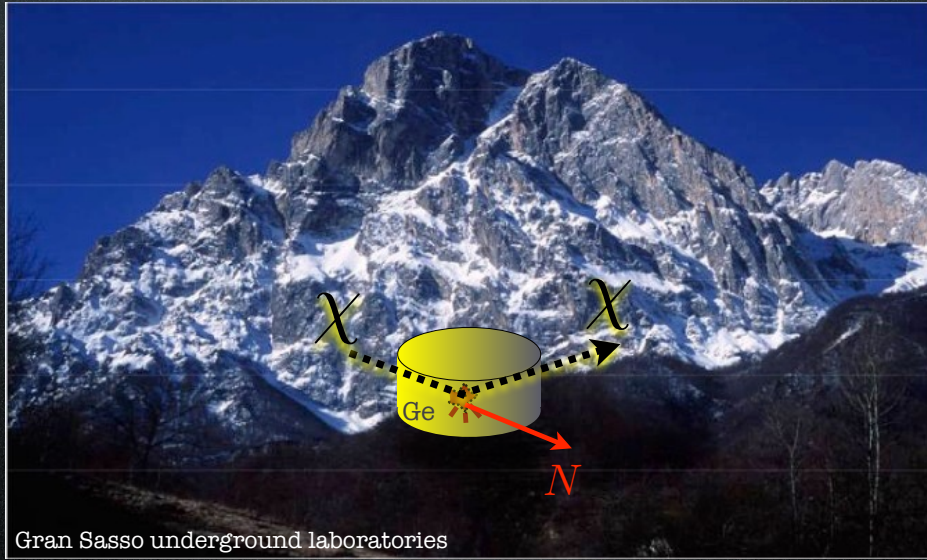
with $1.5 < k < 3.5$ [55]. The MB distribution (4.4) is obtained in the limit $k \rightarrow 0$. These velocity distributions are plotted in fig. 4.2a.

Chapter 5

Direct detection

This section is not ready yet. A great concise and pedagogical reference is [59]. The slides follow.

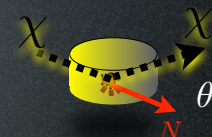
Direct Detection: basics



Direct Detection: basics

recoil energy $E_R = \frac{\mu_\chi^2 v^2}{m_N} (1 - \cos \theta)$

$$\mu_\chi = \frac{m_\chi m_N}{m_\chi + m_N} \rightarrow \begin{cases} m_\chi & \text{for small } m_\chi \\ m_N & \text{for large } m_\chi \end{cases}$$



recoil energy spectrum

$$\frac{dR}{dE_R} = \frac{1}{2} \frac{\rho_\odot}{m_\chi} \frac{\sigma}{\mu^2} \int_{v_{\min}(E_R)}^{v_{\text{esc}}} \frac{1}{v} f(\vec{v}) \, d\vec{v}$$

with $f(\vec{v}) \propto e^{-v^2/V_c^2}$ + motion of Earth
in (static?) halo

$$\sigma \approx \sigma_n^{\text{SI}} A^4 \times \text{nuclear form factors}$$

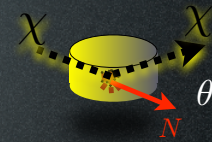
number of events

$$N = \mathcal{E} \mathcal{T} \int_{E_{\text{thres}}}^{E_{\text{max}}} \frac{dR}{dE_R} \, dE_R$$

Direct Detection: basics

recoil energy $E_R = \frac{\mu_\chi^2 v^2}{m_N} (1 - \cos \theta)$

$$\mu_\chi = \frac{m_\chi m_N}{m_\chi + m_N} \rightarrow \begin{cases} m_\chi & \text{for small } m_\chi \\ m_N & \text{for large } m_\chi \end{cases}$$



recoil energy spectrum

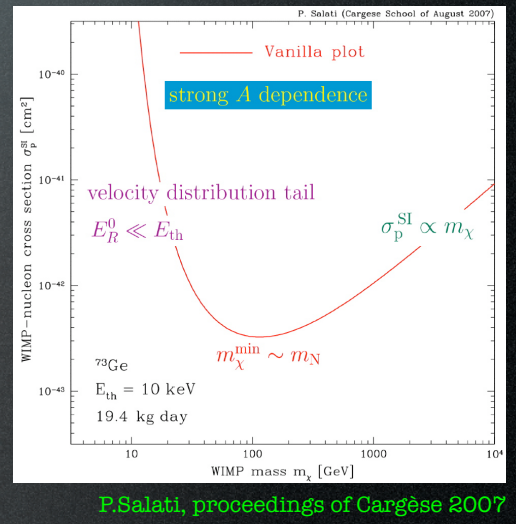
$$\frac{dR}{dE_R} = \frac{1}{2} \frac{\rho_\odot}{m_\chi} \frac{\sigma}{\mu^2} \int_{v_{\min}(E_R)}^{v_{\text{esc}}} \frac{1}{v} f(\vec{v}) \, dv$$

with $f(\vec{v}) \propto e^{-v^2/V_c^2}$ + motion of Earth in (static?) halo

$$\sigma \approx \sigma_n^{\text{SI}} A^4 \times \text{nuclear form factors}$$

number of events

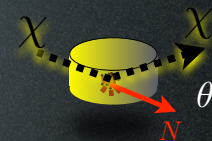
$$N = \mathcal{E} \mathcal{T} \int_{E_{\text{thres}}}^{E_{\max}} \frac{dR}{dE_R} \, dE_R$$



Direct Detection: basics

recoil energy $E_R = \frac{\mu_\chi^2 v^2}{m_N} (1 - \cos \theta)$

$$\mu_\chi = \frac{m_\chi m_N}{m_\chi + m_N} \rightarrow \begin{cases} m_\chi & \text{for small } m_\chi \\ m_N & \text{for large } m_\chi \end{cases}$$



recoil energy spectrum

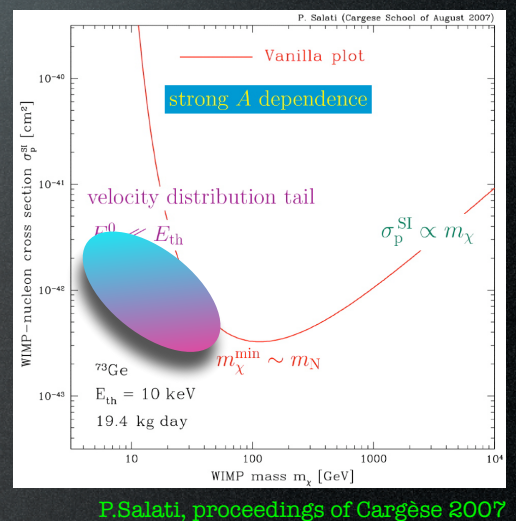
$$\frac{dR}{dE_R} = \frac{1}{2} \frac{\rho_\odot}{m_\chi} \frac{\sigma}{\mu^2} \int_{v_{\min}(E_R)}^{v_{\text{esc}}} \frac{1}{v} f(\vec{v}) \, dv$$

with $f(\vec{v}) \propto e^{-v^2/V_c^2}$ + motion of Earth in (static?) halo

$$\sigma \approx \sigma_n^{\text{SI}} A^4 \times \text{nuclear form factors}$$

number of events

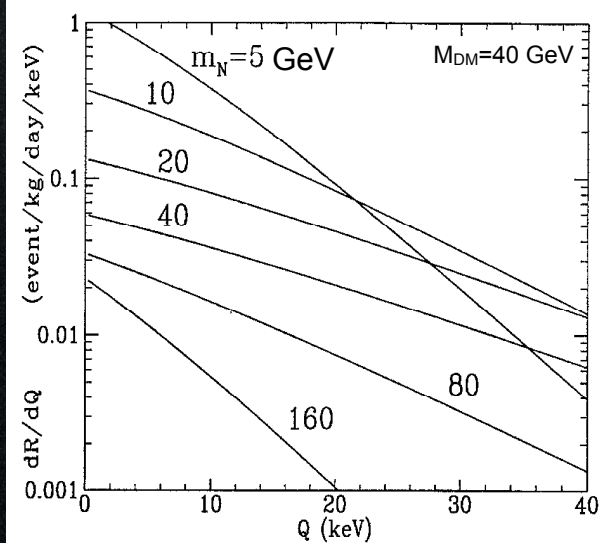
$$N = \mathcal{E} \mathcal{T} \int_{E_{\text{thres}}}^{E_{\max}} \frac{dR}{dE_R} \, dE_R$$



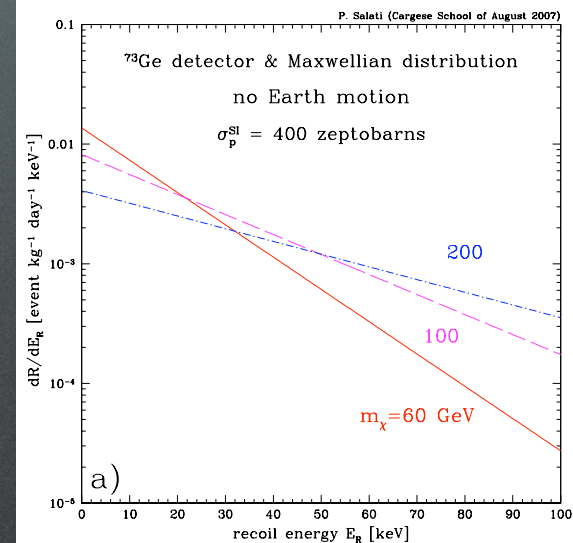
Direct Detection

Recoil spectra

fixed M_{DM}



fixed M_{nucl}



Direct Detection

Strategy #1: silence the Universe

Direct Detection

Strategy #1: silence the Universe

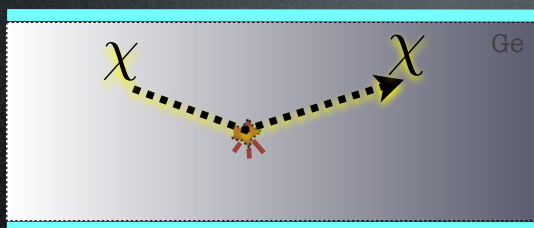
measure two quantities to discriminate Sign & Bkgd,
on event-by-event basis

Direct Detection

Strategy #1: silence the Universe

measure two quantities to discriminate Sign & Bkgd,
on event-by-event basis

E.g. Edelweiss:

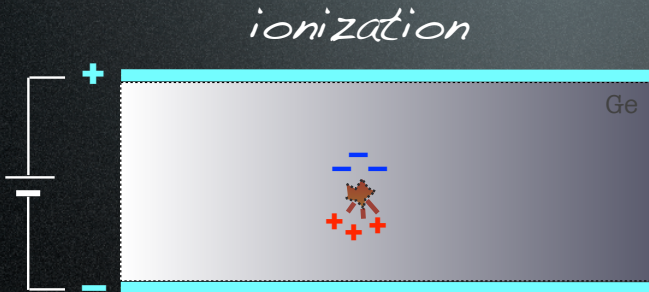


Direct Detection

Strategy #1: silence the Universe

measure two quantities to discriminate Sign & Bkgd,
on event-by-event basis

E.g. Edelweiss:

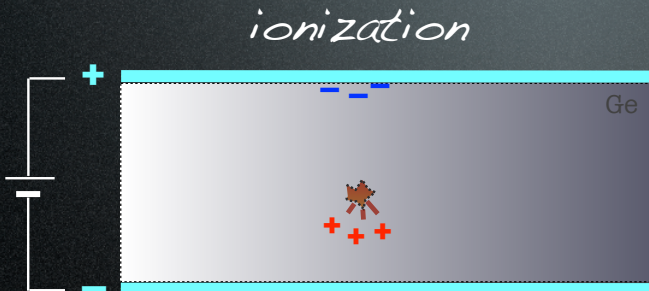


Direct Detection

Strategy #1: silence the Universe

measure two quantities to discriminate Sign & Bkgd,
on event-by-event basis

E.g. Edelweiss:

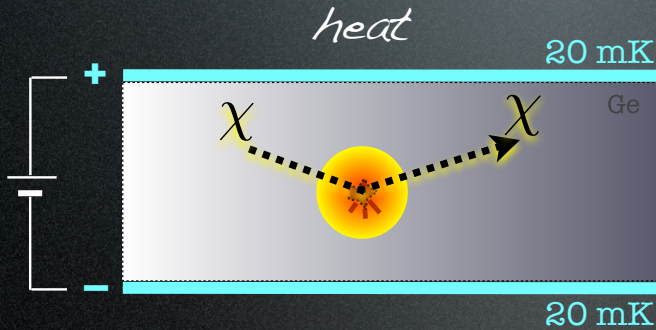


Direct Detection

Strategy #1: silence the Universe

measure two quantities to discriminate Sign & Bkgd,
on event-by-event basis

E.g. Edelweiss:

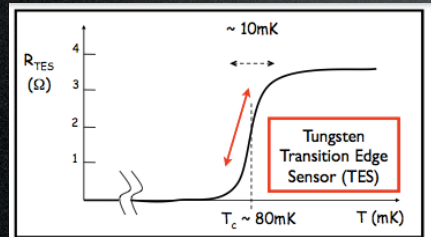
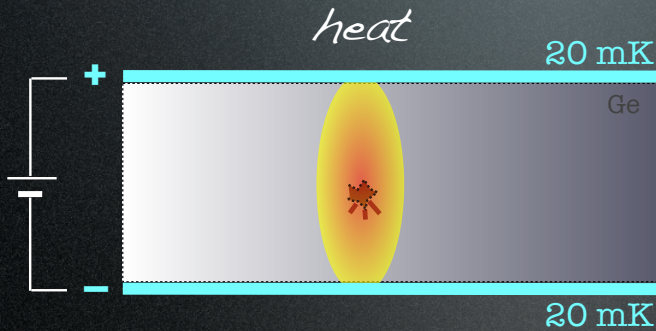


Direct Detection

Strategy #1: silence the Universe

measure two quantities to discriminate Sign & Bkgd,
on event-by-event basis

E.g. Edelweiss:

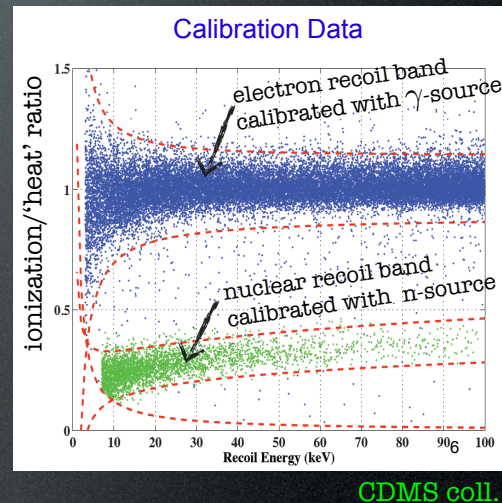
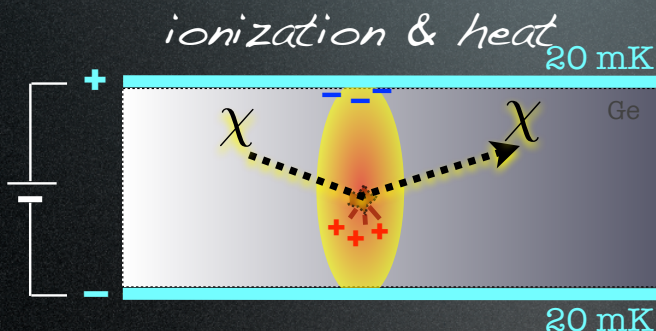


Direct Detection

Strategy #1: silence the Universe

measure two quantities to discriminate Sign & Bkgd,
on event-by-event basis

E.g. Edelweiss:

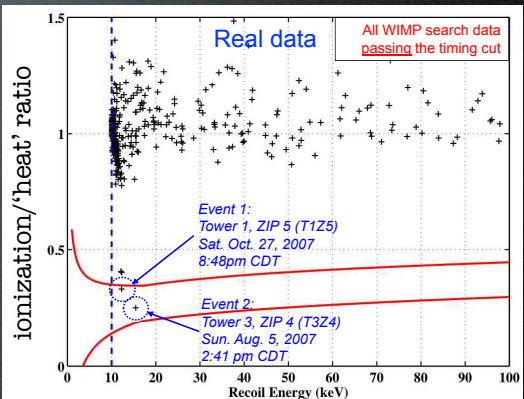
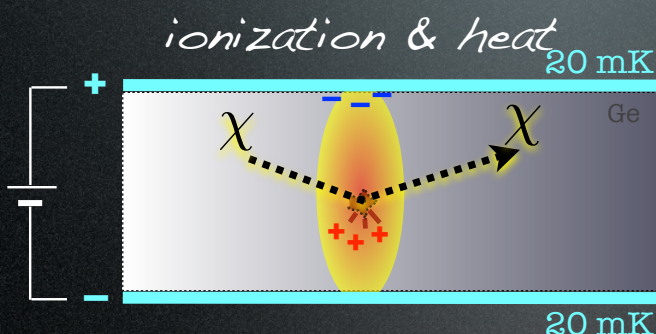


Direct Detection

Strategy #1: silence the Universe

measure two quantities to discriminate Sign & Bkgd,
on event-by-event basis

E.g. Edelweiss:



Direct Detection

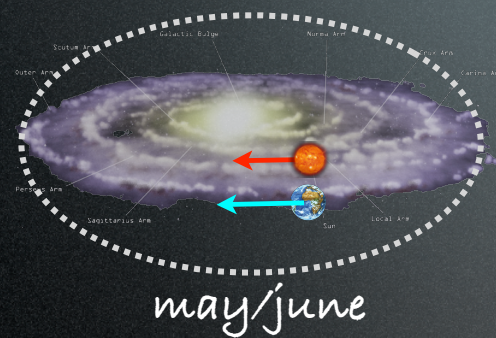
Strategy #2: ride the dark wave

collect all events, and detect an annual modulation

Direct Detection

Strategy #2: ride the dark wave

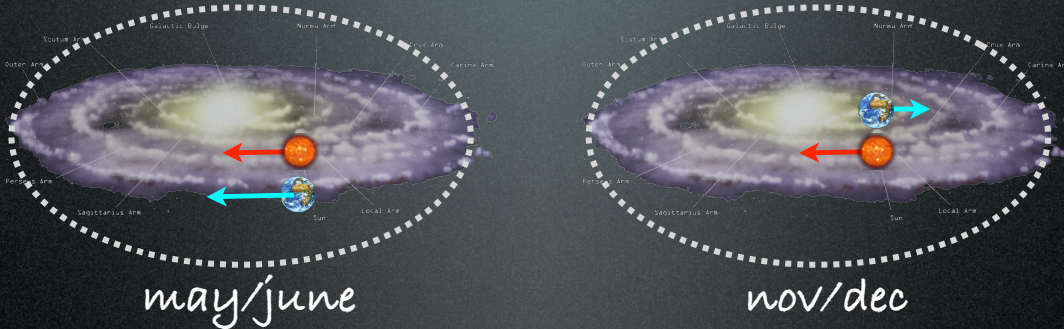
collect all events, and detect an annual modulation



Direct Detection

Strategy #2: ride the dark wave

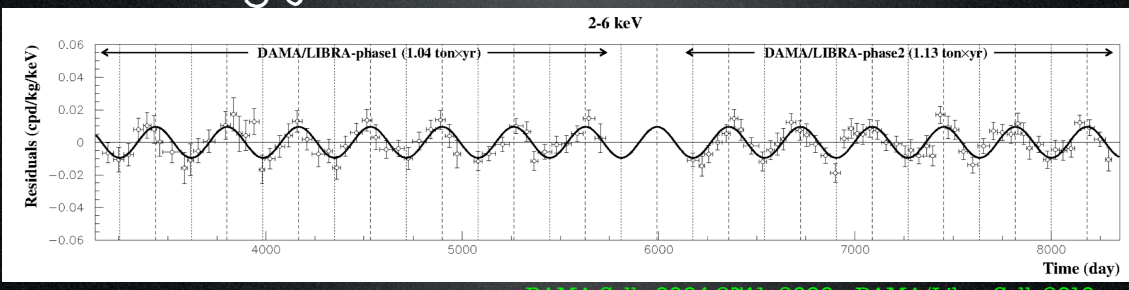
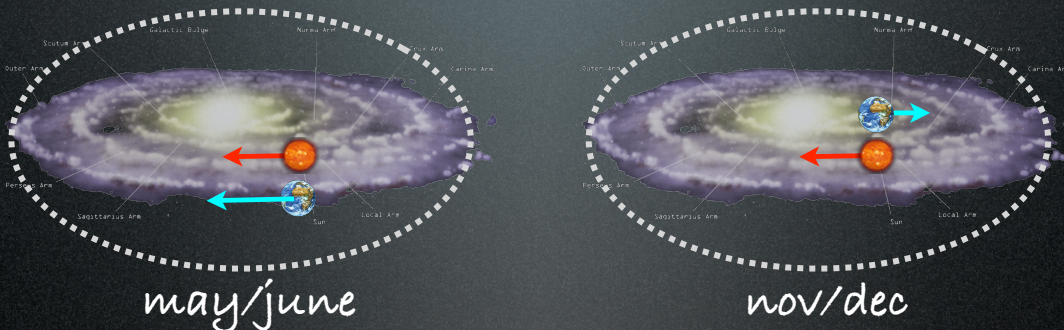
collect all events, and detect an annual modulation



Direct Detection

Strategy #2: ride the dark wave

collect all events, and detect an annual modulation

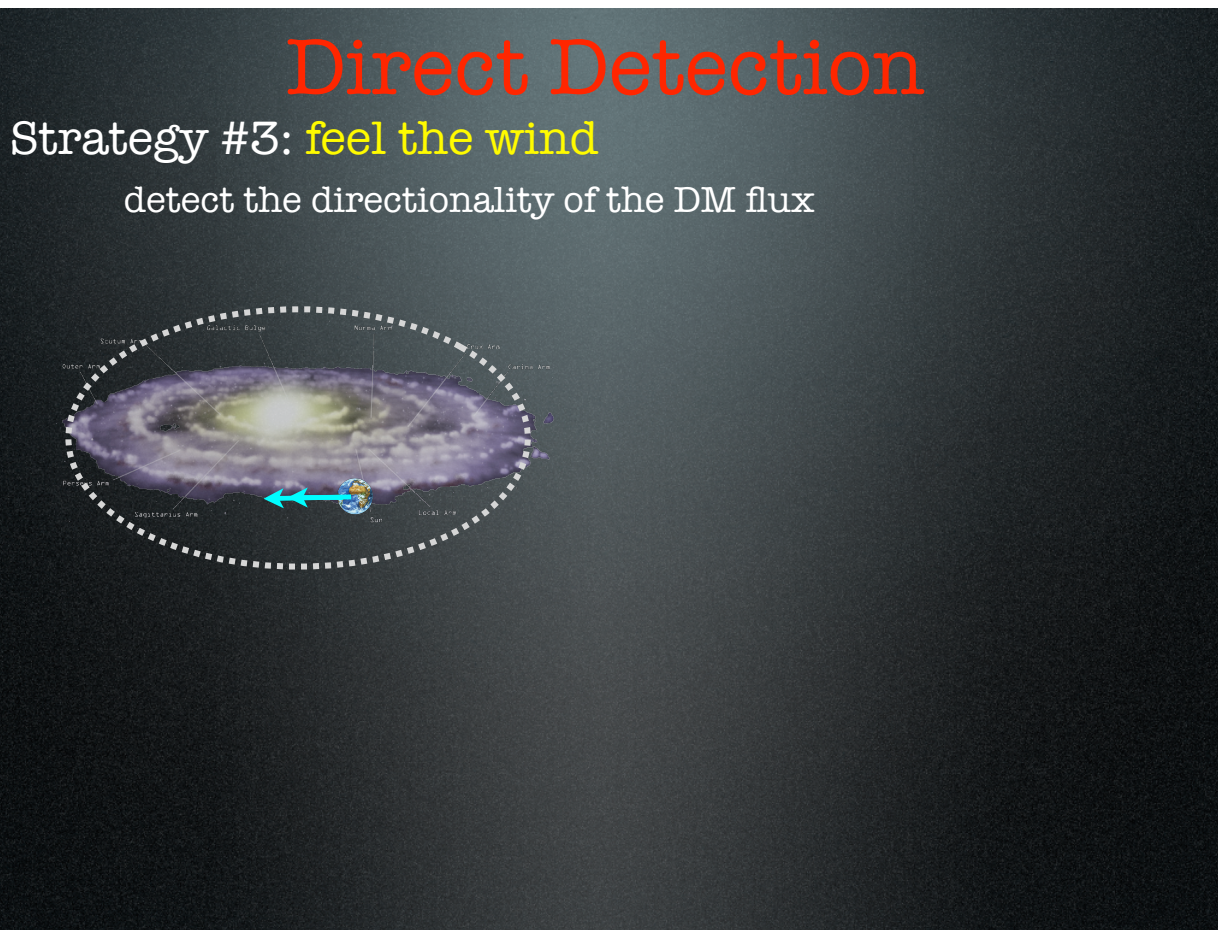


DAMA Coll., 0804.2741, 2008 + DAMA/Libra Coll. 2018

Direct Detection

Strategy #3: feel the wind

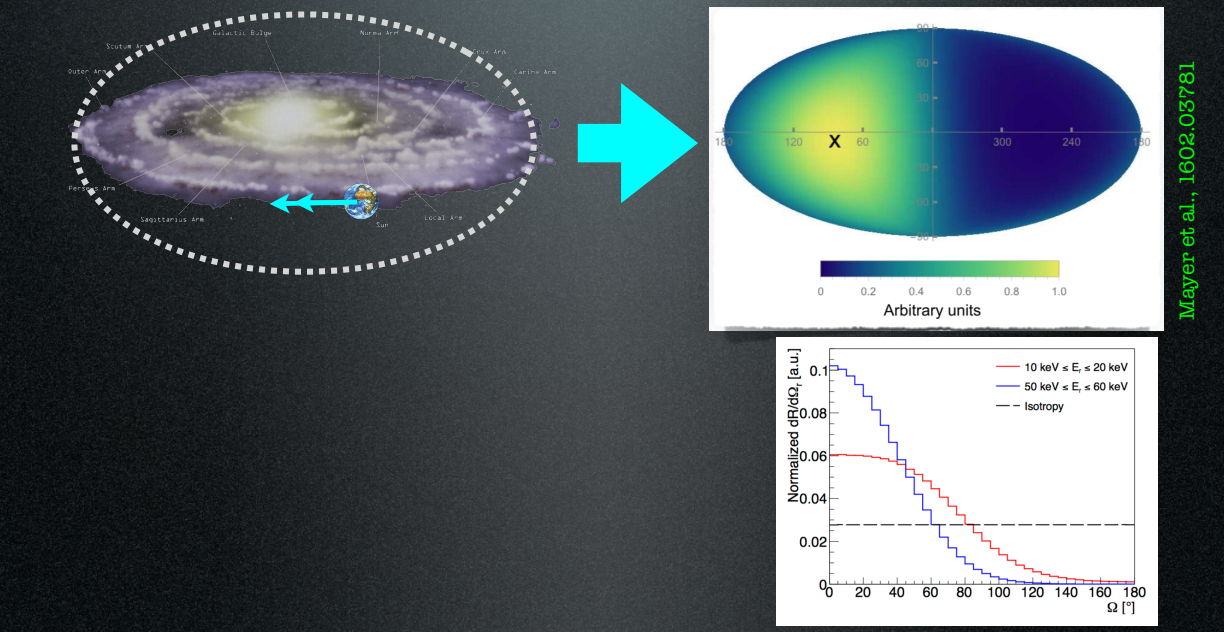
detect the directionality of the DM flux



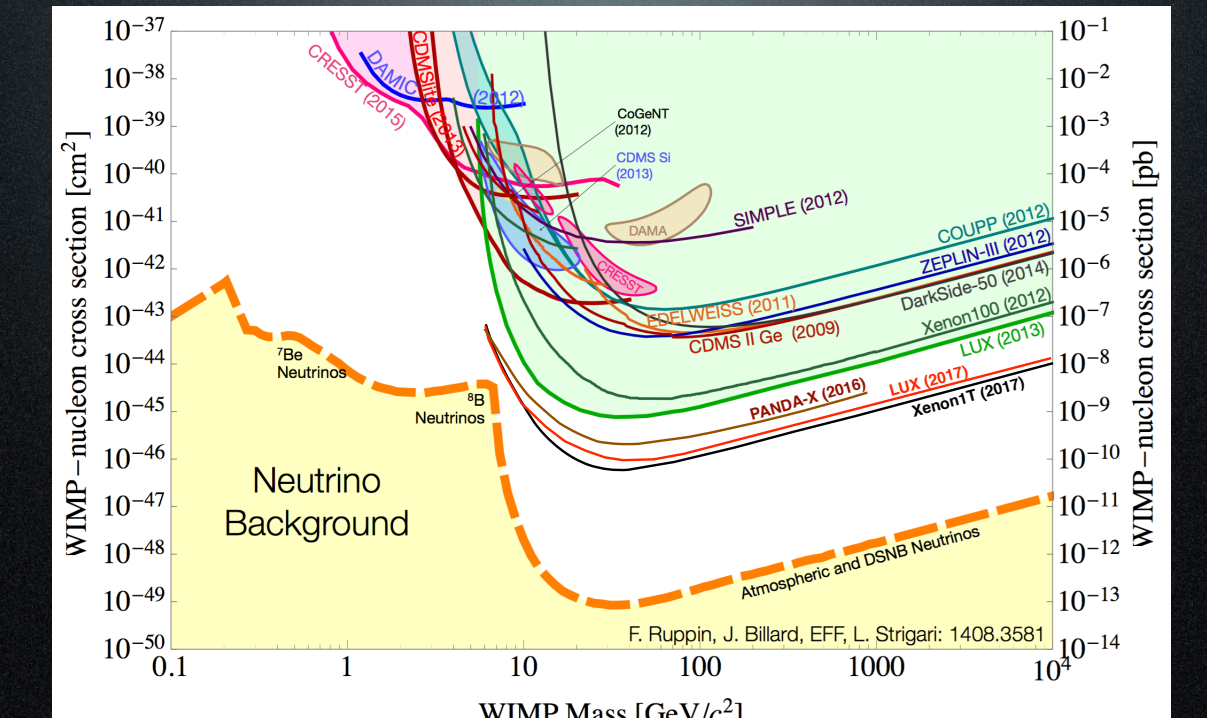
Direct Detection

Strategy #3: feel the wind

detect the directionality of the DM flux

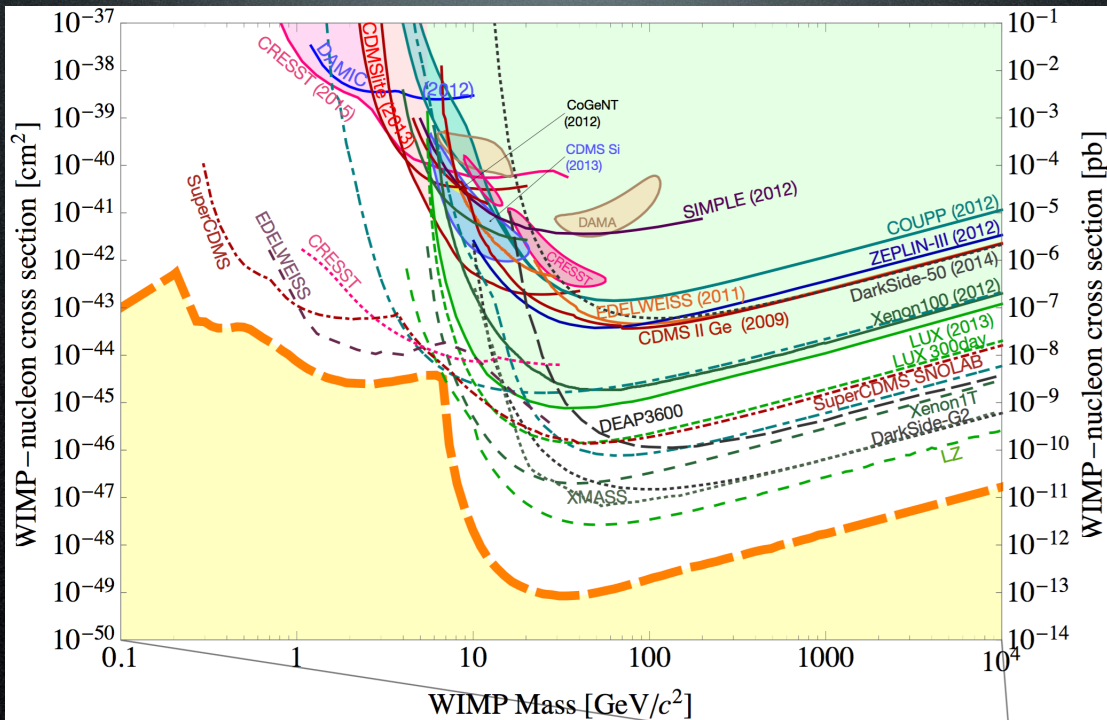


Direct Detection: results



E. Figueroa-Feliciano - ICRC 2015 → updated by hand to status at 04.2018 by M.C.

Direct Detection: future



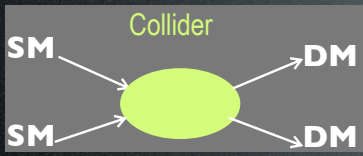
E. Figueroa-Feliciano - ICRC 2015

Chapter 6

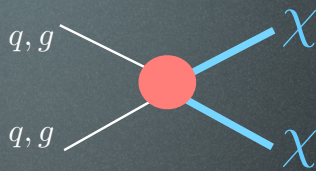
Collider searches

This section is not ready yet. A good reference is [60]. The slides follow.

Production at colliders

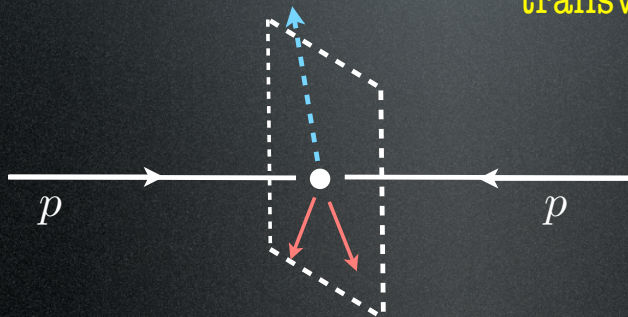


At LHC:



'Problem' is: DM flies away

Signature is: missing $\cancel{E}_{\text{transverse}}$



Before collision: $\vec{P}_T^{\text{tot}} \equiv 0$

(NB: $\vec{P}_L^{\text{tot}} \neq 0$ in general)

After collision: $\vec{P}_T^{\text{vis}} \stackrel{?}{=} 0$

If \neq , then 'MET'

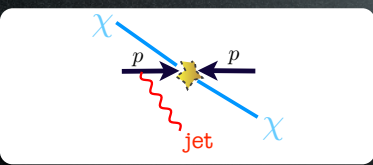
Background: neutrinos (e.g. $W \rightarrow e\nu$)

- model your background and look for anomalies
- construct kinematic variables sensitive to χ mass

Production at colliders

OK, MET is the crucial signature. Then what else?

the bare minimum



'mono-jet'

'started' by
J. Goodman et al.,
1008.1783

- 'new'
- model independent

'mono-photon'

'mono-Z/W'

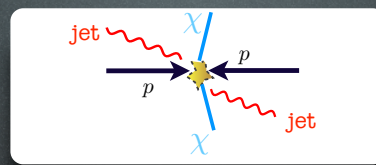
'mono-top'...

'mono-higgs'...



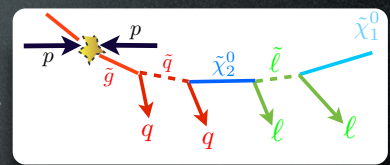
'mono-X'

lots of things



'(forward) di-jets'

- 'clean' topology
- flexible interpretation
(see later)



'trigger on 4j+4l+MET...'

huge literature

- well studied (M_T^2 ...)
- model dependent

NB: not an exhaustive list

Chapter 7

Indirect detection

Indirect detection experiments search for the following signal: pairs of Dark Matter particles that annihilate into Standard Model particles or Dark Matter that decays into SM particles. The latter can be detected by searching for an excess in cosmic rays, collected on Earth, with respect to the presumed astrophysical contribution. Promising sources are generically the regions where DM is expected to be densest, such as the center of our Galaxy, the inner halo of our Galaxy, nearby galaxies dominated by Dark Matter, the center of the Sun, the center of the Earth... However, some of these regions (notably the Galactic Center) are also the most complicated from the point of view of the underlying astrophysics. The best detection opportunities might thus come from selecting targets which are not necessarily the richest in DM but rather for which the signal over background ratio is most favorable. This then also depends on which species of cosmic ray one is looking for. In general terms, the SM particles that we hope to detect are photons, neutrinos, positrons, anti-protons, anti-deuterium and maybe even more exotic anti-nuclei such as anti-helium.

Each one of these messengers has advantages and disadvantages:

- *High-energy photons (γ -rays)* freely propagate in the galactic environment,¹ such that the information lies in both their energy and angular spectrum. However, DM is electrically neutral, so that it produces photons only via some subdominant mechanism, e.g., loops involving charged particles, or as secondary radiation. The photon spectrum is thus expected to be suppressed and highly model-dependent.
- *Low-energy photons (X-rays, radio waves)*. In the case of heavy DM, with mass in the \sim GeV-TeV range, the low energy photons are typically produced as secondary radiation due to electrons and positrons originating from DM annihilation or decay. The X-rays and radio waves are then produced through synchrotron radiation or through bremsstrahlung. Such photons constitute a DM signal, but they are ‘doubly indirect’ and dependent on the astrophysical environment that reprocesses the e^\pm . There are uncertainties due to the strength of magnetic field, gas density, etc. On the other hand, X-rays and other low energy radiation can also arise directly from the decay of light DM particles with masses in the \sim keV to MeV range, e.g., in models with sterile neutrinos.
- *Positrons* diffuse in the galactic magnetic fields, which randomizes their directions. They lose energy via synchrotron emission, Coulomb scattering, ionization, bremsstrahlung and

¹In the extragalactic/cosmological environment, on the other hand, absorption can occur, but its practical impact is limited.

Inverse Compton (IC) scattering processes. The potential DM contribution to positron flux is dominated by the nearby regions of the galaxy. The information about DM lies in the energy spectrum. Furthermore, the e^+ energy spectrum below a few GeV is distorted by the solar activity.

- *Electrons.* Similar comments as for the positrons apply to the electrons, with the disadvantage of a higher astrophysical background and the advantage that, at high energy, it is easier to measure the total $e^- + e^+$ flux rather than the positron flux alone.
- *Anti-protons* diffuse in the galactic magnetic fields, which randomizes their directions. Unlike e^\pm they undergo negligible energy losses, up to some scatterings on matter in the galactic plane. Therefore, even far-away regions of the Galaxy contribute to the flux collected on Earth and, as a consequence, its normalization has significant astrophysical uncertainties. The information about DM lies in the energy spectrum which, again, is distorted by solar activity below a few GeV.
- *Anti-deuterons.* Nuclei of anti-deuterium can be synthesised via the coalescence of an anti-proton and an anti-neutron produced in the DM annihilation or decay. The expected yield is very small. On the other hand, the astrophysical background is also expected to be small and, notably, is expected to peak in a range of energies different from the one of a typical DM signal, thanks to the differing kinematics of the two production mechanisms. The propagation in the galactic environment is analogous to the anti-proton case. Heavier anti-nuclei, such as anti-helium, can be produced in a completely analogous way, with the important penalty of a much suppressed flux, due to the need of coalescing more anti-nucleons.
- *Neutrinos* propagate freely in the Galaxy and can also propagate through the dense matter of the Earth and of the Sun, up to multi-TeV energies. The small interaction cross sections make the detection of neutrinos more difficult than, e.g., of gamma rays. Furthermore, the neutrino energy can be reconstructed only partially because they are measured indirectly via the detection of charged particles (e.g. up-going muons) produced by a neutrino interaction in the rock or water surrounding a neutrino telescope. On the other hand, the neutrino interaction cross section increases with energy, thus partly compensating the decrease in flux for larger DM masses. Possible sources of neutrinos from DM are the same as those already discussed for photons, plus the center of the Sun and, less promising, the Earth.

In the following we discuss each species in turn. This section is mostly based on [63], in which many more details and practical tools are given.

7.1 Energy spectra at production

Dark Matter can annihilate (or decay) in principle into any pair of Standard Model particles. The underlying particle physics model encompassing DM will specify which channels are most relevant, and/or with which branching ratios.

In order to be as model independent and illustrative as possible, here we consider DM annihilations (parameterized by the DM DM cross section σv) and decays (described by the DM decay

rate $\Gamma = 1/\tau$) into all the following primary channels:

$$\begin{aligned} & e_L^+ e_L^-, \, e_R^+ e_R^-, \, \mu_L^+ \mu_L^-, \, \mu_R^+ \mu_R^-, \, \tau_L^+ \tau_L^-, \, \tau_R^+ \tau_R^-, \, \nu_e \bar{\nu}_e, \, \nu_\mu \bar{\nu}_\mu, \, \nu_\tau \bar{\nu}_\tau, \\ & q\bar{q}, \, c\bar{c}, \, b\bar{b}, \, t\bar{t}, \, \gamma\gamma, \, gg, \\ & W_L^+ W_L^-, \, W_T^+ W_T^-, \, Z_L Z_L, \, Z_T Z_T, hh, \end{aligned} \tag{7.1}$$

where $q = u, d, s$ denotes a light quark and h is the Standard Model Higgs boson, with a mass fixed at 125 GeV.² These primary particles undergo parton showers and hadronization, in such a way to produce fluxes of $e^\pm, \bar{p}, \bar{d}, \gamma, \overset{\leftarrow}{\nu}_{e,\mu,\tau}$. This process is followed in most DM studies with the use of Monte Carlo simulation programs, e.g. PYTHIA, mostly designed for collider physics.

Some channels (such as $\gamma\gamma, \nu\bar{\nu}, gg$) are ‘unusual’ as they are often suppressed in many models, but from a model-independent point of view they are as viable as any other. The subscripts L and R on the leptonic channels refer to their left and right polarization, while the L and T on the vector boson ones refer to their longitudinal and transverse polarizations. It is important to distinguish such polarizations for the purposes of electroweak radiation, which we will discuss shortly. The corresponding unpolarized channels can be recovered by means of the following averages:

$$e^+ e^- = \frac{e_L^+ e_L^- + e_R^+ e_R^-}{2}, \quad W^+ W^- = \frac{2 W_T^+ W_T^- + W_L^+ W_L^-}{3}.$$

Electroweak radiation effects have been recognized as relevant for the purposes of DM indirect detection only relatively recently [61]. At large DM masses, such bremsstrahlung corrections are enhanced by one or more powers of $\ln(M_{\text{DM}}/M_W)$ logarithms, which become large for $M_{\text{DM}} \gg M_W$, compensating the suppression due to the additional weak coupling.

Phenomenologically, electroweak radiation effects can be particularly relevant for the leptonic and $\gamma\gamma$ channels. In fact, the emission of W 's and Z 's yields to further hadrons in the final state, and therefore it significantly modifies the flux of γ 's and e^\pm at energies $E \ll M$, M being the DM mass. Moreover, W/Z radiation leads to a \bar{p} contribution, which is instead absent if weak corrections are neglected; this is also true for the neutrino channels, that thereby also give e^\pm 's, γ 's and \bar{p} 's.

MC codes such as PYTHIA currently include some but not all the EW effects needed. One can however include electroweak bremsstrahlung (at leading order in the electroweak couplings) by ‘post-processing’ the output of the codes. Refer to [62] for a dedicated discussion and a detailed presentation of the computational techniques. The enhanced terms are model-independent: in the numerical results presented here they have been turned on abruptly when $M_{\text{DM}} \gtrsim M_W$. In a full DM model, these effects would actually appear in a smooth model-dependent way when increasing the DM mass. The finite non-logarithmic terms, that cannot be computed in a model-independent way, have instead been neglected.

The spectra of $e^\pm, \bar{p}, \bar{d}, \gamma, \overset{\leftarrow}{\nu}_{e,\mu,\tau}$ produced by the annihilation of two DM particles with mass M_{DM} (normalized per annihilation), for four values of M_{DM} , are presented in fig. 7.1. They correspond to the fluxes from the decay of a DM particle with mass $2M_{\text{DM}}$.

We now move on to discuss how these particles, produced anywhere in the galactic halo, reach us on Earth.

²We also consider models $VV \rightarrow 4e$, $VV \rightarrow 4\mu$, $VV \rightarrow 4\tau$ where DM annihilates into some new (light) boson V which then decays into a pair of leptons.

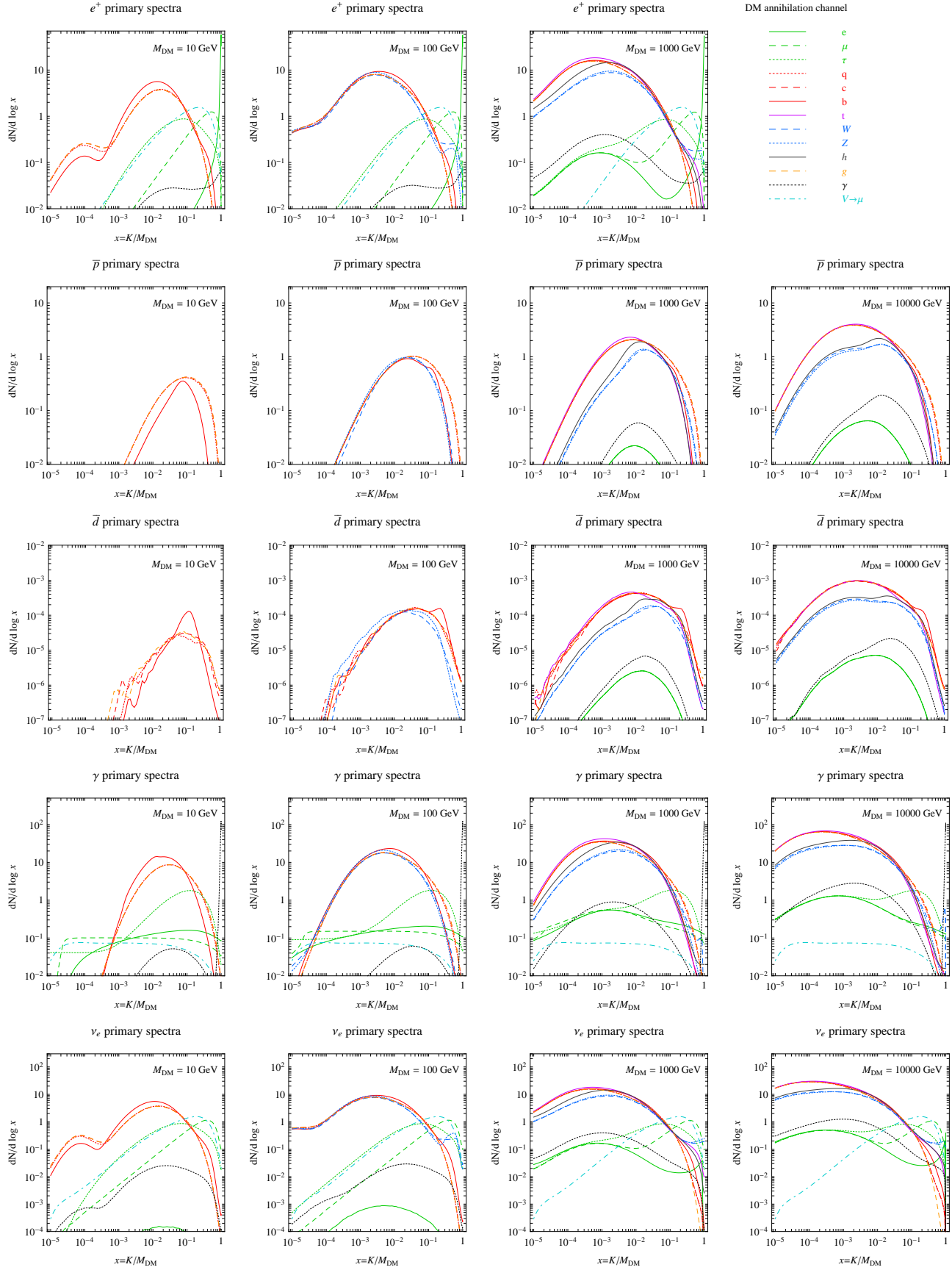


Figure 7.1: **Primary fluxes** of e^\pm , \bar{p} , \bar{d} , γ and ν_e .

7.2 Positrons and electrons

The differential e^\pm flux³ per unit of energy from DM annihilations or decays in any point in space \vec{x} and time t is given by $d\Phi_{e^\pm}/dE(t, \vec{x}, E) = v_{e^\pm} f/4\pi$ (units $1/\text{GeV} \cdot \text{cm}^2 \cdot \text{s} \cdot \text{sr}$) where v_{e^\pm} is the velocity (essentially equal to c in the regimes of our interest). The e^\pm number density per unit energy, $f(t, \vec{x}, E) = dN_{e^\pm}/dE$, obeys the diffusion-loss equation:

$$\frac{\partial f}{\partial t} - \nabla(\mathcal{K}(E, \vec{x}) \nabla f) - \frac{\partial}{\partial E}(b(E, \vec{x})f) = Q(E, \vec{x}) \quad (7.2)$$

with diffusion coefficient function $\mathcal{K}(E, \vec{x})$ and energy loss coefficient function $b(E, \vec{x})$. They respectively describe transport through the turbulent magnetic fields and energy loss due to several processes, such as synchrotron radiation and Inverse Compton scattering (ICS) on CMB photons and on infrared or optical galactic starlight, as we discuss in more detail below. Eq. (7.2) is solved in a diffusive region with the shape of a solid flat cylinder that sandwiches the galactic plane, with height $2L$ in the z direction and radius $R = 20 \text{ kpc}$ in the r direction. The location of the solar system corresponds to $\vec{x} = (r_\odot, z_\odot) = (8.33 \text{ kpc}, 0)$. Boundary conditions are imposed such that the e^\pm density f vanishes on the surface of the cylinder, outside of which electrons and positrons freely propagate and escape. Since steady state conditions hold, the first term of eq. (7.2) vanishes and the dependence on time disappears. Before illustrating the solution method, we briefly comment on the different pieces of the equation.

The e^\pm energy loss coefficient function $b(E, \vec{x})$ is in general dependent on the position \vec{x} , since the energy losses suffered by the e^\pm are sensitive to the environment:

$$-\frac{dE}{dt} \equiv b(E, \vec{x}) = \frac{4\sigma_T}{3m_e^2} E^2 \tilde{u} \quad , \quad \tilde{u} = u_B(\vec{x}) + \sum_i u_\gamma(\vec{x}) R_i^{\text{KN}}(E), \quad (7.3)$$

where $\sigma_T = 8\pi r_e^2/3$, with $r_e = \alpha_{\text{em}}/m_e$, is the Thompson cross section. The first addend in \tilde{u} is associated with synchrotron losses, the second one with ICS losses⁴. $u_B = B^2/2$ is the energy density in galactic magnetic fields B and $u_{\gamma,i} = \int dE n_i(E)$ is the energy density in light. Here i runs over the three main components: CMB, star-light and dust-diffused InfraRed light. For the CMB, $n(E)$ is just the black body spectrum with $T = 2.725 \text{ K}$ and one gets $u_{\gamma,\text{CMB}} = 0.260 \text{ eV/cm}^3$. For IR light and starlight, one has to extract the maps of their distribution and energy profile in the Galaxy from a range of astronomical surveys. The \vec{x} dependence in b is due to the fact that the composition of the background light for ICS is different in different points of the halo (e.g. the center or the periphery of the Galaxy) and the value of the magnetic field also varies (much higher in the center than elsewhere).

The dependence of b on the energy E , in turn, is dictated by the energy dependence of the rates of the different loss processes. In particular, for IC scattering one has $b \propto E^2$ as long

³Notice that with the notation e^\pm we always refer to the independent fluxes of electrons e^- or positrons e^+ , which share the same formalism, and not to their sum (for which we use the notation $e^+ + e^-$ when needed) which of course differs by a trivial factor 2.

⁴So one can also define

$$b_{\text{syn}}(E, \vec{x}) = \frac{4\sigma_T}{3m_e^2} E^2 u_B(\vec{x}) \quad \text{and} \quad b_{\text{IC}}(E, \vec{x}) = \frac{4\sigma_T}{3m_e^2} \sum_i E^2 u_{\gamma,i}(\vec{x}) R_i^{\text{KN}}(E). \quad (7.4)$$

Model	Electrons or positrons		Antiprotons (and antideuterons)			L [kpc]
	δ	\mathcal{K}_0 [kpc 2 /Myr]	δ	\mathcal{K}_0 [kpc 2 /Myr]	V_{conv} [km/s]	
MIN	0.55	0.00595	0.85	0.0016	13.5	1
MED	0.70	0.0112	0.70	0.0112	12	4
MAX	0.46	0.0765	0.46	0.0765	5	15

Table 7.1: *Propagation parameters for charged particles in the Galaxy (from [?, ?]).*

as the scattering happens in the Thomson regime, where the factor $R_i^{\text{KN}}(E) = 1$.⁵ For large enough electron energy the IC scattering enters into the full Klein-Nishina regime, where the γe^\pm scattering rate becomes rapidly smaller than the Thomson approximation, and thus $R_i^{\text{KN}}(E_e) < 1$ reducing $b(E)$. The synchrotron loss rate, instead, is always proportional to the square of the electron/positron energy E^2 .

The *profile of the magnetic field in the Galaxy* is very uncertain and we adopt the conventional one

$$B(r, z) = B_0 \exp[-(r - r_\odot)/r_B - |z|/z_B] \quad (7.5)$$

with $B_0 = 4.78 \mu\text{G}$, $r_B = 10$ kpc and $z_B = 2$ kpc. With these choices, the dominant energy losses are due to ICS everywhere, except in the region of the Galactic Center and for high e^\pm energies, in which case synchrotron losses dominate.

All in all, the $b(E, \vec{x})$ function that we obtain is sampled in fig. 7.2. In the figure, one sees the E^2 behaviour at low energies changing into a softer dependence as the energy increases (the transition happens earlier at the GC, where starlight is more abundant, and later at the periphery of the Galaxy, where CMB is the dominant background). At the GC, it eventually re-settles onto a E^2 slope at very high energies, where synchrotron losses dominate.

The *diffusion coefficient* function \mathcal{K} is also in principle dependent on the position, since the distribution of the diffusive inhomogeneities of the magnetic field changes throughout the galactic halo. However, a detailed mapping of such variations is prohibitive: e.g. they would have different features inside/outside the galactic arms as well as inside/outside the galactic disk, so that they would depend very much on poorly known local galactic geography. Moreover, including a spatial dependence in \mathcal{K} would make the semi-analytic method described below much more difficult to implement numerically. We therefore, as customary, we adopt the parameterization $\mathcal{K}(E, \vec{x}) = \mathcal{K}_0(E/\text{GeV})^\delta = \mathcal{K}_0 \epsilon^\delta$.

The values of the propagation parameters δ , K_0 and L (the height of the diffusion cylinder defined above) are deduced from a variety of cosmic ray data and modelizations. It is customary to adopt the sets presented in Table 7.1, which are found to minimize or maximize the final fluxes.⁶

Finally, DM DM annihilations or DM decays in each point of the halo with DM density $\rho(\vec{x})$

⁵We recall that the Thomson regime in electron-photon Compton scattering is identified by the condition $\epsilon'_{\text{max}} = 2\gamma\epsilon < m_e$, where ϵ denotes the energy of the impinging photon, ϵ' the same quantity in the rest frame of the electron, γ is the Lorentz factor of the electron and m_e is the electron mass. When e^\pm scatter on CMB photons ($\epsilon \simeq 2 \cdot 10^{-4}$ eV) the condition is satisfied up to \sim TeV e^\pm energies. For scatterings on more energetic starlight ($\epsilon \approx 0.3$ eV), the condition breaks down already above \approx few GeV e^\pm energies.

⁶We stress, however, that the determination of these parameters is a whole evolving research area.

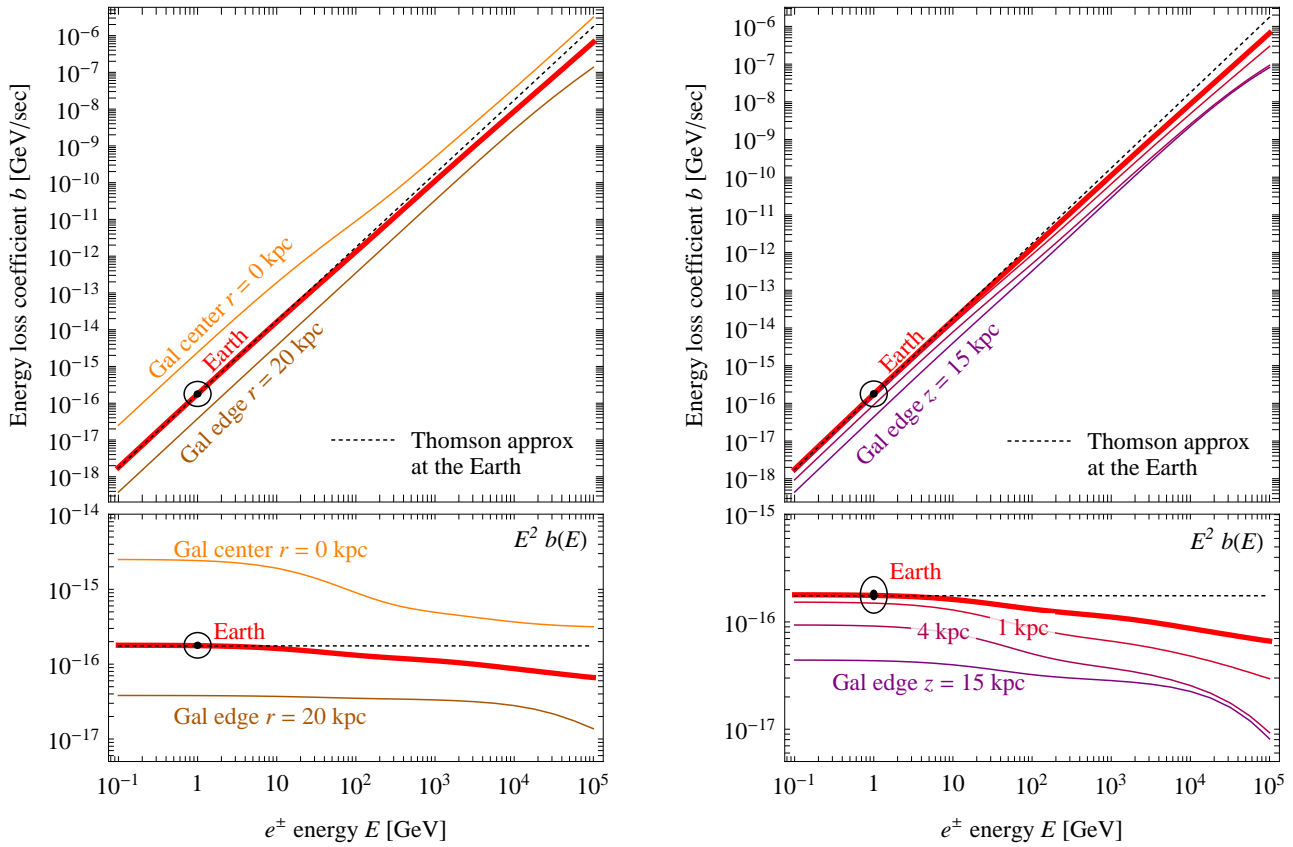


Figure 7.2: **Energy loss coefficient function** for electrons and positrons in the Milky Way. Left panel: at several locations along the galactic radial coordinate r , right panel: above (or below) the location of the Earth along the coordinate z . The dot points at the value of τ_\odot (see next subsection).

provide the source term Q of eq. (7.2), which reads

$$Q = \frac{1}{2} \left(\frac{\rho}{M_{\text{DM}}} \right)^2 f_{\text{inj}}^{\text{ann}}, \quad f_{\text{inj}}^{\text{ann}} = \sum_f \langle \sigma v \rangle_f \frac{dN_{e^\pm}^f}{dE} \quad (\text{annihilation}), \quad (7.6)$$

$$Q = \left(\frac{\rho}{M_{\text{DM}}} \right) f_{\text{inj}}^{\text{dec}}, \quad f_{\text{inj}}^{\text{dec}} = \sum_f \Gamma_f \frac{dN_{e^\pm}^f}{dE} \quad (\text{decay}), \quad (7.7)$$

where f runs over all the channels with e^\pm in the final state, with the respective thermal averaged cross sections σv or decay rate Γ .

With all the ingredients above, the solution for the differential flux of e^\pm $d\Phi_{e^\pm}/dE = v_{e^\pm} f/4\pi$

in each given point of our Galaxy for any injection spectrum can be written as

$$\frac{d\Phi_{e^\pm}}{dE}(E, \vec{x}) = \frac{v_{e^\pm}}{4\pi b(E, \vec{x})} \begin{cases} \frac{1}{2} \left(\frac{\rho(\vec{x})}{M_{\text{DM}}} \right)^2 \sum_f \langle \sigma v \rangle_f \int_E^{M_{\text{DM}}} dE_s \frac{dN_{e^\pm}^f}{dE}(E_s) I(E, E_s, \vec{x}) & (\text{annihilation}) \\ \left(\frac{\rho(\vec{x})}{M_{\text{DM}}} \right) \sum_f \Gamma_f \int_E^{M_{\text{DM}}/2} dE_s \frac{dN_{e^\pm}^f}{dE}(E_s) I(E, E_s, \vec{x}) & (\text{decay}) \end{cases} \quad (7.8)$$

where E_s is the e^\pm energy at production ('s' stands for 'source') and the *generalized halo functions* $I(E, E_s, \vec{x})$ are essentially the Green functions from a source with fixed energy E_s to any energy E . In other words, the halo functions I encapsulate all the astrophysics (there is a halo function I for each choice of DM distribution profile and choice of e^\pm propagation parameters) and are independent of the particle physics model: convoluted with the injection spectra, they give the final spectrum searched for. They obey $I(E, E, \vec{x}) = 1$ and $I(E, E_s, \vec{x}) = 0$ on the boundary of the diffusion cylinder. Neglecting diffusion (i.e. setting $\mathcal{K} = 0$) one would have $I(E, E_s, \vec{x}) = 1$.

The above treatment is pretty general in that it allows to compute the propagated fluxes taking into account the full energy and position dependance of $b(E, \vec{x})$, as discussed above. An approximated formalism had been adopted in the past and we report it here for completeness.

Assuming a space-independent $b = b_T(\epsilon) = \epsilon^2 \text{GeV}/\tau_\odot$ everywhere in the Galaxy, one can define a 'reduced' halo function $\mathcal{I}(\lambda_D, \vec{x})$ (and a simplified differential equation for it) in terms of a single quantity $\lambda_D = \lambda_D(\epsilon, \epsilon_s) = \sqrt{4\mathcal{K}_0\tau_\odot(\epsilon^{\delta-1} - \epsilon_s^{\delta-1})/(1-\delta)}$, which represents the diffusion length of e^\pm injected with energy ϵ_s and detected with energy ϵ . One has the equivalent of eq. (7.8) as

$$\frac{d\Phi_{e^\pm}}{dE}(\epsilon, \vec{x}) = \frac{1}{4\pi} \frac{v_{e^\pm}}{b_T(\epsilon)} \begin{cases} \frac{1}{2} \left(\frac{\rho_\odot}{M_{\text{DM}}} \right)^2 \sum_f \langle \sigma v \rangle_f \int_\epsilon^{M_{\text{DM}}} d\epsilon_s \frac{dN_{e^\pm}^f}{dE}(\epsilon_s) \mathcal{I}(\lambda_D(\epsilon, \epsilon_s), \vec{x}) & (\text{annihilation}) \\ \left(\frac{\rho_\odot}{M_{\text{DM}}} \right) \sum_k \Gamma_k \int_\epsilon^{M_{\text{DM}}/2} d\epsilon_s \frac{dN_{e^\pm}^f}{dE}(\epsilon_s) \mathcal{I}(\lambda_D(\epsilon, \epsilon_s), \vec{x}) & (\text{decay}) \end{cases} \quad (7.9)$$

The function $\mathcal{I}(\lambda_D, r_\odot, z_\odot)$ at the location of the Earth is well reproduced in terms of the fit

$$\mathcal{I}(\lambda_D) = a_0 + a_1 \tanh\left(\frac{b_1 - \ell}{c_1}\right) \left[a_2 \exp\left(-\frac{(\ell - b_2)^2}{c_2}\right) + a_3 \right] \quad (7.10)$$

with $\ell = \log_{10}(\lambda_D/\text{kpc})$ and the coefficients given in the tables in [63].

7.3 Anti-protons

The propagation of antiprotons through the galaxy is described by a diffusion equation analogous to the one for positrons. Again, the number density of antiprotons per unit energy $f(t, \vec{x}, K) = dN_{\bar{p}}/dK$ vanishes on the surface of the cylinder at $z = \pm L$ and $r = R$. $K = E - m_p$ is the \bar{p} kinetic energy, conveniently used instead of the total energy E (a distinction which is of course not particularly relevant when one looks at fluxes originating from TeV-scale DM, i.e. at energies much larger than the proton mass m_p , but important for the low energy tails and in the case

of small DM masses). Since $m_p \gg m_e$ one can neglect the energy loss term that was instead important for positrons. But new terms appear in the diffusion equation for f , which reads

$$\frac{\partial f}{\partial t} - \mathcal{K}(K) \cdot \nabla^2 f + \frac{\partial}{\partial z} (\text{sign}(z) f V_{\text{conv}}) = Q - 2h \delta(z) (\Gamma_{\text{ann}} + \Gamma_{\text{non-ann}}) f, \quad (7.11)$$

where:

- The pure *diffusion term* can again be written as $\mathcal{K}(K) = \mathcal{K}_0 \beta (p/\text{GeV})^\delta$, where $p = (K^2 + 2m_p K)^{1/2}$ and $\beta = v_{\bar{p}}/c = (1 - m_p^2/(K + m_p)^2)^{1/2}$ are the antiproton momentum and velocity. δ and \mathcal{K}_0 are given in Table 7.1.
- The V_{conv} term corresponds to a *convective wind*, assumed to be constant and directed outward from the galactic plane, that tends to push away \bar{p} with energy $T \lesssim 10 m_p$. Its value is given in Table 7.1.
- The *source term* Q due to DM DM annihilations or DM decay has a form fully analogous to eq. (7.6) or (7.7), with E now formally replaced by K .
- The first part of the last term in eq. (7.11) describes the annihilations of \bar{p} on interstellar protons in the galactic plane (with a thickness of $h = 0.1 \text{kpc} \ll L$) with rate $\Gamma_{\text{ann}} = (n_{\text{H}} + 4^{2/3} n_{\text{He}}) \sigma_{p\bar{p}}^{\text{ann}} v_{\bar{p}}$, where $n_{\text{H}} \approx 1/\text{cm}^3$ is the hydrogen density, $n_{\text{He}} \approx 0.07 n_{\text{H}}$ is the Helium density (the factor $4^{2/3}$ accounting for the different geometrical cross section in an effective way) and $\sigma_{p\bar{p}}^{\text{ann}}$ is given by

$$\sigma_{p\bar{p}}^{\text{ann}} = \begin{cases} 661 (1 + 0.0115 K^{-0.774} - 0.984 K^{0.0151}) \text{ mbarn}, & \text{for } K < 15.5 \text{ GeV} \\ 36 K^{-0.5} \text{ mbarn}, & \text{for } K \geq 15.5 \text{ GeV} \end{cases}. \quad (7.12)$$

The second part, similarly, describes the interactions on interstellar protons in the galactic plane in which the \bar{p} 's do not annihilate but lose a significant fraction of their energy. Technically, one should keep them in the flux, with a degraded energy: they are referred to as “tertiary antiprotons”. We adopt instead the simplifying approximation of treating them as if they were removed from the flux. The cross section that we need for the whole last term of eq. (7.11) is then the sum of $\sigma_{p\bar{p}}^{\text{ann}} + \sigma_{p\bar{p}}^{\text{non-ann}} = \sigma_{p\bar{p}}^{\text{inel}}$. It is given as

$$\sigma_{p\bar{p}}^{\text{inel}}(K) = 24.7 (1 + 0.584 K^{-0.115} + 0.856 K^{-0.566}) \text{ mbarn}. \quad (7.13)$$

We find, anyway, that the precise expressions adopted for these cross sections do not significantly impact the final results.

- We neglect, as just said, the effect of “tertiary antiprotons”. It can be re-included in terms of an absorption term proportional to a different $\sigma_{p\bar{p}}^{\text{non-ann}}$, and of a re-injection term Q^{tert} proportional to the integrated cross section over $f(K)$. The full solution of the resulting integro-differential equation can be found in [?]. The effect of tertiaries is mainly relevant at low energies $K \lesssim \text{few GeV}$.

Assuming steady state conditions the first term in the diffusion equation vanishes, and the equation can be solved analytically. In the “no-tertiaries” approximation that we adopt, the solution for the antiproton differential flux at the position of the Earth $d\Phi_{\bar{p}}/dK(K, \vec{r}_{\odot}) = v_{\bar{p}}/(4\pi) f$

acquires a simple factorized form

$$\frac{d\Phi_{\bar{p}}}{dK}(K, \vec{r}_\odot) = \frac{v_{\bar{p}}}{4\pi} \begin{cases} \left(\frac{\rho_\odot}{M_{\text{DM}}}\right)^2 R(K) \sum_f \frac{1}{2} \langle \sigma v \rangle_f \frac{dN_{\bar{p}}^f}{dK} & (\text{annihilation}) \\ \left(\frac{\rho_\odot}{M_{\text{DM}}}\right) R(K) \sum_f \Gamma_f \frac{dN_{\bar{p}}^f}{dK} & (\text{decay}) \end{cases}. \quad (7.14)$$

The f index runs over all the annihilation channels with antiprotons in the final state, with the respective cross sections or decay rates; this part contains the particle physics input. The function $R(K)$ encodes all the astrophysics of production and propagation. There is such a ‘propagation function’ for annihilations and for decays for any choice of DM galactic profile and for any choice of set of propagation parameters among those in Table 7.1. We provide $R(K)$ for all these cases in terms of a fit function

$$\log_{10}[R(K)/\text{Myr}] = a_0 + a_1 \kappa + a_2 \kappa^2 + a_3 \kappa^3 + a_4 \kappa^4 + a_5 \kappa^5, \quad (7.15)$$

with $\kappa = \log_{10} K/\text{GeV}$ and the coefficients reported in the tables in [63].

7.4 Gamma rays

The *differential flux of photons* from a given angular direction $d\Omega$ produced by the annihilation of self-conjugated DM particles (e.g. Majorana fermions) is

$$\frac{d\Phi_\gamma}{d\Omega dE} = \frac{1}{2} \frac{r_\odot}{4\pi} \left(\frac{\rho_\odot}{M_{\text{DM}}}\right)^2 J \sum_f \langle \sigma v \rangle_f \frac{dN_\gamma^f}{dE}, \quad J = \int_{\text{l.o.s.}} \frac{ds}{r_\odot} \left(\frac{\rho(r(s, \theta))}{\rho_\odot}\right)^2 \quad (\text{annihilation}) \quad (7.16)$$

where dN_γ^f/dE is the energy spectrum of photons produced per one annihilation⁷ in the channel with final state f . If DM is not constituted by self-conjugated particles (e.g. in the case of Dirac fermions), then σv must be averaged over DM particles and antiparticles: in practice, the equation above has to be divided by an additional factor of 2 if only particle-antiparticle annihilations are present.

In the case of DM decay, an analogous equation holds

$$\frac{d\Phi_\gamma}{d\Omega dE} = \frac{r_\odot}{4\pi} \frac{\rho_\odot}{M_{\text{DM}}} J \sum_f \Gamma_f \frac{dN_\gamma^f}{dE}, \quad J = \int_{\text{l.o.s.}} \frac{ds}{r_\odot} \left(\frac{\rho(r(s, \theta))}{\rho_\odot}\right) \quad (\text{decay}) \quad (7.17)$$

Here the coordinate r , centered on the Galactic Center, reads $r(s, \theta) = (r_\odot^2 + s^2 - 2 r_\odot s \cos \theta)^{1/2}$, and θ is the aperture angle between the direction of the line of sight and the axis connecting the Earth to the Galactic Center.

The J factor in eq. (7.16) and eq. (7.17) integrates the intervening matter along the line of sight (along which the variable s runs) individuated by the angular direction, and it is conventionally weighted by r_\odot (here assumed to be 8.33 kpc) and the appropriate power of ρ_\odot (here assumed to be 0.3 GeV/cm³) so to be adimensional.⁸ $J(\theta)$ is of course invariant under rotations around the axis which connects the Earth to the GC, due to the assumed spherical symmetry of the DM distribution $\rho(r)$.

⁷Not per initial state particle; not per final state primary particle.

⁸Alternatively, sometimes an analogous factor is defined as $\mathcal{J} = \int_{\text{l.o.s.}} \rho^2(r) = r_\odot \rho_\odot^2 J$ in units of GeV²/cm⁵ (annihilation) or $\mathcal{J} = \int_{\text{l.o.s.}} \rho(r) = r_\odot \rho_\odot J$ in units of GeV/cm² (decay).

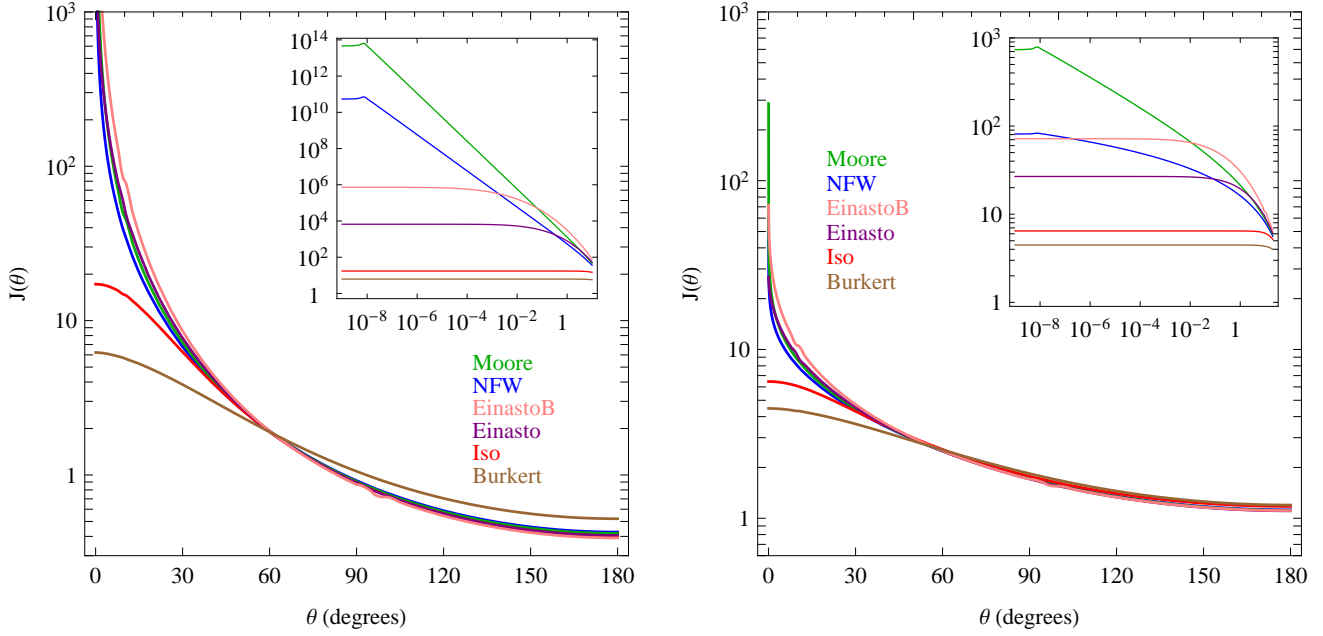


Figure 7.3: **$J(\theta)$ for annihilating (left) and decaying (right) Dark Matter**, for the different DM profiles. The color code individuates the profiles (Burkert, Isothermal, Einasto, EinastoB, NFW, Moore from bottom to top in the inset).

The J factors for the profiles in eq. (4.1) are plotted in fig. 7.3 as a function of θ .

The recipes (7.16) and (7.17) are ready for consumption if one needs the flux of gamma rays from a given direction. More often, of course, one needs the *integrated flux* over a region $\Delta\Omega$, corresponding e.g. to the window of observation or the resolution of the telescope. The J factor is then replaced by the *average J factor* for such region, simply defined as $\bar{J}(\Delta\Omega) = (\int_{\Delta\Omega} J d\Omega) / \Delta\Omega$. The following simple formulæ hold for regions that are disks of aperture θ_{\max} centered around the GC, annuli $\theta_{\min} < \theta < \theta_{\max}$ centered around the GC or generic regions defined in terms of galactic latitude b and longitude ℓ ⁹ (provided they are symmetric around the GC):

$$\begin{aligned} \Delta\Omega &= 2\pi \int_0^{\theta_{\max}} d\theta \sin \theta, & \bar{J} &= \frac{2\pi}{\Delta\Omega} \int d\theta \sin \theta J(\theta), & \text{(disk)} \\ \Delta\Omega &= 2\pi \int_{\theta_{\min}}^{\theta_{\max}} d\theta \sin \theta, & \bar{J} &= \frac{2\pi}{\Delta\Omega} \int d\theta \sin \theta J(\theta), & \text{(annulus)} \\ \Delta\Omega &= 4 \int_{b_{\min}}^{b_{\max}} \int_{\ell_{\min}}^{\ell_{\max}} db d\ell \cos b, & \bar{J} &= \frac{4}{\Delta\Omega} \iint db d\ell \cos b J(\theta(b, \ell)). & \text{($b \times \ell$ region)} \end{aligned} \quad (7.18)$$

⁹Galactic polar coordinates (d, ℓ, b) are defined as

$$x = d \cos \ell \cos b, \quad y = d \sin \ell \cos b, \quad z = d \sin b$$

where the Earth is located at $\vec{x} = 0$ (such that d is the distance from us); the Galactic Center at $x = r_\odot$, $y = z = 0$; and the Galactic plane corresponds to $z \approx 0$. Consequently $\cos \theta = x/d = \cos b \cdot \cos \ell$.

7.5 Secondary photons

Galactic e^\pm generated by DM in the diffusion volume lose essentially all their energy into photons by means of two processes: Inverse Compton and synchrotron radiation. Bremsstrahlung radiation is also important in regions close to the galactic disk (where gas is abundant) and for low energy electrons.

The resulting fluxes of ICS (and bremsstrahlung) γ rays and of microwave synchrotron radiation are thus possible signatures of DM. The ICS flux is particularly promising. One of its features is that it originates from ‘everywhere’ in the diffusion volume of the galactic halo, including regions where the astrophysical background is reduced (e.g. at high latitudes). Moreover, essentially everywhere synchrotron energy losses are sub-dominant with respect to Inverse Compton energy losses, so that, thanks to energy conservation, the resulting ICS γ flux suffers only moderate astrophysical uncertainties.

The microwave synchrotron emission is generated in significant amount from the region close to the Galactic Center (where the intensity of the magnetic field and the density of Dark Matter is highest) and therefore is plagued by more uncertainty and more background. However it can also come from large latitudes.

Finally, the bremsstrahlung emission can be a relevant signature for DM in the conditions mentioned above (large gas density and $\lesssim 10$ GeV e^\pm energy). In any case, it has to be taken into account if one wants to consistently model the other emissions with which it competes.

7.6 Neutrinos from the Sun and from the Earth

A flux of neutrinos is produced inside the Sun or the Earth as a consequence of annihilation of dark matter particles which have been gravitationally captured inside these celestial bodies. The differential neutrino flux is:

$$\frac{d\Phi_\nu}{dE_\nu} = \frac{\Gamma_{\text{ann}}}{4\pi d^2} \frac{dN_\nu}{dE_\nu} \quad (7.19)$$

where d is the distance of the neutrino source from the detector (either the Sun–Earth distance r_{SE} or the Earth radius R_\oplus), dN_ν/dE_ν is the neutrino flux produced per DM annihilation after taking into account neutrino propagation effects (oscillations and absorption), and Γ_{ann} is the DM annihilation rate.

The number N of DM particles captured inside the Sun (or the Earth) varies with time as

$$\frac{dN}{dt} = \Gamma_{\text{capt}} - \Gamma_{\text{evap}} - 2\Gamma_{\text{ann}} \quad (7.20)$$

where Γ_{capt} is the capture rate; Γ_{evap} is the DM evaporation rate proportional to N (and negligible unless DM is lighter than a few GeV); Γ_{ann} is the DM annihilation rate. Since 2 DM annihilate, this factor appears multiplied by 2 and is proportional to N^2 . It can be computed taking into account that DM thermalises within the Sun, acquiring a density distribution $n(r) \propto \exp[-M\phi(r)/T]$, where $\phi(r)$ is the Newton potential and $T = 15.5 \cdot 10^6$ K is the temperature of matter around the center. The annihilation rate is

$$2\Gamma_{\text{ann}} = \int dV n^2(\vec{x}) \langle \sigma v \rangle = C_A N^2, \quad C_A = \langle \sigma v \rangle \left(\frac{2G_N M \rho}{3T} \right)^{3/2} \quad (7.21)$$

where $\rho = 151 \text{ g/cm}^3$ is the density in the center of the Sun.

Neglecting Γ_{evap} and solving eq. (7.20) one finds

$$\Gamma_{\text{ann}} = \frac{\Gamma_{\text{capt}}}{2} \tanh^2 \left(\frac{t}{\tau} \right) \quad (7.22)$$

where $t = 4.5 \text{ Gyr}$ is the age of the Sun and $\tau = 1/\sqrt{\Gamma_{\text{capt}} C_A}$ is the time-scale for the competing processes of capture and annihilation. Equilibrium between capture and annihilation is reached when τ is much smaller than the age t of the body (this is often achieved for the Sun but not for the Earth), such that $\tanh(t/\tau) \approx 1$.

Then, the annihilation rate Γ_{ann} is given by the capture rate Γ_{capt} . If DM interacts so strongly that every DM particle that hits the sun is captured, it is given by

$$\Gamma_{\text{capt}} = \frac{\rho_{\text{DM}}}{M} \langle v_{\text{rel}} \rangle \pi R_{\text{sun}}^2 \approx \frac{1.3 \cdot 10^{26}}{\text{sec}} \frac{\text{TeV}}{M} \frac{\langle v_{\text{rel}} \rangle}{10^{-3}} \quad (7.23)$$

where $R_{\text{sun}} \approx 7 \cdot 10^8 \text{ m}$ is the solar radius. Such a rate is experimentally excluded. So DM must have a cross section small enough that there is a small probability that a DM hitting the Sun is captured. In such a case the capture rate is

$$\Gamma_{\text{capt}} = \frac{\rho_{\text{DM}}}{M} \sum_i \sigma_i \int_0^R dr \ 4\pi r^2 \ n_i(r) \int_0^\infty dv \ 4\pi v^2 \frac{f(v)}{v} (v^2 + v_{\odot \text{esc}}^2) \wp_i(v, v_{\odot \text{esc}}) \quad (7.24)$$

where σ_i is the low-energy DM cross section on nucleus i , assumed to be isotropic; the Sun is assumed to be spherical with radius R and density $\rho(r)$; the sum runs over all kinds of nuclei i with mass m_i and mass fraction ϵ_i , such that $n_i = \rho(r)\epsilon_i/m_i$ is their number density; $f(v)$ is the angular average of the DM velocity distribution (see section 4.2) with respect to the body rest frame, neglecting the gravitational attraction of the body; the gravity of the Sun is taken into account by $v_{\odot \text{esc}}(r)$, which is the escape velocity at radius r , such that $v^2 + v_{\odot \text{esc}}^2$ is the squared velocity that DM acquires when arriving at r .¹⁰ The probability that a scattering leads to DM capture is

$$\wp_i(v, v_{\odot \text{esc}}) = \frac{1}{E_{\max}} \int_{E_{\min}}^{E_{\max}} d\Delta |F_i(\Delta)|^2 \approx \max \left(0, \frac{E_{\max} - E_{\min}}{E_{\max}} \right) \quad (7.25)$$

where $E_{\max}/E = 4m_i M_{\text{DM}}/(M_{\text{DM}} + m_i)^2$ and $E_{\min}/E = v^2/(v^2 + v_{\odot \text{esc}}^2)$ are the maximal and minimal energy loss Δ that a particle can suffer in the scattering process, provided that it is captured; $|F_i(\Delta)|^2 = e^{-\Delta/E_0}$ with $E_0 = 3/2m_i r_i^2$ (spin-dependent) or $E_0 = 5/2m_i r_i^2$ (spin-independent) (where r_i is the effective nuclear radius) is a form factor that describes the suppression of the DM/nucleus cross section at large energy transfer.

The fraction of scatterings that lead to capture is larger for nuclei with mass m_i comparable to the DM mass M . Fig. 7.4 shows the capture rate in the Sun. In the limit of heavy DM, $M \gg m_i \sim 100 \text{ GeV}$, DM can be captured only if very slow, $v < 2v_{\text{esc}}\sqrt{m_i/M}$: the capture rate is then proportional to $1/M^2$. In this limit

$$\Gamma_{\text{capt}} \simeq \frac{5.9 \cdot 10^{22}}{\text{sec}} \left(\frac{\rho_{\text{DM}}}{0.3 \text{ GeV/cm}^3} \right) \left(\frac{100 \text{ GeV}}{M} \right)^2 \left(\frac{270 \text{ km/sec}}{v_0} \right)^3 \frac{\sigma_{\text{SD}} + 1200 \sigma_{\text{SI}}}{10^{-40} \text{ cm}^2} \quad (7.26)$$

having approximated DM interactions with nuclei as a spin-dependent and a spin-independent cross section on nucleons.

¹⁰We neglected the effect of other bodies in the solar system, which presumably is a good approximation.

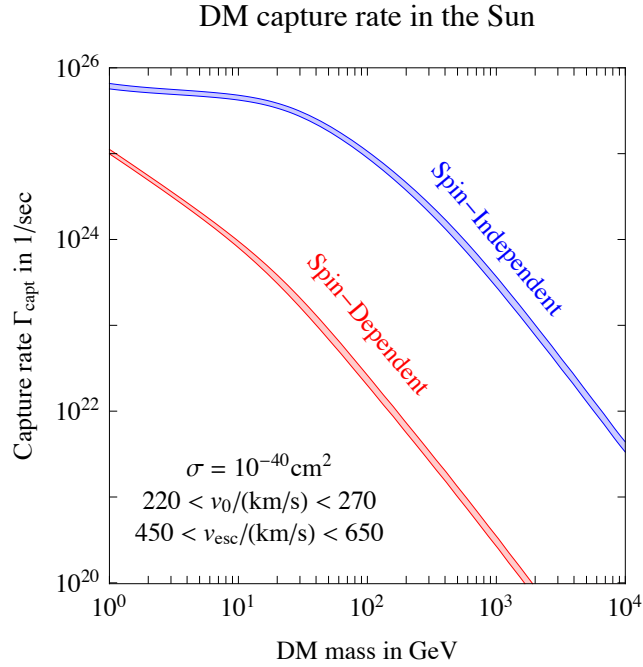


Figure 7.4: Capture rate Γ_{capt} of DM particles in the Sun. The capture rate is proportional to the cross-section σ , and we consider both Spin-Dependent and Spin-Independent scattering.

The neutrino energy spectra from DM annihilations in the Sun, dN_ν/dE_ν in eq. (7.19), are computed similarly to those in vacuum with two differences.

First, one needs to take into account that particles produced from DM annihilations interact with matter in the Sun. As a result, particles with larger cross section and longer life-times loose energy before decaying into neutrinos. This is the case of π and μ , giving rise to large neutrino fluxes at low energies, below the detection threshold of experiments like ICECUBE.

Second, one needs to take into account neutrino oscillations in the Sun and outside together with neutrino absorption and energy losses in the Sun. As a result, neutrinos produced in the center of the Sun only exit with sub-TeV energies.

Appendix A

Cosmology

We collect here some of the main relevant results of big-bang cosmology.

A.1 Expansion

The expanding Universe, assumed to be homogenous and isotropic (which is what it is observed to be, at least on large enough scales) is described by the translation and rotation invariant Friedmann-Lemaître-Robertson-Walker (FLRW) metric

$$ds^2 = -dt^2 + a(t) \left[\frac{dr^2}{1 - k r^2} r^2 d\theta^2 + r^2 \sin^2 \theta d\phi^2 \right] \stackrel{\text{(if } k=0)}{=} -dt^2 + a^2(t)[dx^2 + dy^2 + dz^2]. \quad (\text{A.1})$$

where $a(t)$ is the scale factor and $k = 0, \pm 1$ is a constant that describes the global geometry ($k = 0$ flat, $k = +1$ closed i.e. the geometry if a sphere, $k = -1$ open i.e. the geometry if a hyperbolic surface). The fact that a depends on time encodes the expansion. In the usual convention, $a(t)$ is adimensional and normalized to unity today $a(t = \text{today}) = a_0 = 1$. One also defines the (cosmological) redshift z as $1 + z = 1/a$, so today $z_0 = 0$.

The matter-energy content of the Universe is modeled as a generic fluid, whose stress-energy tensor is constrained by homogeneity and isotropy to have the form

$$T_\nu^\mu = \text{diag}(\rho, P, P, P), \quad (\text{A.2})$$

where ρ is the energy density and p the pressure density. In such a Universe, Einstein's equations of General Relativity $R_{\mu\nu} - \frac{R}{2}g_{\mu\nu} = 8\pi G T_{\mu\nu}$ specialize to the Friedmann equations

$$H^2 = \frac{8\pi G}{3}\rho - \frac{k}{a^2}, \quad (\text{A.3})$$

$$\frac{\ddot{a}}{a} = -\frac{4\pi G}{3}(\rho + 3P), \quad (\text{A.4})$$

where \cdot denotes the derivative with respect to time t . Here $H \equiv \dot{a}/a$ is called the Hubble expansion rate. Its present value is $H = H_0$ with

$$H_0 = h \frac{100 \text{ km}}{\text{sec} \cdot \text{Mpc}} = \frac{h}{9.78 \cdot 10^9 \text{ yr}} = 2.1 h \cdot 10^{-33} \text{ eV}, \quad h \approx 0.7 \quad (\text{A.5})$$

(where pc = 3.26 lyr is the parsec).

Some equations simplify if one uses, instead of time t , a variable η called *conformal time* and defined as the comoving distance traveled by light: $d\eta \equiv dt/a(t) = da/Ha^2$.

It is fun to note that the first Friedmann equation could have been derived by Newton centuries before Einstein, Friedmann, Robertson and Walker. Indeed, modeling the Universe as a sphere with radius $a(t)$ composed by a constant density $\rho(t)$, Newtonian gravity predicts that it evolves according to

$$\ddot{a} = -\frac{GM(r < a)}{a^2} = -\frac{4\pi G\rho(t)}{3}a. \quad (\text{A.6})$$

Taking into account that for matter one has $\rho(t) \propto 1/a^3(t)$ this equation can be integrated, obtaining the usual conservation of energy

$$\frac{d}{dt} \left[\frac{1}{2}\dot{a}^2 - \frac{4\pi}{3}G\rho a^2 \right] = 0,$$

from which eq. (A.3) follows. Here k plays the role of energy constant. The critical case of ‘zero energy’ $k = 0$ corresponds to a density equal to the ‘critical density’

$$\rho = \rho_{\text{cr}} \equiv 3H^2/8\pi G \quad (\text{A.7})$$

and describes a Universe that expands for free (the double of zero energy is zero energy). This is the case predicted by inflationary cosmology in GR, and is compatible with present observations of the actual Universe.

A.2 Matter-energy content

Many components of the Universe are described by a toy equation of state

$$P = w\rho \quad \text{with } w \text{ a constant.} \quad (\text{A.8})$$

The relativistic conservation law for the energy momentum tensor $T^{\mu\nu}_{;\nu} = 0$ just gives the first law of thermodynamics:

$$dU = -P dV \quad U = \rho V \quad (\text{A.9})$$

The explicit solution is $\rho \propto a^{-3(1+w)}$. The relevant special cases are:

- $w = 0$ describes *non-relativistic matter* (‘dust’), $P_m = 0$ and $\rho_m \propto 1/a^3$;
- $w = 1/3$ describes *relativistic particles* (‘radiation’): $P_r = \rho_r/3$ and $\rho_r \propto 1/a^4$;
- $w = -1$ describes *vacuum energy*: $P_V = -\rho_V$, that do not depend on (i.e. is constant with) a .

The actual Universe is composed by a sum of different components: matter, radiation and dark energy. The latter has properties close to vacuum energy, and it might be a cosmological constant Λ . The present energy densities of these components

$$\Omega_i = \rho_i/\rho_{\text{cr}} \quad \sum_i \Omega_i \simeq 1 \quad (\text{A.10})$$

are measured [2] to be

$$\Omega_\Lambda \approx 69\%, \quad \Omega_m \approx 5\% + 26\%, \quad \Omega_r \approx 0.0049\% + 0.0034\%. \quad (\text{A.11})$$

Matter is made of two components: normal baryonic matter (5%) and the unknown Dark Matter (26%). Radiation is also made of two components: photons and neutrinos, here approximated as massless. We see that matter started dominating the Universe at $a > a_{\text{eq}} = \Omega_r/\Omega_m \approx 1/3100$ i.e. $t_{\text{eq}} \approx 60$ kyr.

The age of the Universe is given by

$$T_U = \int_0^1 \frac{da}{a H} = \frac{1}{H_0} \int_0^1 \frac{da}{a \sqrt{\Omega_\Lambda + \Omega_m/a^3 + \Omega_r/a^4}} = \frac{1}{H_0} \times \begin{cases} 1/2 & \text{if } \Omega_r = 1 \\ 2/3 & \text{if } \Omega_m = 1 \\ 0.96 & \text{true case} \end{cases}. \quad (\text{A.12})$$

In general, one can hence explicitly solve the Friedmann equation (A.3)

$$\frac{\dot{a}}{a} = H = H_0 \sqrt{\frac{\rho}{\rho_0}} = H_0 \sqrt{\Omega_\Lambda + \frac{\Omega_m}{a^3} + \frac{\Omega_r}{a^4}}. \quad (\text{A.13})$$

Simple analytic results hold in the ages where matter or radiation was dominating the total energy density:

$$a(t) = \begin{cases} (3tH_0\sqrt{\Omega_m}/2)^{2/3} & \text{during matter domination at } 1 \gg a \gg a_{\text{eq}} \\ (2tH_0\sqrt{\Omega_r})^{1/2} & \text{during radiation domination at } a \ll a_{\text{eq}} \end{cases}. \quad (\text{A.14})$$

A.3 Particles in thermal equilibrium

A gas of relativistic particles at temperature T has energy $E \sim T$, wavelength $\lambda \sim 1/T$ and consequently number density n_{eq} and energy density ρ_{eq} approximatively given by

$$n_{\text{eq}} \sim T^3, \quad \rho_{\text{eq}} \sim T^4. \quad (\text{A.15})$$

For non relativistic particles, $T \ll m$, one instead has $E \simeq m$ such that $\rho_{\text{eq}} = mn_{\text{eq}}$ and both densities get suppressed by a Boltzmann factor $e^{-m/T}$ (unless there is a conserved quantum number that prevents such suppression, like baryon number in the case of baryonic matter).

The precise formulæ for the thermal densities of a gas of particles with mass m and g degrees of freedom are:

$$n_{\text{eq}}(T) = g \int \frac{d^3 p}{(2\pi)^3} f_{\text{eq}} = \frac{g}{2\pi^2} \int_m^\infty f_{\text{eq}} E p dE \quad (\text{A.16})$$

$$\rho_{\text{eq}}(T) = g \int \frac{d^3 p}{(2\pi)^3} E f_{\text{eq}} = \frac{g}{2\pi^2} \int_m^\infty f_{\text{eq}} E^2 p dE \quad (\text{A.17})$$

$$p_{\text{eq}}(T) = g \int \frac{d^3 p}{(2\pi)^3} \frac{p^2}{3E} f_{\text{eq}} = \frac{g}{6\pi^2} \int_m^\infty f_{\text{eq}} p^3 dE \quad (\text{A.18})$$

where $f_{\text{eq}} = 1/(e^{E/T} + c)$ is the Fermi-Dirac distribution for fermions ($c = +1$) or the Bose-Einstein distribution for bosons ($c = -1$). A simple useful approximation is the Boltzmann limit $c = 0$.

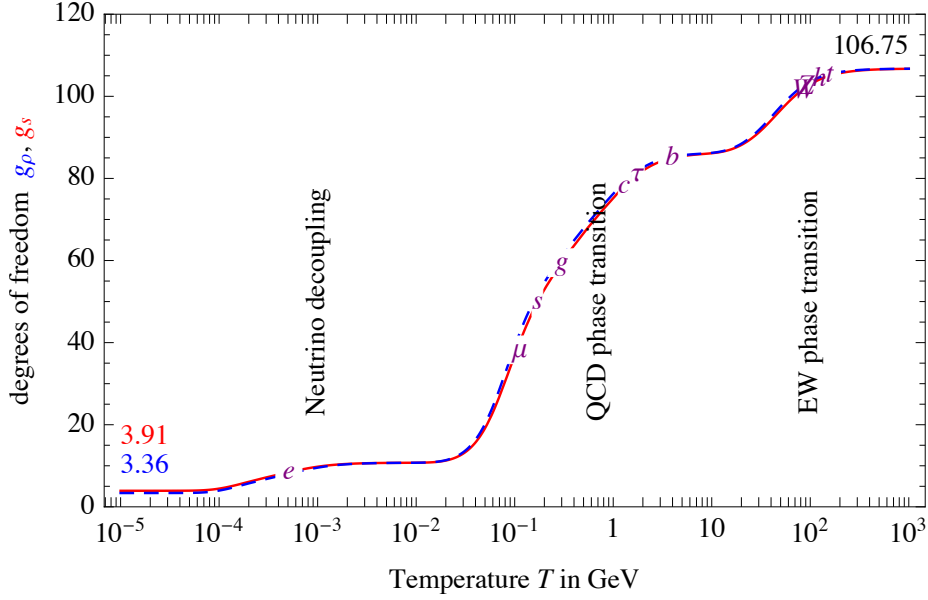


Figure A.1: Degrees of freedom of the SM $g_s(T)$ (red) and $g_\rho(T)$ (blue dashed), increasing up to 106.75 as function of the temperature T .

▷ In the ultra-relativistic limit $T \gg m$ the integrals can be performed with the explicit results

$$n_{\text{eq}}(T \gg m) = \frac{g}{\pi^2} T^3 \times \begin{cases} 3\zeta(3)/4 & c = +1 \\ 1 & c = 0 \\ \zeta(3) & c = -1 \end{cases} \quad (\text{A.19})$$

$$\rho_{\text{eq}}(T \gg m) = \frac{g}{\pi^2} T^4 \times \begin{cases} 7\pi^4/240 & c = +1 \\ 3 & c = 0 \\ \pi^4/30 & c = -1 \end{cases} \quad (\text{A.20})$$

and $p_{\text{eq}} = \rho_{\text{eq}}/3$. The total energy density in relativistic species, which can have different temperatures, writes

$$\rho_R(T) = \frac{\pi^2}{30} g_\rho(T) T^4, \quad \text{with } g_\rho(T) = \sum_{m \ll T} g_b \left(\frac{T_b}{T}\right)^4 + \frac{7}{8} \sum_{m \ll T} g_f \left(\frac{T_f}{T}\right)^4, \quad (\text{A.21})$$

where the sums run over bosons and fermions respectively.

▷ In the non-relativistic limit $T \ll m$ all distributions reduce to the Boltzmann result:

$$n_{\text{eq}}(T \ll m) = g(MT/2\pi)^{3/2} e^{-m/T}, \quad p_{\text{eq}} \ll \rho_{\text{eq}} \simeq mn_{\text{eq}}. \quad (\text{A.22})$$

Since the Universe cannot exchange heat with any “outside”, its evolution in thermal equilibrium conserves the entropy $S = sV$ where V is the volume and

$$s = \frac{\rho + p}{T} \equiv \frac{2\pi^2}{45} g_s(T) T^3 \quad \text{is the entropy density.} \quad (\text{A.23})$$

Up to factors of order one, s is essentially the total number density of particles, n_{eq} . Conservation of S implies that the temperature T decreases during expansion as $1/a$, up to the decrease in g_s that takes place when the various SM particles become non relativistic. The entropy is dominated by ultra-relativistic particles, such that summing over all particles one has

$$g_s = \sum_{m \ll T} g_b \left(\frac{T_b}{T} \right) + \frac{7}{8} \sum_{m \ll T} g_f \left(\frac{T_f}{T} \right). \quad (\text{A.24})$$

At $T \gg m_e$ all SM fermions and bosons are in thermal equilibrium and consequently have the same temperature T : the value of $g_s(T)$ in the SM is shown in fig. A.1. At $T \gg M_t$, such that all SM particles are ultra-relativistic, one has $g_s = \frac{7}{8}2 \cdot 3 \cdot 15 + 2(1 + 3 + 8) + 2 \cdot 2 = 106.75$, slightly lower than 118, the total number of SM degrees of freedom. See [?] for the expansion rate at $T \sim \Lambda_{\text{QCD}}$ [?]. After neutrino decoupling, at $T \ll m_e$, the Universe contains photons and neutrinos with different temperatures, $T_\nu = T_\gamma(4/11)^{1/3}$. Measuring the entropy in units of the photon temperature one has $g_s = 2 + \frac{7}{8}2 \cdot 3 \frac{4}{11} = \frac{43}{11} \simeq 3.91$.

Bibliography

- [1] **General and historical reviews.** *The classics.* G. Jungman, M. Kamionkowski, K. Griest, “Supersymmetric dark matter”, Phys. Rept. 267 (1996) 195 [[arXiv:hep-ph/9506380](#)]. G. Bertone, D. Hooper, J. Silk, “Particle dark matter: Evidence, candidates and constraints”, Phys. Rept. 405 (2004) 279 [[arXiv:hep-ph/0404175](#)].
- Recent.* L. Bergström, “Nonbaryonic dark matter: Observational evidence and detection methods”, Rept. Prog. Phys. 63 (2000) 793 [[InSpires:Bergstrom:2000pn](#)]. M. Taoso, G. Bertone, A. Masiero, “Dark Matter Candidates: A Ten-Point Test”, JCAP 0803 (2007) 022 [[arXiv:0711.4996](#)]. J. Einasto, “Dark Matter” [[arXiv:0901.0632](#)]. A.H.G. Peter, “Dark Matter: A Brief Review” [[arXiv:1201.3942](#)]. L.E. Strigari, “Galactic Searches for Dark Matter”, Phys. Rept. 531 (2013) 1 [[arXiv:1211.7090](#)]. A. Del Popolo, “Nonbaryonic Dark Matter in Cosmology”, Int. J. Mod. Phys. D23 (2014) 1430005 [[arXiv:1305.0456](#)]. M. Lisanti, “Lectures on Dark Matter Physics” [[arXiv:1603.03797](#)]. G. Bertone, D. Hooper, “A History of Dark Matter” [[arXiv:1605.04909](#)]. K. Freese, “Status of Dark Matter in the Universe”, Int. J. Mod. Phys. D26 (2017) 1730012 [[arXiv:1701.01840](#)]. J. de Swart, G. Bertone, J. van Dongen, “How Dark Matter Came to Matter”, Nature Astron. 1 (2017) 0059 [[arXiv:1703.00013](#)]. T. Plehn, “Yet Another Introduction to Dark Matter” [[arXiv:1705.01987](#)]. M. Drees and G. Gerbier in PDG Collaboration, “Review of Particle Physics”, Chin. Phys. C40 (2016) 100001 [[InSpires:Patrignani:2016xqp](#)].
- DM density distribution.** M. Kuhlen, M. Vogelsberger, R. Angulo, “Numerical Simulations of the Dark Universe: State of the Art and the Next Decade”, Phys. Dark Univ. 1 (2012) 50 [[arXiv:1209.5745](#)]. C.S. Frenk, S.D.M. White, “Dark matter and cosmic structure”, Annalen Phys. 524 (2012) 507 [[arXiv:1210.0544](#)]. J.I. Read, “The Local Dark Matter Density”, J. Phys. G41 (2014) 063101 [[arXiv:1404.1938](#)].
- Direct detection.** R.J. Gaitskell, “Direct detection of dark matter”, Ann. Rev. Nucl. Part. Sci. 54 (2004) 315 [[InSpires:Gaitskell:2004gd](#)]. K. Freese, M. Lisanti, C. Savage, “Colloquium: Annual modulation of dark matter”, Rev. Mod. Phys. 85 (2013) 1561 [[arXiv:1209.3339](#)]. M. Schumann, “Dark Matter 2014”, EPJ Web Conf. 96 (2015) 01027 [[arXiv:1501.01200](#)]. T. Marrodán Undagoitia, L. Rauch, “Dark matter direct-detection experiments”, J. Phys. G43 (2015) 013001 [[arXiv:1509.08767](#)].
- Indirect detection.** S. Profumo, “Astrophysical Probes of Dark Matter” [[arXiv:1301.0952](#)]. A. Ibarra, D. Tran, C. Weniger, “Indirect Searches for Decaying Dark Matter”, Int. J. Mod. Phys. A28 (2013) 1330040 [[arXiv:1307.6434](#)] J. Conrad, J. Cohen-Tanugi, L.E. Strigari, “WIMP searches with gamma rays in the Fermi era: challenges, methods and results”, J. Exp. Theor. Phys. 121 (2016) 1104 [[arXiv:1503.06348](#)]. J.M. Gaskins, “A review of indirect searches for particle dark matter”, Contemp. Phys. 57 (2016) 496 [[arXiv:1604.00014](#)]. L.E. Strigari, “Dark Matter in Dwarf Spheroidal Galaxies and Indirect Detection: A Review”, Rept. Prog. Phys. 81 (2018) 056901 [[InSpires:Strigari:2018utn](#)].
- Collider searches.** F. Kahlhoefer, “Review of LHC Dark Matter Searches”, Int. J. Mod. Phys. A32 (2017) 1730006 [[arXiv:1702.02430](#)].
- Particle physics candidates for DM.** F.D. Steffen, “Dark Matter Candidates - Axions, Neutralinos, Gravitinos, and Axinos”, Eur. Phys. J. C59 (2008) 557 [[arXiv:0811.3347](#)]. J.L. Feng, “Dark Matter Candidates from Particle Physics and Methods of Detection”, Ann. Rev. Astron. Astrophys. 48 (2010) 495 [[arXiv:1003.0904](#)]. A. Ringwald, “Exploring the Role of Axions and Other WISPs in the Dark Universe”, Phys. Dark Univ. 1 (2012) 116 [[arXiv:1210.5081](#)]. K-Y. Choi, J.E. Kim, L. Roszkowski, “Review of axino dark matter”, J. Korean Phys. Soc. 63 (2013) 1685 [[arXiv:1307.3330](#)]. M. Drewes et al., “A White Paper on keV Sterile Neutrino Dark Matter”, JCAP 1701 (2017) 025 [[arXiv:1602.04816](#)]. G. Arcadi, M. Dutra, P. Ghosh, M. Lindner, Y. Mambrini, M. Pierre, S. Profumo, F.S. Queiroz, “The Waning

- of the WIMP? A Review of Models, Searches, and Constraints” [[arXiv:1703.07364](#)]. N. Bernal, M. Heikinheimo, T. Tenkanen, K. Tuominen, V. Vaskonen, “The Dawn of FIMP Dark Matter: A Review of Models and Constraints” [[arXiv:1706.07442](#)]. L. Roszkowski, E.M. Sessolo, S. Trojanowski, “WIMP dark matter candidates and searches - current issues and future prospects” [[arXiv:1707.06277](#)].
- Alternatives to DM.** C. Skordis, “The Tensor-Vector-Scalar theory and its cosmology”, Class. Quant. Grav. 26 (2009) 143001 [[arXiv:0903.3602](#)]. B. Famaey, S. McGaugh, “Modified Newtonian Dynamics (MOND): Observational Phenomenology and Relativistic Extensions”, Living Rev. Rel. 15 (2011) 10 [[arXiv:1112.3960](#)].
- Books.** G. Bertone (editor), “Particle Dark Matter: Observations, Models and Searches”, Cambridge University Press (2010) [[InSpire:Bertone:2010zza](#)]. S. Profumo, “An Introduction to Particle Dark Matter”, World Scientific (2017) .
- [2] PLANCK Collaboration, “Planck 2015 results. XIII. Cosmological parameters”, Astron. Astrophys. 594 (2015) A13 [[arXiv:1308.3419](#)].
- [3] **Hubble constant.** A. Riess *et al*, “A 2.4% Determination of the Local Value of the Hubble Constant”, Astrophys. J. 826 (2016) 56 [[arXiv:1604.01424](#)]. A. Riess *et al*, “New Parallaxes of Galactic Cepheids from Spatially Scanning the Hubble Space Telescope: Implications for the Hubble Constant” [[arXiv:1801.01120](#)]. A. Riess *et al*, “Milky Way Cepheid Standards for Measuring Cosmic Distances and Application to Gaia DR2: Implications for the Hubble Constant” [[arXiv:1804.10655](#)].
- [4] Particle Data Group, “Review of Particle Physics”, Chin. Phys. C 40 (2016) 100001 [[link](#)].
- [5] **Rotation curves. Historical measurements and interpretations.** V.C. Rubin, J. Ford, “Rotation of the Andromeda Nebula from a Spectroscopic Survey of Emission Regions”, Astrophys. J. 159 (1970) 379 [[InSpire:Rubin:1970zza](#)]. K. Freeman, “On the Disks of Spiral and S0 Galaxies”, Astrophysical Journal 160 (1970) 811. V.C. Rubin, J. Ford, N. Thonnard, “Extended rotation curves of high-luminosity spiral galaxies. IV. Systematic dynamical properties, Sa through Sc”, Astrophys. J. 225 (1978) L107 [[InSpire:Rubin:1978kmz](#)]. S.M. Faber, J.S. Gallagher, “Masses and mass-to-light ratios of galaxies”, Ann. Rev. Astron. Astrophys. 17 (1979) 135 [[InSpire:Faber:1979pp](#)]. V.C. Rubin, N. Thonnard, J. Ford, “Rotational properties of 21 SC galaxies with a large range of luminosities and radii, from NGC 4605 /R = 4kpc/ to UGC 2885 /R = 122 kpc/”, Astrophys. J. 238 (1980) 471 [[InSpire:Rubin:1980zd](#)]. K.G. Begeman, A.H. Broeils, R.H. Sanders, “Extended rotation curves of spiral galaxies: Dark haloes and modified dynamics”, Mon. Not. Roy. Astron. Soc. 249 (1991) 523 [[InSpire:Begeman:1991iy](#)].
- More recent works.* M. Persic, P. Salucci, F. Stel, “The Universal rotation curve of spiral galaxies: 1. The Dark matter connection”, Mon. Not. Roy. Astron. Soc. 281 (1995) 27 [[arXiv:astro-ph/9506004](#)]. E. Corbelli, P. Salucci, “The Extended Rotation Curve and the Dark Matter Halo of M33”, Mon. Not. Roy. Astron. Soc. 311 (1999) 441 [[InSpire:Corbelli:1999af](#)]. Y. Sofue, Y. Tutui, M. Honma, A. Tomita, T. Takamiya, J. Koda, Y. Takeda, “Central rotation curves of spiral galaxies”, Astrophys. J. 523 (1999) 136 [[InSpire:Sofue:1999jy](#)]. Y. Sofue, V. Rubin, “Rotation curves of spiral galaxies”, Ann. Rev. Astron. Astrophys. 39 (2000) 137 [[arXiv:astro-ph/0010594](#)]. P. Salucci, A. Lapi, C. Tonini, G. Gentile, I. Yegorova, U. Klein, “The Universal Rotation Curve of Spiral Galaxies. 2. The Dark Matter Distribution out to the Virial Radius”, Mon. Not. Roy. Astron. Soc. 378 (2007) 41 [[InSpire:Salucci:2007tm](#)]. F. Donato, G. Gentile, P. Salucci, C.F. Martins, M.I. Wilkinson, G. Gilmore, E.K. Grebel, A. Koch, R. Wyse, “A constant dark matter halo surface density in galaxies”, Mon. Not. Roy. Astron. Soc. 397 (2009) 1169 [[arXiv:0904.4054](#)].
- Recent works for the Milky Way (including publicly available data).* M. Pato, F. Iocco, G. Bertone, “Dynamical constraints on the dark matter distribution in the Milky Way”, JCAP 1512 (2015) 001 [[arXiv:1504.06324](#)]. F. Iocco, M. Pato, G. Bertone, “Evidence for dark matter in the inner Milky Way”, Nature Phys. 11 (2015) 245 [[arXiv:1502.03821](#)]. Y. Huang *et al*, “The Milky Way’s rotation curve out to 100 kpc and its constraint on the Galactic mass distribution” [[arXiv:1604.01216](#)]. M. Pato, F. Iocco, “galkin: a new compilation of the Milky Way rotation curve data”, SoftwareX 6 (2017) 54 [[arXiv:1703.00020](#)].
- [6] **Disk stability.** J. Ostriker, p. Peebles, “A Numerical Study of the Stability of Flattened Galaxies: or, can Cold Galaxies Survive?”, Astrophysical Journal 186 (1973) 467-480. E. Athanassoula, “Bar-halo interaction and bar growth”, Astrophys. J. 569 (2002) L83 [[InSpire:Athanassoula:2002db](#)]. A.J. Benson, “Galaxy Formation Theory”, Phys. Rept. 495 (2010) 33 [[arXiv:1006.5394](#)]. F. Combes, “Dark matter

- distribution and its impact on the evolution of galaxy disks”, Mem. Soc. Astron. Ital. Suppl. 25 (2012) 45 [[arXiv:1210.5124](#)].
- Galaxy-galaxy lensing.** T.G. Brainerd, R.D. Blandford, I. Smail, “Measuring galaxy masses using galaxy - galaxy gravitational lensing”, *Astrophys. J.* 466 (1995) 623 [[InSpires:Brainerd:1995da](#)]. I.P. Dell’Antonio, J.A. Tyson, “Galaxy dark matter: Galaxy-galaxy lensing in the Hubble deep field”, *Astrophys. J.* 473 (1996) L17 [[InSpires:DellAntonio:1996ylb](#)]. H. Hoekstra, H.K.C. Yee, M.D. Gladders, “Properties of galaxy dark matter halos from weak lensing”, *Astrophys. J.* 606 (2003) 67 [[InSpires:Hoekstra:2003pn](#)]. M. Bartelmann, M. Maturi, “Weak gravitational lensing” [[arXiv:1612.06535](#)].
- [7] F. Zwicky, “Die Rotverschiebung von extragalaktischen Nebeln”, *Helv. Phys. Acta* 6 (1933) 110 [[InSpires:Zwicky:1933gu](#)].
- [8] **Bullet cluster and other colliding clusters.** D. Clowe, M. Bradac, A.H. Gonzalez, M. Markevitch, S.W. Randall, C. Jones, D. Zaritsky, “A direct empirical proof of the existence of dark matter”, *Astrophys. J.* 648 (2006) L109 [[arXiv:astro-ph/0608407](#)]. D. Harvey, R. Massey, T. Kitching, A. Taylor, E. Tittley, “The non-gravitational interactions of dark matter in colliding galaxy clusters”, *Science* 347 (2015) 1462 [[arXiv:1503.07675](#)].
- DM self-interaction limits.** M. Markevitch, A.H. Gonzalez, D. Clowe, A. Vikhlinin, L. David, W. Forman, C. Jones, S. Murray, W. Tucker, “Direct constraints on the dark matter self-interaction cross-section from the merging galaxy cluster 1E0657-56”, *Astrophys. J.* 606 (2003) 819 [[arXiv:astro-ph/0309303](#)]. S.W. Randall, M. Markevitch, D. Clowe, A.H. Gonzalez, M. Bradac, “Constraints on the Self-Interaction Cross-Section of Dark Matter from Numerical Simulations of the Merging Galaxy Cluster 1E 0657-56”, *Astrophys. J.* 679 (2007) 1173 [[arXiv:0704.0261](#)]. F. Kahlhoefer, K. Schmidt-Hoberg, M.T. Frandsen, S. Sarkar, “Colliding clusters and dark matter self-interactions”, *Mon. Not. Roy. Astron. Soc.* 437 (2014) 2865 [[arXiv:1308.3419](#)].
- [9] **Cosmic shear.** van Waerbeke et al., “Detection of correlated galaxy ellipticities on CFHT data: First evidence for gravitational lensing by large scale structures”, *Astron. Astrophys.* 358 (2000) 30 [[InSpires:vanWaerbeke:2000rm](#)]. D.J. Bacon, A.R. Refregier, R.S. Ellis, “Detection of weak gravitational lensing by large-scale structure”, *Mon. Not. Roy. Astron. Soc.* 318 (2000) 625 [[InSpires:Bacon:2000sy](#)]. D.M. Wittman, J.A. Tyson, D. Kirkman, I. Dell’Antonio, G. Bernstein, “Detection of weak gravitational lensing distortions of distant galaxies by cosmic dark matter at large scales”, *Nature* 405 (2000) 143 [[arXiv:astro-ph/0003014](#)]. N. Kaiser, G. Wilson, G.A. Luppino, “Large scale cosmic shear measurements” [[InSpires:Kaiser:2000if](#)]. R. Massey et al., “Dark matter maps reveal cosmic scaffolding”, *Nature* 445 (2007) 286 [[InSpires:Massey:2007wb](#)]. R. Massey, T. Kitching, J. Richard, “The dark matter of gravitational lensing”, *Rept. Prog. Phys.* 73 (2010) 086901 [[arXiv:1001.1739](#)].
- [10] PLANCK Collaboration, “Planck 2015 results. I. Overview of products and scientific results”, *Astron. Astrophys.* 594 (2016) A1 [[arXiv:1502.01582](#)].
- [11] M. Tegmark, M. Zaldarriaga, “Separating the early universe from the late universe: Cosmological parameter estimation beyond the black box”, *Phys. Rev. D* 66 (2002) 103508 [[InSpires:Tegmark:2002cy](#)]. S. Dodelson, M. Liguori, “Can Cosmic Structure form without Dark Matter?”, *Phys. Rev. Lett.* 97 (2006) 231301 [[InSpires:Dodelson:2006zt](#)].
- [12] C. Skordis, “The Tensor-Vector-Scalar theory and its cosmology”, *Class. Quant. Grav.* 26 (2009) 143001 [[arXiv:0903.3602](#)].
- [13] **Cosmology books.** E. W. Kolb and M. S. Turner, “The Early Universe”, *Frontiers in Physics* (Addison Wesley Publishing Co.) 69 (1990) 1 [[InSpires:Kolb:1990vq](#)]. S. Dodelson, “Modern cosmology”, Academic Press, Amsterdam (The Netherlands) (2003) [[InSpires:Dodelson:2003ft](#)].
- [14] **Discovery of Neptune.** U.-J. Le Verrier, “Sur la planète qui produit les anomalies observées dans le mouvement d’Uranus - Détermination de sa masse, de son orbite et de sa position actuelle”, *Comptes Rendus hebdomadaires des Séances de l’Académie des Sciences Tome* 23 (juillet-décembre 1846) 428-438, available on the website of the Bibliothèque nationale de France. J. C. Adams, “On the perturbations of Uranus”, Appendices to various nautical almanacs between the years 1834 and 1854 (1846) 265-293, available online.

- [15] **Non-discovery of Vulcan.** U.-J. Le Verrier, “Lettre [...] sur la théorie de Mercure et sur le mouvement du périhélie de cette planète”, Comptes Rendus hebdomadaires des Séances de l’Académie des Sciences Tome 49 (juillet-décembre 1859) 379-383, [available on the website](#) of the Bibliothèque nationale de France. E. M. Lescarbault, U.-J. Le Verrier, “Passage d’une planète sur le disque du Soleil, observé à Orgères (Eure-et-Loir)”, Comptes Rendus hebdomadaires des Séances de l’Académie des Sciences Tome 50 (janvier-juin 1860) 40-45, [available on the website](#) of the Bibliothèque nationale de France. A. Einstein, “Explanation of the Perihelion Motion of Mercury from the General Theory of Relativity”, Sitzungsber. Preuss. Akad. Wiss. Berlin (Math. Phys.) 1915 (1915) 831. A. Einstein, “Die Grundlage der allgemeinen Relativitätstheorie”, Annalen de Physik 49 (7) (1916) 769-822.
- [16] H. Desmond, “A statistical investigation of the mass discrepancy-acceleration relation”, Mon. Not. Roy. Astron. Soc. 464 (2017) 4160 [[arXiv:1607.01800](#)].
- [17] S. McGaugh, F. Lelli, J. Schombert, “Radial Acceleration Relation in Rotationally Supported Galaxies”, Phys. Rev. Lett. 117 (2016) 201101 [[arXiv:1609.05917](#)].
- [18] B.W. Keller, J.W. Wadsley, “La Fin du MOND? Λ CDM is Fully Consistent with SPARC Acceleration Law” [[arXiv:1610.06183](#)].
- [19] A.D Ludlow et al., “The Mass-Discrepancy Acceleration Relation: a Natural Outcome of Galaxy Formation in CDM halos” [[arXiv:1610.07663](#)].
- [20] **MOND.** M. Milgrom, “*A modification of the Newtonian dynamics as a possible alternative to the hidden mass hypothesis*”, Astrophysical J. 270 (1983) 365. For a recent review see S.S. McGaugh, “A tale of two paradigms: the mutual incommensurability of Λ CDM and MOND”, Can. J. Phys. 93 (2014) 250 [[arXiv:1404.7525](#)].
- [21] A. Aguirre, J. Schaye, E. Quataert, “Problems for MOND in clusters and the Ly-alpha forest”, Astrophys. J. 561 (2001) 550 [[arXiv:astro-ph/0105184](#)].
- [22] **Theories possibly underlying MOND.** J. Bekenstein and M. Milgrom, “*Does the missing mass problem signal the breakdown of Newtonian gravity?*”, Astrophys. J. 286 (1984) 7. J.D. Bekenstein, “Relativistic gravitation theory for the MOND paradigm”, Phys. Rev. D70 (2004) 083509 [[arXiv:astro-ph/0403694](#)]. G.W. Angus, B. Famaey, HS. Zhao, “Can MOND take a bullet? Analytical comparisons of three versions of MOND beyond spherical symmetry”, Mon. Not. Roy. Astron. Soc. 371 (2006) 138 [[arXiv:astro-ph/0606216](#)]. B. Famaey, S. McGaugh, “Modified Newtonian Dynamics (MOND): Observational Phenomenology and Relativistic Extensions”, Living Rev. Rel. 15 (2011) 10 [[arXiv:1112.3960](#)]. J. Khoury, “Another Path for the Emergence of Modified Galactic Dynamics from Dark Matter Superfluidity”, Phys. Rev. D93 (2016) 103533 [[arXiv:1602.05961](#)].
- [23] E.P. Verlinde, “Emergent Gravity and the Dark Universe” [[arXiv:1611.02269](#)]. See however K. Pardo, “Testing Emergent Gravity with Isolated Dwarf Galaxies” [[arXiv:1706.00785](#)].
- [24] **MACHOs.** *Original published proposals.* M Petrou, “Dynamical Models of Spheroidal Systems”, PhD thesis Churchill College (July 1981) Cambridge (this is the first document in which the ‘massive halo object’ idea is put forward and which does a detailed calculation of the lensing effect; however, the document is not published on a journal and not available online – obtained thanks to private communications with the author). B. Paczynski, “Gravitational microlensing by the galactic halo”, Astrophys. J. 304 (1986) 1 [[InSpire:Paczynski:1985jf](#)]. K. Griest, “Galactic Microlensing as a Method of Detecting Massive Compact Halo Objects”, Astrophys. J. 366 (1991) 412 [[InSpire:Griest:1990vu](#)].
- Lensing surveys.*
- MACHO Collaboration, “The MACHO project: Microlensing results from 5.7 years of LMC observations”, Astrophys. J. 542 (2000) 281 [[arXiv:astro-ph/0001272](#)]. EROS-2 Collaboration, “Limits on the Macho Content of the Galactic Halo from the EROS-2 Survey of the Magellanic Clouds”, Astron. Astrophys. 469 (2006) 387 [[arXiv:astro-ph/0607207](#)]. OGLE Collaboration, “The OGLE View of Microlensing towards the Magellanic Clouds. III. Ruling out sub-solar MACHOs with the OGLE-III LMC data”, Mon. Not. Roy. Astron. Soc. 413 (2010) 493 [[arXiv:1012.1154](#)]. OGLE Collaboration, “The OGLE View of Microlensing towards the Magellanic Clouds. IV. OGLE-III SMC Data and Final Conclusions on MACHOs”, Mon. Not. Roy. Astron. Soc. 416 (2011) 2949 [[arXiv:1106.2925](#)]. K. Griest, A.M. Cieplak, M.J. Lehner, “Experimental Limits on Primordial Black Hole Dark Matter

from the First 2 yr of Kepler Data”, *Astrophys. J.* 786 (2014) 158 [[arXiv:1307.5798](#)]. H. Niikura, M. Takada, N. Yasuda, R.H. Lupton, T. Sumi, S. More, A. More, M. Oguri, M. Chiba, “Microlensing constraints on $10^{-10} M_\odot$ -scale primordial black holes from high-cadence observation of M31 with Hyper Suprime-Cam” [[arXiv:1701.02151](#)]. EROS collaboration’s [webpage](#). MOA collaboration’s [webpage](#). OGLE collaboration’s [webpage](#). Super-MACHO collaboration’s [webpage](#).

Reviews and constraints.

B.J. Carr, K. Kohri, Y. Sendouda, J’. Yokoyama, “New cosmological constraints on primordial black holes”, *Phys. Rev. D* 81 (2009) 104019 [[arXiv:0912.5297](#)]. A.S. Josan, A.M. Green, K.A. Malik, “Generalised constraints on the curvature perturbation from primordial black holes”, *Phys. Rev. D* 79 (2009) 103520 [[arXiv:0903.3184](#)]. B. Carr, F. Kuhnel, M. Sandstad, “Primordial Black Holes as Dark Matter”, *Phys. Rev. D* 94 (2016) 083504 [[arXiv:1607.06077](#)]. T.D. Brandt, “Constraints on MACHO Dark Matter from Compact Stellar Systems in Ultra-Faint Dwarf Galaxies”, *Astrophys. J.* 824 (2016) L31 [[arXiv:1605.03665](#)]. A.M. Green, “Astrophysical uncertainties on stellar microlensing constraints on multi-Solar mass primordial black hole dark matter” [[arXiv:1705.10818](#)].

[25] **Primordial Black Holes as DM.**

Original proposal. Ya. Bo. Zeldovich, I. D. Novikov, “The hypothesis of cores retarded during expansion and the hot cosmological model”, *Soviet Astronomy* 10 (1967) 602, translated from *Astronomicheskii Zhurnal* 43 (1966) 758. S. Hawking, “Gravitationally collapsed objects of very low mass”, *Mon. Not. Roy. Astron. Soc.* 152 (1971) 75 [[InSpire:Hawking:1971ei](#)]. G. Chapline, “Cosmological effects of primordial black holes”, *Nature* 253 (1975) 251.

PBH formation. See B.J. Carr, “Primordial black holes as a probe of cosmology and high energy physics”, *Lect. Notes Phys.* 631 (2003) 301 [[arXiv:astro-ph/0310838](#)], M.Y. Khlopov, “Primordial Black Holes”, *Res. Astron. Astrophys.* 10 (2008) 495 [[arXiv:0801.0116](#)] and references therein.

Black Hole evaporation. S.W. Hawking, “Black hole explosions”, *Nature* 248 (1974) 30 [[InSpire:Hawking:1974rv](#)]. S.W. Hawking, “Particle Creation by Black Holes”, *Commun. Math. Phys.* 43 (1975) 199 [[InSpire:Hawking:1974sw](#)]. J.H. MacGibbon, “Can Planck-mass relics of evaporating black holes close the universe?”, *Nature* 329 (1987) 308 [[InSpire:MacGibbon:1987my](#)].

Constraints. M. Ricotti, J.P. Ostriker, K.J. Mack, “Effect of Primordial Black Holes on the Cosmic Microwave Background and Cosmological Parameter Estimates”, *Astrophys. J.* 680 (2007) 829 [[arXiv:0709.0524](#)]. F. Capela, M. Pshirkov, P. Tinyakov, “Constraints on primordial black holes as dark matter candidates from capture by neutron stars”, *Phys. Rev. D* 87 (2013) 123524 [[arXiv:1301.4984](#)]. S. Clesse, J. García-Bellido, “Detecting the gravitational wave background from primordial black hole dark matter” [[arXiv:1610.08479](#)]. D. Gaggero, G. Bertone, F. Calore, R.M.T. Connors, M. Lovell, S. Markoff, E. Storm, “Searching for Primordial Black Holes in the radio and X-ray sky” [[arXiv:1612.00457](#)]. Y. Ali-Haïmoud, M. Kamionkowski, “Cosmic microwave background limits on accreting primordial black holes”, *Phys. Rev. D* 95 (2017) 043534 [[arXiv:1612.05644](#)]. V. Poulin, P.D. Serpico, F. Calore, S. Clesse, K. Kohri, “Squeezing spherical cows: CMB bounds on disk-accreting massive Primordial Black Holes” [[arXiv:1707.04206](#)]. Y. Ali-Haïmoud, E.D. Kovetz, M. Kamionkowski, “The merger rate of primordial-black-hole binaries” [[arXiv:1709.06576](#)].

PBHs DM at the origin of the LIGO GW events. S. Bird, I. Cholis, J.B. Muñoz, Y. Ali-Haïmoud, M. Kamionkowski, E.D. Kovetz, A. Raccanelli, A.G. Riess, “Did LIGO detect dark matter?”, *Phys. Rev. Lett.* 116 (2016) 201301 [[arXiv:1603.00464](#)]. S. Clesse, J. García-Bellido, “The clustering of massive Primordial Black Holes as Dark Matter: measuring their mass distribution with Advanced LIGO”, *Phys. Dark Univ.* 15 (2017-03) 142 [[arXiv:1603.05234](#)]. M. Sasaki, T. Suyama, T. Tanaka, S. Yokoyama, “Primordial Black Hole Scenario for the Gravitational-Wave Event GW150914”, *Phys. Rev. Lett.* 117 (2016) 061101 [[arXiv:1603.08338](#)]. I. Cholis, E.D. Kovetz, Y. Ali-Haïmoud, S. Bird, M. Kamionkowski, J.B. Muñoz, A. Raccanelli, “Orbital eccentricities in primordial black hole binaries”, *Phys. Rev. D* 94 (2016) 084013 [[arXiv:1606.07437](#)].

Prospects and future searches. M.A. Abramowicz, J.K. Becker, P.L. Biermann, A. Garzilli, F. Johansson, L. Qian, “No observational constraints from hypothetical collisions of hypothetical dark halo primordial black holes with galactic objects”, *Astrophys. J.* 705 (2008) 659 [[arXiv:0810.3140](#)]. M. Kesden, S. Hanasoge, “Transient solar oscillations driven by primordial black holes”, *Phys. Rev. Lett.* 107 (2011) 111101 [[arXiv:1106.0011](#)]. B.J. Carr, K. Kohri, Y. Sendouda, J’. Yokoyama, “Constraints on primordial black holes from the Galactic gamma-ray background”, *Phys. Rev. D* 94 (2016) 044029 [[arXiv:1604.05349](#)]. K.

- Schutz, A. Liu, “Pulsar timing can constrain primordial black holes in the LIGO mass window”, Phys. Rev. D95 (2017) 023002 [[arXiv:1610.04234](#)].
- Extended mass function.* S. Clesse, J. García-Bellido, “Massive Primordial Black Holes from Hybrid Inflation as Dark Matter and the seeds of Galaxies”, Phys. Rev. D92 (2015) 023524 [[arXiv:1501.07565](#)]. F. Kühnel, K. Freese, “Constraints on Primordial Black Holes with Extended Mass Functions”, Phys. Rev. D95 (2017) 083508 [[arXiv:1701.07223](#)]. B. Carr, M. Raidal, T. Tenkanen, V. Vaskonen, H. Veermäe, “Primordial black hole constraints for extended mass functions” [[arXiv:1705.05567](#)]. A.M. Green, “Microlensing and dynamical constraints on primordial black hole dark matter with an extended mass function”, Phys. Rev. D94 (2016) 063530 [[arXiv:1609.01143](#)]. N. Bellomo, J.L. Bernal, A. Raccanelli, L. Verde, “Primordial Black Holes as Dark Matter: Converting Constraints from Monochromatic to Extended Mass Distributions” [[arXiv:1709.07467](#)].
- [26] S. Clesse, J. García-Bellido, “Seven Hints for Primordial Black Hole Dark Matter” [[arXiv:1711.10458](#)].
- [27] LIGO Collaboration, “Observation of Gravitational Waves from a Binary Black Hole Merger”, Phys. Rev. Lett. 116 (2016) 061102 [[arXiv:1602.03837](#)].
- [28] J.R. Espinosa, D. Racco, A. Riotto, “A Cosmological Signature of the Standard Model Higgs Vacuum Instability: Primordial Black Holes as Dark Matter”, Phys. Rev. Lett. 120 (2018) 121301 [[arXiv:1710.11196](#)].
- [29] S. Tremaine, J.E. Gunn, “Dynamical Role of Light Neutral Leptons in Cosmology”, Phys. Rev. Lett. 42 (1979) 407 [[InSpire:Tremaine:1979we](#)]. C. Di Paolo, F. Nesti, F.L. Villante, “Phase space mass bound for fermionic dark matter from dwarf spheroidal galaxies” [[arXiv:1704.06644](#)].
- [30] C. Di Paolo, F. Nesti, F.L. Villante, “Phase space mass bound for fermionic dark matter from dwarf spheroidal galaxies” [[arXiv:1704.06644](#)].
- [31] R. Hlozek, D. Grin, D.J.E. Marsh, P.G. Ferreira, “A search for ultralight axions using precision cosmological data”, Phys. Rev. D91 (2015) 103512 [[arXiv:1410.2896](#)].
- [32] K. Petraki, R. R. Volkas, “Review of asymmetric dark matter”, Int. J. Mod. Phys. A 28 (2013) 1330028 [[arXiv:1305.4939](#)].
- [33] L.J. Hall, K. Jedamzik, J. March-Russell, S.M. West, “Freeze-In Production of FIMP Dark Matter”, JHEP 1003 (2009) 080 [[arXiv:0911.1120](#)].
J. McDonald, “Thermally generated gauge singlet scalars as selfinteracting dark matter”, Phys. Rev. Lett. 88 (2001) 091304 [[arXiv:hep-ph/0106249](#)].
- [34] J.F. Navarro, C.S. Frenk, S.D.M. White, “The Structure of cold dark matter halos”, Astrophys. J. 462 (1996) 563 [[InSpire:Navarro:1995iw](#)].
- [35] A.W. Graham, D. Merritt, B. Moore, J. Diemand, B. Terzic, “Empirical models for Dark Matter Halos. I. Nonparametric Construction of Density Profiles and Comparison with Parametric Models”, Astron. J. 132 (2005) 2685 [[arXiv:astro-ph/0509417](#)].
- [36] J.F. Navarro et al., “The Diversity and Similarity of Cold Dark Matter Halos”, Mon. Not. Roy. Astron. Soc. 402 (2008) 21 [[arXiv:0810.1522](#)].
- [37] K. G. Begeman, A. H. Broeils, R. H. Sanders, “Extended rotation curves of spiral galaxies: Dark haloes and modified dynamics”, MNRAS 249 (1991) 523.
- [38] J.N. Bahcall, R.M. Soneira, “The Universe at faint magnitudes. 2. Models for the predicted star counts”, Astrophys. J. Suppl. 44 (1980) 73 [[InSpire:Bahcall:1980fb](#)].
- [39] A. Burkert, “The Structure of dark matter halos in dwarf galaxies”, Astrophys. J. 447 (1995) L25 [[arXiv:astro-ph/9504041](#)].
See also: P. Salucci and A. Burkert, “Dark Matter Scaling Relations”, Astrophys. J. 537 (2000) L9-L12 [[arXiv:astro-ph/0004397](#)]. G. Gentile, P. Salucci, U. Klein, D. Vergani and P. Kalberla, “The cored distribution of dark matter in spiral galaxies”, Mon. Not. Roy. Astron. Soc. 351 (2004) 903 [[arXiv:astro-ph/0403154](#)]. P. Salucci, A. Lapi, C. Tonini, G. Gentile, I. Yegorova and U. Klein, “The universal rotation curve of spiral galaxies. II: The dark matter distribution out to the virial radius”, Mon. Not. Roy. Astron. Soc. 378 (2007) 41 [[arXiv:astro-ph/0703115](#)].

- [40] J. Diemand, B. Moore and J. Stadel, “Convergence and scatter of cluster density profiles”, Mon. Not. Roy. Astron. Soc. 353 (2004) 624 [[arXiv:astro-ph/0402267](#)].
- [41] R. Catena, P. Ullio, “A novel determination of the local dark matter density”, JCAP 1008 (2009) 004 [[arXiv:0907.0018](#)].
- [42] M. Weber, W. de Boer, “Determination of the Local Dark Matter Density in our Galaxy”, Astron. Astrophys. 509 (2009) A25 [[arXiv:0910.4272](#)].
- [43] P. Salucci, F. Nesti, G. Gentile, C.F. Martins, “The dark matter density at the Sun’s location”, Astron. Astrophys. 523 (2010) A83 [[arXiv:1003.3101](#)].
- [44] deBoer2 IS MISSING
- [45] SDSS Collaboration, “The Milky Way’s Circular Velocity Curve to 60 kpc and an Estimate of the Dark Matter Halo Mass from Kinematics of 2400 SDSS Blue Horizontal Branch Stars”, Astrophys. J. 684 (2008) 1143 [[arXiv:0801.1232](#)].
- [46] T. Sakamoto, M. Chiba, T.C. Beers, “The Mass of the Milky Way: Limits from a newly assembled set of halo objects”, Astron. Astrophys. 397 (2002) 899 [[InSpire:Sakamoto:2002zr](#)].
- [47] N. Przybilla, A. Tillich, U. Heber, R-D. Scholz, “Weighing the Galactic dark matter halo: a lower mass limit from the fastest halo star known”, Astrophys. J. 718 (2010) 37 [[arXiv:1005.5026](#)].
- [48] S. Gillessen, F. Eisenhauer, S. Trippe, T. Alexander, R. Genzel, F. Martins, T. Ott, “Monitoring stellar orbits around the Massive Black Hole in the Galactic Center”, Astrophys. J. 692 (2008) 1075 [[arXiv:0810.4674](#)].
- [49] J. Bovy, D.W. Hogg, H-W. Rix, “Galactic masers and the Milky Way circular velocity”, Astrophys. J. 704 (2009) 1704 [[arXiv:0907.5423](#)]. A. M. Ghez et al., “Measuring Distance and Properties of the Milky Way’s Central Supermassive Black Hole with Stellar Orbits”, Astrophys. J. 689 (2008) 1044 [[arXiv:0808.2870](#)].
- [50] F.J. Kerr, D. Lynden-Bell, “Review of galactic constants”, Mon. Not. Roy. Astron. Soc. 221 (1986) 1023 [[InSpire:Kerr:1986hz](#)]. See also M. Shen and Z. Zhu, “A Kinematical Calibration of the Galactocentric Distance”, Chin. Astron. Astrophys. 7 (2007) 120 for a recent compilation.
- [51] M. Fairbairn, T. Schwetz, “Spin-independent elastic WIMP scattering and the DAMA annual modulation signal”, JCAP 0901 (2008) 037 [[arXiv:0808.0704](#)].
- [52] M. Kuhlen, N. Weiner, J. Diemand, P. Madau, B. Moore, D. Potter, J. Stadel, M. Zemp, “Dark Matter Direct Detection with Non-Maxwellian Velocity Structure”, JCAP 1002 (2009) 030 [[arXiv:0912.2358](#)].
- [53] M. Vogelsberger, A. Helmi, V. Springel, S.D.M. White, J. Wang, C.S. Frenk, A. Jenkins, A.D. Ludlow, J.F. Navarro, “Phase-space structure in the local dark matter distribution and its signature in direct detection experiments”, Mon. Not. Roy. Astron. Soc. 395 (2008) 797 [[arXiv:0812.0362](#)].
- [54] F.S. Ling, E. Nezri, E. Athanassoula, R. Teyssier, “Dark Matter Direct Detection Signals inferred from a Cosmological N-body Simulation with Baryons”, JCAP 1002 (2009) 012 [[arXiv:0909.2028](#)].
- [55] M. Lisanti, L.E. Strigari, J.G. Wacker, R.H. Wechsler, “The Dark Matter at the End of the Galaxy”, Phys. Rev. D83 (2010) 023519 [[arXiv:1010.4300](#)].
- [56] J. Stadel, D. Potter, B. Moore, J. Diemand, P. Madau, M. Zemp, M. Kuhlen, V. Quilis, “Quantifying the heart of darkness with GHALO - a multi-billion particle simulation of our galactic halo”, Mon. Not. Roy. Astron. Soc. 398 (2008) L21 [[arXiv:0808.2981](#)].
- [57] M. Kuhlen, N. Weiner, J. Diemand, P. Madau, B. Moore, D. Potter, J. Stadel, M. Zemp, “Dark Matter Direct Detection with Non-Maxwellian Velocity Structure”, JCAP 1002 (2009) 030 [[arXiv:0912.2358](#)].
- [58] RAVE Collaboration, “The RAVE Survey: Constraining the Local Galactic Escape Speed”, Mon. Not. Roy. Astron. Soc. 379 (2007) 755 [[InSpire:Smith:2006ym](#)].
- [59] P. Salati, “Indirect and direct dark matter detection”, PoS CARGESE 2007 (2007) 009.
- [60] F. Kahlhoefer, “Review of LHC Dark Matter Searches”, Int. J. Mod. Phys. A 32 (2017) 1730006 [[arXiv:1702.02430](#)].

- [61] The potential relevance of the effect is pointed out in M. Kachelriess, P.D. Serpico, “Model-independent dark matter annihilation bound from the diffuse γ ray flux”, Phys. Rev. D76 (2007) 063516 [[arXiv:0707.0209](#)]. See also N.F. Bell, J.B. Dent, T.D. Jacques, T.J. Weiler, “Electroweak Bremsstrahlung in Dark Matter Annihilation”, Phys. Rev. D78 (2008) 083540 [[arXiv:0805.3423](#)]. More recent analyses and a more complete appraisal of the phenomenological importance of the effect have been performed in: M. Kachelriess, P.D. Serpico, M.A. Solberg, “On the role of electroweak bremsstrahlung for indirect dark matter signatures”, Phys. Rev. D80 (2009) 123533 [[arXiv:0911.0001](#)]. P. Ciafaloni, A. Urbano, “TeV scale Dark Matter and electroweak radiative corrections”, Phys. Rev. D82 (2010) 043512 [[arXiv:1001.3950](#)]. N.F. Bell, J.B. Dent, T.D. Jacques, T.J. Weiler, “W/Z Bremsstrahlung as the Dominant Annihilation Channel for Dark Matter”, Phys. Rev. D83 (2010) 013001 [[arXiv:1009.2584](#)].
- [62] P. Ciafaloni, D. Comelli, A. Riotto, F. Sala, A. Strumia, A. Urbano, “Weak Corrections are Relevant for Dark Matter Indirect Detection”, JCAP 1103 (2010) 019 [[arXiv:1009.0224](#)].
- [63] M. Cirelli, G. Corcella, A. Hektor, G. Hutsi, M. Kadastik, P. Panci, M. Raidal, F. Sala, A. Strumia, “PPPC 4 DM ID: A Poor Particle Physicist Cookbook for Dark Matter Indirect Detection”, JCAP 1103 (2010) 051 [[arXiv:1012.4515](#)].